STUDIES ON SELF-ASSEMBLY AND NETWORKS OF SOME COPPER(II) COMPLEXES AND COORDINATION POLYMERS

A Thesis
Submitted for the Degree of
Doctor of Philosophy

By
SUNIRBAN DAS

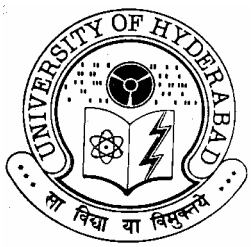

School of Chemistry
University of Hyderabad
Hyderabad 500 046
India

April 2006

To My
Parents and Sister

STATEMENT

I hereby declare that the matter embodied in the thesis entitled ***"Studies on self-assembly and networks of some copper(II) complexes and coordination polymers"*** is the result of investigations carried out by me in the School of Chemistry, University of Hyderabad, Hyderabad, India under the supervision of **Prof. Samudranil Pal**.

In keeping with the general practice of reporting scientific investigations, due acknowledgements have been made wherever the work described is based on the findings of other investigators. Any omission or error that might have crept in is regretted.

April 2006 **Sunirban Das**

PROF. SAMUDRANIL PAL
SCHOOL OF CHEMISTRY
UNIVERSITY OF HYDERABAD
HYDERABAD-500 046, INDIA

Phone: +91-40-2313 4756
(office)
Fax: +91-40-2301 2460
Email: spsc@uohyd.ernet.in

17th April 2006

CERTIFICATE

Certified that the work embodied in the thesis entitled ***"Studies on self-assembly and networks of some copper(II) complexes and coordination polymers"*** has been carried out by **Mr. Sunirban Das** under my supervision and that the same has not been submitted elsewhere for any degree.

Prof. Samudranil Pal
(Thesis Supervisor)

Dean
School of Chemistry
University of Hyderabad

Preface

The terms ‘self-assembly’ and ‘networks’ are very much common in the study of supramolecular chemistry. Self-assembly of molecular unit can be achieved by the recognition through various non-covalent interactions. Whereas, the term network readily appeared for the simplification of the supramolecular structural motifs and correlation between them. Solid state structures of the transition metal complexes occupied a vast area in the supramolecular chemistry. The assembly patterns are very sensitive to the conformation, substitution and also to the solvent of crystallizations. This thesis is an attempt to rationalized these problems in a few sets of copper(II) complexes.

Copper(II) chemistry has spread over a vast area of natural system and also of great research interests. Chapter 1 gives an overview of the coordination preference of copper(II) ion in synthetic and biological system with the importance of non-covalent interactions in various field with the reference of copper(II) complexes. The importance of copper(II) coordination polymers are also discussed in this chapter.

The conformational flexibility, the location of peripheral functional group and substituent exert the crystal packing. Chapter 2 to 4 highlight the variation of solid state structures of the complexes with the minute variation of the peripheral functional position and conformation of the ligand. Whereas, chapter 5 and 6 deal with discrepancy of the structural motif with the variation of the substituent location. Chaper 7 gives the impact of length and the conformational flexibility of the spacers on the networks of the coordination polymers.

Hyderabad *Sunirban Das*
April 2006

Acknowledgement

I express my deep sense of gratitude and profound respect to my research supervisor ***Prof. Samudranil Pal*** *for his invaluable guidance, support and constant encouragement. I have learned a great deal from him and consider my association with him to be a rewarding experience. He has been quite helpful to me in both academic and personal fronts.*

I would like to thank the former and present Dean, School of Chemistry, for their constant inspiration and for the available facilities. I am extremely thankful individually to all the faculty members of the school for their help, cooperation and encouragement at various stages of my stay in the campus.

I convey my sincere thank to Prof. A. R. Chakravarty, Prof. S. Vasudevan (IISc, Bangalore) and Prof. Wataru Fujita (Nagoya University) for providing the variable temperature Magnetic data. I would also like to convey my sincere thank to Prof. A. Nangia (University of Hyderabad) for providing me the DSC and TGA facility.

I thank all my seniors in the lab: Drs. Sangeetha, Satyanarayan, Tin, Mariappan, Gupta and Vamsee, with whom I am associated at various stages of my stay in the lab. I acknowledge my junior friends in the lab: Raji, Anindita and Rajesh. I cherish my association with all of them. My special thanks to Abhik, my friend and labmate, for his help and encouragement in many ways.

I thank all the non-teaching staff of the school for their cooperation. They had all been quite helpful, Raghavaiah and Suresh in particular.

Financial assistance from CSIR, DST and UPE, New Delhi is greatly acknowledged.

Friends are a wholesome lot and it is indeed a difficult task to mention them all here. I acknowledge whole-heartedly the contribution of each and every one of them. Even then, my association with Sougata, Raju, Totan, Nibu and Band of brothers from Mitchell and Aurabindo hostels are memorable. Also I highly acknowledge Anoop, Pavan, Bala, Ghreeh, Padu, Param, Vanki, Pradip, Sunil, Thakur, Prasad, Biju, Sarat, Philip, Mala, Jaggu, Rajesh, Sivaia and Madhu for many reasons.

I pitch high to thanks my 'Picnic', 'Movie', 'Bindaas' and 'Tea' group that include Pandua, Lungi, Baba, Saki, Sandi, Kedo, Panchu, BKS, DD, Didi, Kedar, PKM, Bishu, Tak, Jethu, Ullas, Bhat, Bachha, Bhaswati, Ghona, Padu, Bips, Tanmoy, Pati, Sandip, Sapto, Ghata, Ariandam, Rumpa, Aham-rifels and also many more to add on.

Without my parent's and sister relentless support and blessings I would not have reached to this stage of my life. I owe every think to them.

Contents

Chapter 1

Introduction

This chapter provides an overview of the fundamental importance of divalent copper ion in biology and materials science with respect to coordination behavior and structural topology. The importance of weak intermolecular interactions in the biological and materials science with a particular reference to copper(II) species have been discussed briefly. The development and the applications of the covalently bridged coordination polymers have been mentioned briefly.

1.1. Coordination chemistry of copper(II): A brief survey

Since the starting of modern coordination chemistry with Werner, chemists are constantly engaged with the understanding of bonding principles responsible for the energetics and structure of the coordination compounds. The resulting supramolecular structure with various non-covalent intermolecular interactions and their effect on the chemical and physical properties of the coordination complexes are now becoming contemporary field of chemical research. The over all structural patterns are mainly depends upon the preferential coordination of the specified metal ion and the design and conformational flexibility of the ligands. In the solid state, the nature of the solvent of crystallization also plays an important role to hold a particular structural motif. The coordination chemistry of copper is of particular interest for the better understanding of various enzymatic processes in biology, organic catalytic reactions, optical and magnetic properties, host-guest chemistry etc. There is an adequate abundance of copper containing proteins in the biological systems to carry on the electron transfer and oxidative catalytic reactions. With addition, the importance of copper containing species in materials science kept interest for the understanding of coordination as well as the supramolecular chemistry of copper.

In the following subsections, the possible coordination modes, the biological essentiality and clinical use of the copper(II) species have been discussed.

1.1.1. Preferential coordination geometry

Four-coordinated copper(II) centers are relatively abundant in the literature.[1–3] Structural variations in these systems are usually indicated by a tetrahedral distortion index which depends on the L-M-L angles and the dihedral angle between the two planes, each of which contain the central copper ion and two *cis* ligands.[3] Among the four-coordinate species, most of the complexes are either perfectly planar or slightly distorted planar due to the structural constraints. According to the point of electronic stability, the square planar complexes of copper(II) shows apical interaction with the available coordinating site from the same type of neighboring molecules or from the solvent molecules to get stability through 18-electron rule.[4] A vast number of five- or six-coordinate copper(II) complexes have been also isolated with long axial bonds due to Jahn-Teller distortion of the d^9 copper(II) center.[1,5] The geometries of the five-coordinate complexes usually range from square-pyramidal (C_{4v}) to trigonal-bipyramidal (D_{3h}), with most of the complexes falling between ideal square-pyramidal and trigonal-bipyramidal geometries, somewhere along the classical Berry pathway.[4,6] Magnetic orbital for square-planar, square-pyramidal and elongated octahedral species is $d_{x^2-y^2}$ and that for trigonal-bipyramidal species is d_{z^2}. Whereas, in most five coordinate copper(II) complexes it varies between these two orbitals. This is due to different structural disposition of five-coordinate copper(II) species between square-pyramidal and trigonal-bipyramidal. Few higher than six-coordinated copper(II) complexes are also reported in the literature.[7–11] Seven-coordinate complexes are mostly pentagonal bipyramidal with a few hexagonal pyramidal species.[7–9] Some heterometallic halogen clusters and bi-caped complexes with borane or carborane have been reported where higher than even seven coordination of copper(II) is present.[10,11] In higher coordinated copper(II) complexes $d_{x^2-y^2}$ will be serving as the magnetic orbital, however, the energy gap between $d_{x^2-y^2}$ and d_{z^2} will be less compared to that in lower coordinated structures.[12]

1.1.2. Copper(II) in biology

Copper is an abundant trace metal in biological systems and is often found as a co-factor in proteins, spanning over a wide range of functions.[2] Copper is found more in brain and heart than any where else except in liver, where it is stored as copper thionein and released in the form of a complex with serum albumin.[13] High metabolic

rate of brain and heart requires relatively large amount of copper metalloenzymes such as, tyrosinase, cytochrome *c* oxidase, dopamine-β-hydroxylase, monamine oxidases and Cu-Zn superoxide dismutase. Copper containing proteins can be found in electron transfer processes and in fibrinolytic pathways (e.g., cytochrome *c* oxidase, Cu/Zn superoxide dismutase).[2,13] Copper as well as other metals in biological systems are usually directly associated with the protein residues and using protein engineering, much can be learned about these systems in terms of properties, structure, function and their interplay.[14–16] In most biological systems copper is bound to protein through imidazole imine nitrogen atom of histidine moiety or amide oxygen of the amino acid.[17,18] Copper proteins can be divided in two categories, proteins that help catalytic processes and the electron transfer proteins. But here we will discuss them according to their structural point of view. Copper containing proteins according to the coordination geometry around the copper centre can be classify into three classes as described below.[19,20]

(i) Type I (Blue copper protein)

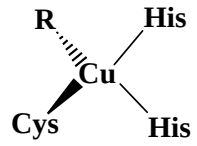

R = S_{Met} (azurin, plastocyanin, laccase)
R = O_{Glu} (phytocyanins)
R = H_2O (ceruloplasmin)

$Cu(N_{His})_2S_{Cys}R$

In blue copper proteins, copper center is coordinated to two histidine nitrogen atoms and one cystine sulphur atom. The fourth coordination site is satisfied by the sulphur atom from methionine (azurin, plastocyanin, laccase), or oxygen atom from glutamine (phytocyanins) or the water molecule (ceruloplasmin).[21,22]

(ii) Type II (Non-blue copper protein)

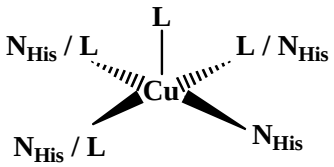

L = O or S ligands

$Cu(N_{His})_mL_n$ (m = 1 to 4; n = 0 to 3; m+n = 4 or 5)

Although these proteins are monomeric and similar to the Type I, but they do not possess the beautiful blue colour.[23] The copper center is coordinated to nitrogen atom from histidine and sulphur atom from methionine and/or the oxygen atom of the carboxylate group. The main proteins in this group are non-blue oxidases (amine, diamine, galactose and lysyl oxidase), nitrite reductase, dioxygenase, monooxygenase and Cu-Zn–superoxide dismutase.[24–26] These proteins are mainly known for their catalytic activities.

(iii) Type III (Dimeric copper protein)

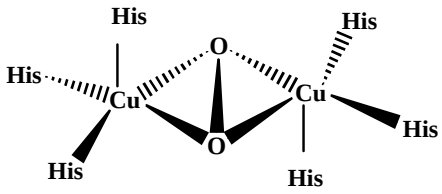

$[Cu_2(\mu\text{-}O_2)(N_{His})_6]$

In this type of proteins, metal centers form a dinuclear $\mu\text{-}\eta^2\text{:}\eta^2$ peroxo copper active site, which is generated from the reduction of molecular oxygen. These are mainly found in haemocyanins,[27] and also in tyrosinase[28] and catechol oxidase.[29]

The most important copper protein cytochrome *c* oxidase, has slightly different structural feature than the above mentioned types with two kinds of copper sites. While one of the copper centre (Cu_A) resembles the Type III but bridged by cystine sulphur instead of oxygen atom, the other copper site (Cu_B) is terminally bridged with *haem* iron through reduced dioxygen. *Haem*/copper oxidases (Cu_B) catalyse the four electron reduction of dioxygen to water, which is coupled to the generation of a proton electrochemical gradient across the membranes in which they are embedded.[30,31] Another important copper protein is superoxide dismutase, universally known as CuZnSOD,[32] where the copper center is distorted square pyramidal (falls in the Type II category) with four histidine nitrogen atoms and a water molecule in the coordination sphere. One of the imidazole moiety serves as the bridging group between the copper and zinc centers.[33]

It is evident that copper containing proteins are essential in the electron transfer and catalytic oxidase processes of several biological systems. Therefore, copper

complexes with different ligand systems or with peptides can serve as drugs for several diseases caused due to deficiency of copper.[34] Copper has an esteemed place in medical biochemistry, although until recently it has been restricted predominantly to organic drugs. Several research has been done in the area of chemotherapeutic use of copper(II) chemistry, which has led to the developments in anti cell growth, infection control, antibacterial activity and anti-inflammatory drugs.[35,36] For the rheumatoid and other degenerative diseases the commercially used drugs such as Dicuprene, Alcuprin, Cuprimyl, and Permalon are copper-salicylate preparation.[37] Copper ascorbate has strong anti-viral properties.[38] Copper peptide complexes have been used for several skin diseases and to protect hair loss. Even simple copper salts such as copper sulfate solution has found its use in promoting normal cardiovascular health and blood circulation, the formation and maintenance of strong bone mass, the inhibition of free radicals, and proper cell replication. Copper salts are also used for the production of collagen and elastin, the proteins responsible for keeping blood vessels, skin and connective tissues supple and elastic.[39] Even the copper arm bands are well known to reduce arthritis. However, the overdose of copper can lead to the toxic effects such as zinc deficiency, over-stimulation, psychosis and liver damage.

1.2. The molecular assembly

Molecular chemistry has provided a very powerful arsenal of procedures for the construction of a wide range of sophisticated molecules and materials from atoms linked by covalent bonds.[40] Beyond the regime of molecular chemistry based on covalent bonds, there lies the field of supramolecular chemistry whose aim is to develop highly complex chemical systems from components interacting via strong covalent bonds or non-covalent intermolecular forces.[41] By the appropriate manipulation of these interactions, supramolecular chemistry has progressively become the chemistry of molecular information, which involves the storage of information at the molecular level and in the structural features, its retrieval, transfer, and processing at the supramolecular level through molecular recognition processes operating via specific interactional algorithms.[42] This has paved the way towards apprehending chemistry as also an information science. A step beyond preorganization, consists of the design of systems capable of spontaneously generating well-defined supramolecular architectures by self-assembly from their

components.[43] They have been implemented for the generation of a variety of discrete functional architectures of either organic or inorganic nature.[44] Self-organization processes also give access to advanced supramolecular materials, such as supramolecular polymers and liquid crystals, and provide an original approach to nanoscience and nanotechnology. The energy range of these interactions beyond the self-organization is intermediate between van der Waals interactions and covalent bonds, which allows self-organization by selection as well as by design at both the molecular and supramolecular levels.

1.2.1. Non-covalent interaction in coordination complexes

During most of the 20th century, chemists have been concerned with making and breaking of strong chemical bonds. With the growth of molecular biology, asymmetric catalysis, supramolecular chemistry and crystal engineering, chemistry is now focused on weak interactions.[41,45,46] The study of supramolecular chemistry provides an understanding of how molecular recognition and self-assembly occur in biology and imparts characteristic properties in materials science.[47] The biological phenomena such as immune response, enzyme catalysis, drug activity and ion channel gating all rely on molecular recognition. Supramolecular systems can also act as nano-scale devices such as molecular switches and machines. An important synthetic strategy employed in metallo-supramolecular chemistry utilizes ligands that can coordinate to a metal ion through primary coordination sites, while at the same time participating in additional bonding interactions through peripheral sites. These supplementary sites may propagate secondary connections via strong hydrogen bonding through the peripheral functional groups or with guest molecules. The weak hydrogen bonding such as C–H···X (X = O, N, halogen), halogen-halogen interaction, sulphur-sulphur interaction and stacking interaction also play important roles in the recognition, magnetic and electronic processes.[48] In the following subsections, the importance of non-covalent interactions in the biological and materials science with a particular reference to copper(II) species have been discussed.

1.2.1.1. In bioinorganic chemistry

Transition metal complexes with potential biological activity are being investigated more frequently than ever before.[49,50] The ternary copper(II) complexes

with distorted square-planar or square-pyramidal geometry are mostly studied for their oxidase and strong cytotoxic properties.[39,51] It has been found that these complexes are far more active than their corresponding organic counter parts. Like all the metalloproteins, the biological activities of the copper proteins are also controlled by the non-covalent interactions between the organic moieties. Among the non-covalent interactions hydrogen bonding[52,53] and stacking interactions[54] are especially common. These interactions are most useful tools for stabilizing the ternary structure of protein, reactivity of the metalloenzymes, the recognition process and nucleic acid chemistry.[55–57] Recognition through non-covalent bonding is the main aim for the production of drug molecules in the pharmaceutical companies.

Furthermore, great deal of research has been done on proper designing of transition metal complexes, which can selectively cleave the nucleic acid chain in DNA or RNA.[58] Since Sigman and coworkers[59,60] have shown the DNA binding ability and chemotherapeutic activity of the copper complexes of 1,10-phenanthroline, a huge number of papers have been published on the use of copper complexes as DNA binding and cleaving agent. In this context, various kinds of ligands have been used, however, the extended heterocyclic rings have received the priority due to their strong binding ability through staking interactions.[61,62] During the last few years, another importance of copper(II) complexes as DNA cleaving agent has been identified, which has its use in photodynamic therapy (PDT).[63] In this process, the near infrared absorption due to the d-d transition of the copper(II) ion has been utilized for the excitation of the drug molecules. The weakly coordinated water molecule has also been used for the hydrolytic cleavage of DNA.[64]

1.2.1.2. In catalysis

The control of reaction rates and equilibria is central to modern chemical sciences. To realize this, a wide variety of sophisticated reagents, catalysts and methodologies have been developed. However, in developing these tools and in discussing the factors governing rates and equilibria, the enthalpic contribution has traditionally been more or over emphasized as far as the “strong interactions” making covalent or ionic bonds are concerned, whilst the entropic contribution has not been explicitly or extensively considered in general to play a crucial role. In contrast, living organisms employ a more smart strategy, controlling biological reactions and

equilibria not only by enthalpy, but also through entropy factors. In the recent years, chemists have demonstrated that the entropy related factors and therefore the "weak interactions" indeed play the decisive roles particularly in catalysis and photochemical processes.[65,66] Consolidating the knowledge, experience and research potentials of photochemistry, thermodynamics, bioinorganic chemistry, supramolecular chemistry and other relevant areas of research, a novel multidisciplinary region of science, i.e. "Entropy Control" is being developed in recent times.[66]

1.2.1.3. In materials science

Non-covalent interactions such as hydrogen bonding, cation–π and π–π interactions are well know tools to generate new metal-organic hybrid materials for their use as magnetic, semiconducting, optical and logic device materials. Intermolecular spin exchange interaction through hydrogen bonding and stacking interactions has been well documented in several cases.[67] For the case of cooper(II) complexes, the resulting antiferro- or ferromagnetic coupling depends upon the approach of hydrogen bonding or cation–π interactions along the equatorial or the axial site.[68] Whereas the mode of spin coupling through stacking interaction predominantly depends upon the coordination geometry of the metal ion and part of the organic moiety involved in the π–π interaction.[69] Weak interactions are found to be responsible for the appropriate orientation of the molecule to generate non-centrosymmetric solid useful as potential second order NLO material in several cases.[70] It has been also found that π–stacked molecular assembly plays an essential role in semiconducting materials such as the pentacene type organic semiconductors.[71] In this regard, the neutral transition metal complexes of extended tetrathiafulvalene (TTF) ditholate ligands are extensively studied.[72]

1.2.2. Ternary copper(II) species

The ternary square-planar complexes of copper(II) are of considerable interest for their structural, magnetic, electron transfer and catalytic properties and as models for some metalloenzymes containing copper in the active sites.[73,74] Such copper(II) complexes are also effective to hydrolyze the inactive peptide bond in several proteins and phosphoester back bone of DNA.[75–78] It is known that π–π interactions

stabilize the tertiary structure of proteins, control the reactivity of the metalloenzymes and dictate the molecular recognition process and also play important role in nucleic acid chemistry.[53−55,79,80] Ternary complexes have been used to model the active site structures and catalytic properties of several *type-II* copper proteins.[81,82] Sigel *et al.* have studied the stacking interactions of the aromatic rings in ternary complexes. Such weak interactions have profound influence on the structure and function of these complexes.[83,84] In this context it is worth to study the recognition motifs of ternary copper(II) complexes with ligands containing amide functionality.

1.2.3. Coordination polymeric structures

The development of rational synthetic routes to novel supramolecular architectures, like molecular boxes, catenanes, rotaxanes, knots and helicates, as well as new two- and three-dimensional frameworks has recently been pursued in inorganic and coordination chemistry.[85,86] These metal containing materials are not only interesting for their new topologies,[87] but also have many potential applications in electrical conductivity,[88] nonlinear optical properties,[89] magnetism,[90] host-guest chemistry,[91] ion-exchange[92] and catalysis.[93] Over the past fifty years, research on porous materials has resulted in a number of applications, which have made a direct impact on domestic life and large scale industrial processes. The basic concepts in coordination polymer chemistry are the use of metal centres with different selected coordination geometries and suitable spacer ligands. Zeolite-like polymeric species have been prepared, that are tailored or functionalized for molecular selectivity or catalytic applications.[94−97]

Development in the crystal engineering of coordination polymers require further information on:

(i) new topological types, to be related to the nature of the metal centres, the dimensions and conformational flexibilities of the ligands, the dimensions and donor properties of the counter-ions and the presence of guest molecules;
(ii) the effect of supramolecular interactions (hydrogen bonding, π–stacking, and others);
(iii) the effects of interdigitation (complementary molecular shapes and steric requirements); and
(iv) the degree of interpenetration and its control.

Polycarboxylate ligands play an important role in designing polynuclear metal complexes with interesting properties. They usually adopt binding modes as diverse as terminal monodentate, chelating to one metal center, bridging bidentate in a *syn–syn*, *syn–anti*, and *anti–anti* configuration to two metal centers, and bridging tridentate to two metal centers.[98,99] On the other hand, the rigid rod-like spacer molecules 4,4'-bipyridine (bpy) and pyrazine (pz) have been found useful building blocks for the construction of various types of metal-organic coordination frameworks.[100,101]

1.3. Motivation behind the thesis

A large number of small molecular units with various functional groups as coordination sites have been synthesized and studied for mimicking various biological activities and their potential use in the materials science. Still, there is a lack of proper structural study with combined variation of ligand conformational flexibility, position of the peripheral functional group and the nature and the position of the substitutent on the ligands. This prompted us to undertake the study of coordination complexes with the aim of detailed structural analysis by varying each of the above mentioned factors. We have chosen the ternary copper(II) complexes with (i) tridentate Schiff bases derived from aroylhydrazine and acetylacetone or salicyladehyde and different aza-heterocyclic bases as the ancillary ligand, (ii) tridentate Schiff bases 2-N-(picolinylidene)phenol having methyl substitution at different positions of the phenolate ring and halide as the ancillary ligand to investigate various non-covalent interactions and the resulting supramolecular structures.

The polymeric coordination compounds with mixed bridging ligands are of particular interest for their use in various fields of science. The conformationally flexible dicarboxylate ligands are excellent bridging groups to design various topological solids with the use of proper metal ions and co-bridging ligands. The remarkable coordination abilities of succinate ligands and of rigid planar bidentate diimines have prompted us to design and synthesize new microporous polymeric copper(II) coordination compounds containing both these ligands.

References

1 Hathaway, B. J. Copper, In *Comprehensive Coordination Chemistry*; Pergamon Press: Oxford, U.K., 1987; Vol. 5, pp 533-774.

2 Addison, A. W. In *Copper Coordination Chemistry: Biochemical and Inorganic Perspectives*; Karlin, K. D.; Zubieta, J., Eds; Adenine Press: New York, 1983.

3 Solomon, E. I.; Baldwin, M. J.; Lowery, M. D. *Chem. Rev.* **1992**, *92*, 521.

4 Mitchell, P. R.; Parish, R. V. *J. Chem. Educ*. **1969**, *46*, 811.

5 Adiison, A. W.; Rao, T. N.; Reedijk, J.; Van Rijn, J.; Verschoor, G. C. *J. Chem. Soc., Dalton Trans.* **1984**, 1449.

6 Addison, A. W.; Rao, T. N.; Sinn, E. *Inorg. Chem.* **1984**, *23*, 1957.

7 Drew, M. G. B.; Nelson, J.; Nelson, S. M. *J. Chem. Soc., Dalton Trans.* **1981**, 1685.

8 Marquez, V. E.; Anacona, J. R.; Lorono, D. *Polyhedron* **2004**, *23*, 1317.

9 Eichhofer, A.; Fenske, D.; Holstein, W. *Angew. Chem., Int. Ed.* **1993**, *32*, 242.

10 Strotmeyer, K. P.; Fritsky, I. O.; Ott, R.; Pritzkow, H.; Kramer, R. *Supramol. Chem.* **2003**, *15*, 529.

11 Wing, R. M. *J. Am. Chem. Soc.* **1968**, *90*, 4828.

12 Kahn, O. *Angew. Chem., Int. Ed.* **1985**, *24*, 834.

13 Sarkar, B.; Kruck, T. P. A. *Biochemistry of Copper*; Academic Press: New York, 1966; p 183.

14 Bertini, I.; Messori, L.; Viezzoli, M. S. In *Handbook of Metal-Ligand Interactions in Biological Fluids: Bioinorganic Chemistry*; Berthon, G., Ed.; Marcel Dekker: New York, 1995; Vol. 1, pp 156-174.

15 Sarkar, B. *Chem. Rev.* **1999**, *99*, 2535.

16 Sorenson, J. R. J. In *Handbook of Metal-Ligand Interactions in Biological Fluids: Bioinorganic Medicine*; Berthon, G., Ed.; Marcel Dekker: New York, 1995; Vol. 2, pp 1128.

17 Holm, R. H.; Kennepohl, P.; Solomon, E. I. *Chem. Rev.* **1996**, *96*, 2239.

18 Aronoff-Spencer, E.; Burns, C. S.; Avdievich, N. I.; Gerfen, G. J.; Peisach, J.; Antholine, W. E.; Ball, H. L.; Cohen, F. E.; Prusiner, S. B.; Millhauser, G. L. *Biochemistry* **2000**, *39*, 13760.

19 Abolmaali, B.; Taylor, H. V.; Weser, U. *Structure and Bonding* **1998**, *91*, 91.

20 Adman, E. T. *Adv. Protein Chem.* **1991**, *42*, 145.

21 Andrew, C. R.; SandersLoehr, J. *Acc. Chem. Res.* **1996**, *29*, 365.

22 Canters, G. W.; Gilardi, G. *FEBS Lett.* **1993**, *325*, 39.

23 Sigel, H.; Song, B. *Met. Ions Biol. Syst.* **1996**, *32*, 135.

24 Ettinger, M. J. *Biochemistry* **1974**, *13*, 1242.
25 Averill, B. A. *Chem. Rev.* **1996**, *96*, 2951.
26 Bannister, J. V.; Bannister, W. H.; Rotilio, G. *CRC Crit. Rev. Biochem.* **1987**, *22*, 111.
27 Ellerton, H. D.; Ellerton, N. F.; Robinson, H. A. *Prog. Biophys. Mol. Biol.* **1983**, *41*, 143.
28 Fontecave, M.; Eklund, H. *Structure* **1995**, *3*, 1127.
29 Lerch, K.; Germann, U. A. *Prog. Clin. Biol. Res.* **1988**, *274*, 331.
30 FergusonMiller, S.; Babcock, G. T. *Chem. Rev.* **1996**, *96*, 2889.
31 Farver, O.; Pecht, I. In *Copper Proteins*; Spiro, T. G., Eds.; Wiley, New York, 1981; pp. 151-192.
32 Fridovich, I. *Adv. Exp. Med. Biol.* **1976**, *74*, 530.
33 Bannister, W. H.; Bannister, J. V.; Barra, D.; Bond, J.; Bossa, F. *Free Radic. Res. Commun.* **1991**, *12-13*, 349.
34 Sarkar, B. *Handbook on Metals in Clinical and Analytical Chemistry*; Marcel Dekker: New York, 1995; p 339.
35 Milanino, R.; Conforti, A.; Franco, L.; Marrella, M.; Velo, G. *Agents & Actions* **1985**, *16*, 504.
36 Lewis, A. J. *Agents & Actions* **1984**, *15*, 513.
37 Sorenson, J. R. J.; Hangarter, W. *Inflammation* **1977**, *2*, 217.
38 Reinhammar, B.; Aasa, R.; Vänngard, T.; Maritano, S.; Marchesini, A. *Biochim. Biophys. Acta Protein Struc. Mol. Enzym.* **1997**, *1337,* 191.
39 DiSilvestro, R. A.; Marten, J.; Skehan, M. *J. Am. Coll. Nutr.* **1992**, *11*, 177.
40 Pauling, L. *The nature of the chemical bond*; Cornell University Press: Ithaca, New York, 1939.
41 Lehn, J.-M. *Supramolecular Chemistry: Concepts and Perspectives*; VCH, Weinheim, 1995.
42 Lehn, J.-M. *Angew. Chem., Int. Ed.* **1990**, *29*, 1304.
43 Lehn, J.-M. *Angew. Chem., Int. Ed.* **1988**, *27*, 89.
44 Wells, A. F. *Further Studies of Three-Dimensional Nets*; American Crystallographic Association, New York, 1979.
45 Dunitz, J. D. *The Crystal as a Supramolecular Entity, Perspectives in Supramolecular Chemistry*; Desiraju, G. R., Eds; Wiley, Chichester, 1995; Vol. 2, pp. 1-30.
46 Desiraju, G. R. *Curr. Opin. Sol. Stat. Mat. Sci*. **1997**, *2*, 451.
47 Bond, A. D.; Jones, W. In *Supramolecular Organization and Materials Design*; Jones, W., Rao, C. N. R., Eds.; Cambridge University Press: Cambridge, 2002.

48 Desiraju, G. R.; Steiner, T. *The Weak Hydrogen Bond In Structural Chemistry and Biology*; Oxford University Press: Oxford, 1999.
49 Lovejoy, D. B.; Richardson, D. R. *Curr. Med. Chem.* **2003**, *10*, 1035.
50 Buss, J. L.; Torti, F. M.; Torti, S. V. *Curr. Med. Chem.* **2003**, *10*, 1021.
51 Klinman, J. P. *Chem. Rev*. **1996**, *96*, 2541.
52 Sabat, M.; Lippert, B. *Met. Ions Biol. Syst*. **1996**, *33*, 143.
53 Sigel, A.; Sigel, H. *Metal Ions in Biological Systems*; Dekker, New York, 1996.
54 Yamauchi, O.; Odani, A.; Masuda, H.; Sigel, H. *Met. Ions Biol. Syst*. **1996**, *32*, 207.
55 Hunter, C. A.; Sanders, J. K. M. *J. Am. Chem. Soc.* **1990**, *112*, 5525.
56 Pyle, A. M.; Barton, J. K. *Prog. Inorg. Chem*. **1990**, *38*, 413.
57 Sigman, D. S.; Bruise, T. W.; Mazumdar, A.; Sutton, C. L. *Acc. Chem. Res*. **1993**, *26*, 98.
58 Erkkila, K. E.; Odom, D. T.; Barton, J. K. *Chem. Rev*. **1999**, *99*, 2777.
59 Sigman, D. S. *Acc. Chem. Res*. **1986**, *19*, 180.
60 Sigman, D. S.; Mazumder, A.; Perrin, D. M. *Chem. Rev*. **1993**, *93*, 2295.
61 Patra, A. K.; Dhar, S.; Nethaji, M.; Chakravarty, A. R. *Chem. Commun*. **2003**, 1562.
62 Patra, A. K.; Dhar, S.; Nethaji, M.; Chakravarty, A. R. *J. Chem. Soc., Dalton Trans.* **2005**, 896.
63 Dhar, S.; Senapati, D.; Reddy, P. A. N.; Das, P. K.; Chakravarty, A. R. *Chem. Commun*. **2003**, 2452.
64 Dhar, S.; Reddy, P. A. N.; Chakravarty, A. R. *J. Chem. Soc., Dalton Trans.* **2004**, 697.
65 Inoue, Y.; Sugahara, N.; Wada, T. *Pure Appl. Chem*. **2001**, *73*, 475.
66 Griesbeck, A. G.; Meierhenrich, U. J. *Angew. Chem., Int. Ed.* **2002**, *41*, 3147.
67 Li, L.-L.; Lin, K.-J.; Ho, C.-J.; Sun, C.-P.; Yang, H.-D. *Chem. Commun*. **2006**, 1286.
68 Desplanches, C.; Ruiz, E.; Rodriguez-Fortea, A.; Alvarez, S. *J. Am. Chem. Soc.* **2002**, *124*, 5197.
69 Huang, L. W.; Yang, C. J.; Lin, K. J. *Chem. Eur. J.* **2002**, *8*, 396.
70 Prakash, M. J.; Radhakrishnan, T. P. *Cryst. Growth Des.* **2005**, *5*, 721.
71 Ohta, H.; Kambayashi, T.; Nomura, K.; Hirano, M.; Ishikawa, K.; Takezoe, H.; Hosono, H. *Adv. Mater.* **2004**, *16*, 312.
72 Tanaka, H.; Kobayashi, H.; Kobayashi, A. *J. Am. Chem. Soc.* **2002**, *124*, 10002.

73 Fenton, D. E. *Advances in inorganic and bio-organic mechanisms*; Sykes, A. G., Eds.; Academic Press: London, 1983, vol. 2; pp. 187.

74 Fenton, D. E. *Metal clusters in proteins*; Que Jr., L., Eds.; ACS: Washington, DC, 1988.

75 Polzin, G. M.; Burstyn, J. N. *Metal Ions in Biological Systems*; Marcel Dekker: New York, 2001; pp 104-143.

76 Hegg, E. L.; Burstyn, J. N. *Coord. Chem. Rev.* **1998**, *173*, 133.

77 Hegg, E. L.; Burstyn, J. N. *J. Am. Chem. Soc.* **1995**, *117*, 7015.

78 Gallagher, J.; Zelenko, O.; Walts, A. D.; Sigman, D. S. *Biochemistry* **1998**, *37*, 2096.

79 Ito, N.; Philips, S. E. V.; Stevens, C.; Ogel, Z. B.; McPherson, M. J.; Keen, J. N.; Yadav, K. D. S.; Knowles, P. F. *Nature* **1991**, *350*, 87.

80 Yamauchi, O.; Odani, A.; Takani, M. *J. Chem. Soc., Dalton Trans.* **2002**, 3411.

81 Sigel, H.; Tribolet, R.; Yamauchi, O. *Comments Inorg. Chem.* **1990**, *9*, 305.

82 Sigel, H. *Angew. Chem. Int. Ed. Engl.* **1975**, *14*, 394.

83 Sigel, H. *Pure Appl. Chem.* **1989**, *61*, 923.

84 Sigel, H. *Angew. Chem. Int. Ed. Engl.* **1982**, *21*, 389.

85 Leininger, S.; Olenyuk, B.; Stang, P. J. *Chem. Rev*. **2000**, *100*, 853.

86 Moulton, B.; Zaworotko, M. J. *Chem. Rev*. **2001**, *101*, 1629.

87 Carlucci, L.; Ciani, G.; Proserpio, D. M. *Coord. Chem. Rev*. **2003**, *246*, 247.

88 Liu, S. Q.; Kuroda-Sowa, T.; Konaka, H.; Suenaga, Y.; Maekawa, M.; Mizutani, T.; Ning, G. L.; Munakata, M. *Inorg. Chem*. **2005**, *44*, 1031.

89 Evans, O. R.; Lin, W. *Acc. Chem. Res*. **2002**, *35*, 511.

90 Liu, T.-F.; Sun, H.-L.; Gao, S.; Zhang, S.-W.; Lau, T.-C. *Inorg. Chem*. **2003**, *42*, 4792.

91 Yaghi, O.; O'Keeffe, M.; Ockwig, N. W.; Chae, H. K.; Eddaoudi, M.; Kim, J. *Nature* **2003**, *423*, 705.

92 Manos, M. J.; Iyer, R. G.; Quarez, E.; Liao, J. H.; Kanatzidis, M. G. *Angew. Chem., Int. Ed.* **2005**, *44*, 3552.

93 Seidel, S. R.; Stang, P. J. *Acc. Chem. Res.* **2002**, *35*, 224.

94 Rosi, N. L.; Eckert, J.; Eddaoudi, M.; Vodak, D. T.; O'Keeffe, M.; Yaghi, O. M. *Science* **2003**, *300*, 1127.

95 Kitagawa, S.; Uemura, K. *Chem. Soc. Rev.* **2005**, *34*, 109.

96 Hu, A. G.; Ngo, H. L.; Lin, W. B. *Angew. Chem., Int. Ed.* **2004**, *43*, 2501.

97 Yoshizawa, M.; Tamura, M.; Fujita, M. *J. Am. Chem. Soc.* **2004**, *126*, 6846.

98 Policar, C.; Lambert, F.; Cesario, M.; Morgenstern-Badarau, I. *Eur. J. Inorg. Chem.* **1999**, 2201.

99 Levstein, P. R.; Calvo, R. *Inorg. Chem.* **1990**, *29*, 1581.

100 Lloret, F.; De Munno, G.; Julve, M.; Cano, J.; Ruiz, R.; Caneschi, A. *Angew. Chem., Int. Ed.* **1998**, *37*, 135.

101 Tong, M. L.; Ye, B. I.; Cai, J. W.; Chen, X. M.; Ng, S. W. *Inorg. Chem.* **1998**, *37*, 2645.

Chapter 2

Stacked one-dimensional assembly of a ternary square-planar copper(II) complex[§]

This chapter describes the synthesis, characterization and physical properties of a mixed-ligand copper(II) complex, [Cu(bhac)(dmpz)] (**1**), with a tridentate Schiff base, acetylacetone benzoylhydrazone (H_2bhac) and a monodentate heterocycle, 3,5-dimethylpyrazole (dmpz). The molecular structure of the complex has been determined by X-ray crystallography. In **1** the metal centre is in square-planar N_2O_2 coordination environment. The whole molecule is essentially planar, barring a small variation in the orientation of the dmpz plane with respect to the {Cu(bhac)} plane. In the solid state, two types of π-π interactions on two sides of [Cu(bhac)(dmpz)] molecule lead to a one-dimensional arrangement of the complex molecules with sequential short [3.5952(8) Å] and long [5.5960(12) Å] Cu···Cu distances. Solid state as well as frozen solution EPR spectral measurements reveal an antiferromagnetically coupled dicopper(II) system and indicate a magnetic exchange interaction mediated by π-π interaction. Magnetic susceptibility data in the temperature range of 10–300 K are consistent with this observation. The magnitude of the coupling constant *J*, obtained by least-squares fitting of the data using the Bleany–Bowers expression, is −6.0 (1) cm^{-1}.

2.1. Introduction

Among various non-covalent intermolecular interactions π-π interaction plays crucial roles in determining the supramolecular structural motifs as well as the physical properties of the resulting solid. Complex molecules containing ligands with aromatic fragments or chelate rings having sufficient π–delocalization can participate in intermolecular π–π interactions and form various stacked structural modes.[1–3]

[§] This work has been published in *New J. Chem*, **2003**, *27*, 1102-1107.

Herein, we report the synthesis and X-ray structure of a square-planar ternary copper(II) complex with dianionic O,N,O-donor deprotonated acetylacetone benzoylhydrazone (H_2bhac) and the monodenate neutral N-donor 3,5-dimethylpyrazole (dmpz) (Figure 2.1). The mononuclear complex, [Cu(bhac)(dmpz)] (**1**), forms a one-dimensional chain *via* intermolecular π-π interactions involving metallated chelate rings of the tridentate ligand and the dmpz moiety with successive long and short Cu···Cu distances. EPR and cryomagnetic studies reveal an antiferromagnetic metal ion spin-coupling.

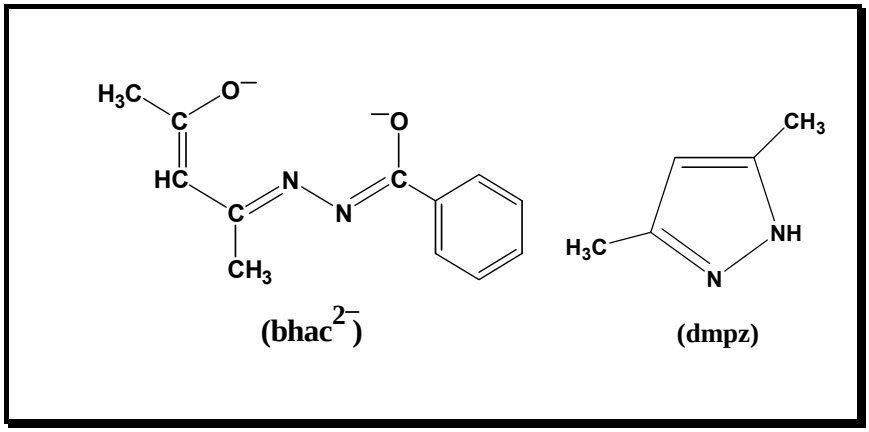

Figure 2.1.

2.2. Experimental section

2.2.1. Materials

The Schiff base, H_2bhac, was prepared by the condensation of one mole equivalent of acetylacetone with one mole equivalent of benzoylhydrazine in boiling methanol. Yield obtained was 85 %. All other chemicals and solvents used in this work were of analytical grade available commercially and were used without further purification.

2.2.2. Physical measurements

Microanalytical (C, H, N) data were obtained with a Perkin Elmer Model 240C elemental analyzer. The infrared spectrum was recorded by using a KBr pellet on a Jasco-5300 FT-IR spectrophotometer. Solution electrical conductivity was measured with a Digisun DI-909 conductivity meter. A Shimadzu 3101-PC UV/vis/NIR spectrophotometer was used to record the electronic spectrum. A CH-Instruments model 620A electrochemical analyzer was used for the cyclic voltammetric experiments with a chloroform solution of the complex containing tetrabutylammonium perchlorate (TBAP) as supporting electrolyte. The three electrode measurements were carried out at 298 K under a dinitrogen atmosphere with a platinum disk working electrode, a platinum wire auxiliary electrode and a saturated calomel reference electrode (SCE). Under identical conditions the $E_{1/2}$ value of Fc^+/Fc (Fc, ferrocene) couple was 0.48 V. The potentials reported in this work are uncorrected for junction contributions. The X-ray powder diffraction pattern was collected on a Philips PW-3710 diffractometer using Cu Kα radiation (λ = 1.54184 Å). The EPR spectra were recorded on a Jeol JES-FA200 spectrometer. The variable temperature (10−300 K) magnetic susceptibility measurements were performed using the Faraday technique with a set-up comprising a George Associates Lewis coil force magnetometer, a CAHN microbalance and an Air Products cryostat. $Hg[Co(NCS)_4]$ was used as the standard. A diamagnetic correction (-155×10^{-6} emu mol^{-1} for [Cu(bhac)(dmpz)] (**1**)) calculated from Pascal's constants,[4] was used to obtain the molar paramagnetic susceptibilities.

2.2.3. Synthesis

[Cu(bhac)(dmpz)] (1)

A dry ethanol solution (15 mL) of $Cu(O_2CCH_3).2H_2O$ (199 mg, 1 mmol) was added to another dry ethanol solution (20 mL) of H_2bhac (261 mg, 1.2 mmol) and 3,5-dimethylpyrazole (dmpz) (96 mg, 1 mmol). The resulting green mixture was stirred at room temperature for 2 h. The mixture was then evaporated on a steam bath to 1/4 of the original volume and slowly cooled to room temperature. The brown needles deposited were collected by filtration and dried in air. Yield was 320 mg (86%). A single crystal suitable for X-ray structure determination was selected from this material. Anal. calcd. for $C_{17}H_{20}N_4O_2Cu$: C, 54.32; H, 5.36; N, 14.90; found: C, 54.10; H, 5.34; N, 14.73. Selected IR bands (cm^{-1}): 3310(m), 1597(s), 1568(m), 1512(s), 1489(m), 1412(s), 1346(w), 1269(s), 1209(w), 1169(m), 1140(w), 1065(w), 1036(s), 949(m), 789(s), 766(m), 687(s), 602(m), 567(w), 474(w), 438(s), 407(w). UV/ Vis [$CHCl_3$; λ_{max}/nm (ε/dm^3 mol^{-1} cm^{-1})]: 577 (107), 373 (17 700), 360sh (16 900), 245 (20 400).

2.2.4. X-ray crystallography

A crystal of dimension 0.48×0.28×0.24 mm^3 was used for data collection on an Enraf–Nonius Mach-3 single crystal diffractometer using graphite monochromated Mo Kα radiation (λ = 0.71073 Å) by the ω-scan method at 298 K. Unit cell parameters were determined by the least-squares fit of 25 reflections having θ values in the range 9−11˚. Intensities of 3 check reflections were measured every 1.5 h during the data collection to monitor the crystal stability. No decay was observed in 28 h of exposure. The ψ-scans of 6 reflections with θ in the range 5–21˚ and χ within 80–89˚ were used for an empirical absorption correction.[5] The structure was solved by direct methods in the $P\bar{1}$ space group and refined on F^2 by full-matrix least-squares procedures. The asymmetric unit contains a single molecule of [Cu(bhac)(dmpz)]. All non-hydrogen atoms were refined using anisotropic thermal parameters. Hydrogen atoms were placed geometrically by using a riding model and included in the structure factor calculation, but not refined. Calculations were done using the programs in WinGX[6] for data reduction and absorption correction, and the

SHELX-97 programs[7] for structure solution and refinement. Ortex6a[8] and Platon98 packages[9] were used for molecular graphics.

Table 2.1. Crystallographic parameter for **[Cu(bhac)(dmpz)]** (**1**).

Chemical formula	$CuC_{17}H_{20}N_4O_2$
Formula weight	375.91
Crystal system	Triclinic
Space group	$P\bar{1}$
T/K	298
a (Å)	7.2563(13)
b (Å)	10.6168(16)
c (Å)	12.0608(19)
α (°)	103.213(12)
β (°)	103.625(14)
γ (°)	101.443(13)
2θ(°) range	3.62–49.94
V (Å^3)	847.3(2)
Z	2
μ (mm^{-1})	1.306
N-collected	2980
N-unique	2980
N [$I \geq 2\sigma(I)$]	2554
Parameters	221
*R*1,[a] *wR*2[b] [$I \geq 2\sigma(I)$]	0.0305, 0.0779
*R*1,[a] *wR*2[b] [all data]	0.0398, 0.0827
GOF[c] on F^2	1.015
Largest peak and hole (*e* Å^{-3})	0.297, –0.368

[a] $R1 = \sum||F_o| - |F_c||/\sum|F_o|$. [b] $wR2 = \{\sum[(F_o^2 - F_c^2)^2]/\sum[w(F_o^2)^2]\}^{1/2}$.

[c] $GOF = \{\sum[w(F_o^2 - F_c^2)^2]/(n - p)\}^{1/2}$ where n is the number of reflections and p is the number of parameters refined; $w = 1/[\sigma^2(F_o^2) + (aP)^2 + bP]$.

2.3. Results and discussion

2.3.1. Synthesis and characterization

In ethanolic medium, the reaction of $Cu(O_2CCH_3)_2{\cdot}2H_2O$, H_2bhac and dmpz in a 1:1:1 mole ratio affords the green complex in good yield. Elemental analysis data are satisfactory with the formula [Cu(bhac)(dmpz)]. The complex is electrically non-conducting in acetonitrile solution.

The infrared spectrum of the complex does not display the amide C=O stretch (~1675 cm^{-1})[10] expected for the free H_2bhac. Thus, in the complex the metal ion is in a +2 oxidation state and coordinated to the enolate-O, the imine-N and the deprotonated amide-O atoms of the completely deprotonated Schiff base ($bhac^{2-}$). A strong band observed at 1597 cm^{-1} is possibly associated with the C=N–N=C moiety of $bhac^{2-}$.[11] The fourth coordination site is satisfied by the imine-N of dmpz. The X-ray structure (*vide infra*) confirms such coordination of $bhac^{2-}$ and dmpz and the +2 oxidation state of the metal ion. The sharp band observed at 3310 cm^{-1} is assigned to the N–H group of dmpz.

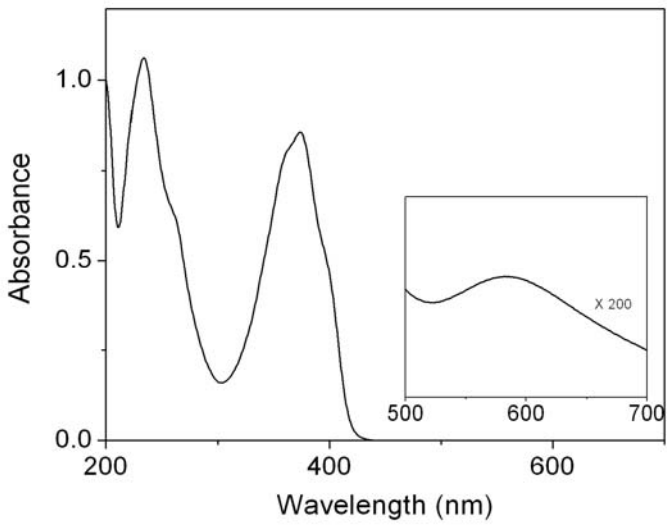

Figure 2.2. Electronic absorption spectrum of **[Cu(bhac)(dmpz)]** (**1**) in chloroform solution. Inset: Magnified d−d transition in same solution.

The electronic spectrum of the complex in chloroform solution displays a weak band at 577 nm. Absorptions in this region observed for square-planar or square-pyramidal copper(II) Schiff base complexes have been assigned to d-d transitions.[12] The intense absorptions displayed in the range of 374−245 nm are likely to be due to ligand-to-metal charge transfer and intraligand transitions (Figure 2.2).

2.3.2. Electrochemical properties

In chloroform solution, the complex is redox active. The cyclic voltammogram of the complex displays an irreversible oxidation at 0.63 V (*vs.* SCE) (Figure 2.3). On the cathodic side of SCE (up to −1.0 V) no redox response is observed. The current height of the oxidation response is comparable with known one-electron redox processes under identical conditions.[13] No such response is observed for either deprotonated $bhac^{2-}$ or dmpz under the same conditions. The iron(III) complex of $bhac^{2-}$ displays a metal-centred one-electron oxidation response at 0.4 V.[14] Thus, the oxidation observed for [Cu(bhac)(dmpz)] is assigned to a Cu(II) → Cu(III) process. The irreversible nature suggests that the corresponding oxidized species is unstable on the cyclic voltammetry time scale.

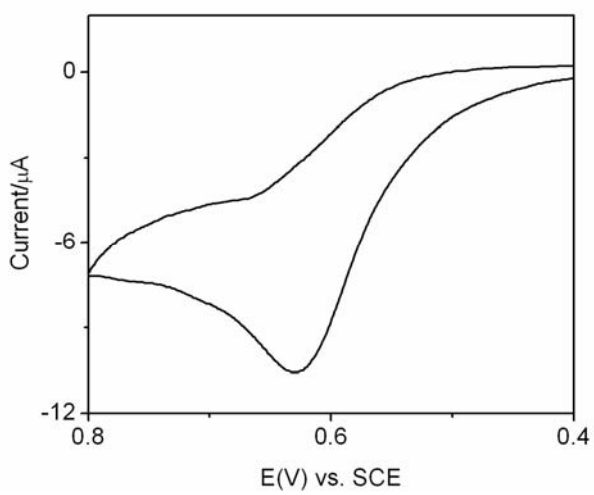

Figure 2.3. Cyclic voltammogram (scan rate 100 mVs^{-1}) of ~10^{-3} M solution of **[Cu(bhac)(dmpz)]** (**1**) in chloroform solution (0.1 M TBAP) at platinum electrode (298 K).

2.3.3. Description of molecular structure

The molecular structure of [Cu(bhac)(dmpz)] (**1)** is depicted in Figure 2.4. The bond parameters associated with the metal ion are listed in Tables 2.2 and 2.3. The copper(II) centre is in a square-planar N_2O_2 coordination environment constituted by the enolate-O, the imine-N and the deprotonated amide-O coordinating $bhac^{2-}$ and the imine-N coordinating dmpz. The N2–C6 [1.304(3) Å] and C6–O2 [1.300(3) Å] distances are consistent with the deprtonated form of the amide functionality in $bhac^{2-}$.[15] The C2–C3 [1.363(4) Å] and C2–O1 [1.300(3) Å] distances indicate the enolate form of the –HC=C(CH3)–O^- fragment of $bhac^{2-}$.[16] The chelate bite angles for the five-and six-membered rings formed by $bhac^{2-}$ are 81.66(8) and 93.75(8)°, respectively. The Cu(II)–O(amide) distance [1.9168(18) Å] is shorter than the distances [1.976(2)–2.063(2) Å] found in copper(II) complexes in which the O-coordinating amide functionality is protonated[17] and comparable with the distances [1.914(4)–1.989(5) Å] observed for complexes in which the copper(II) is coordinated to deprotonated amide-O. The Cu(II)–N(imine) distance [1.915(2) Å] is unexceptional. The Cu–O1 distance [1.9123(18) Å] is within the range reported for

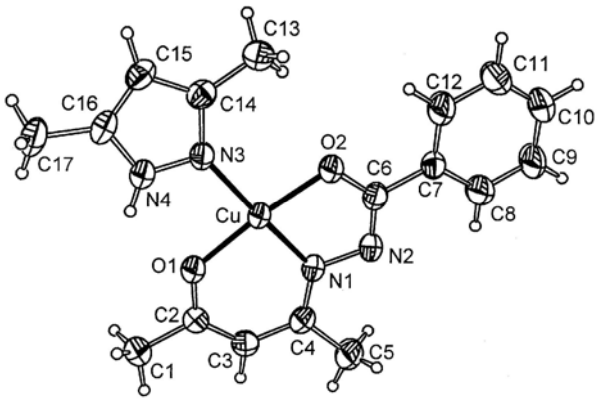

Figure 2.4. Molecular structure of **[Cu(bhac)(dmpz)]** (**1**) and the atom labeling scheme. All non-hydrogen atoms are represented by their 50% probability thermal ellipsoids.

copper (II) to enolate-O bonds.[18] The Cu–N3 distance [1.998(2) Å] is similar to the values observed for copper(II) species containing a non-bridging neutral pyrazole moiety.[19] There is no displacement of the metal ion from the N_2O_2 square-plane. The maximum and minimum deviations from the CuN_2O_2 mean plane are 0.047(1) and 0.012(1) Å for O2 and Cu, respectively. The whole {Cu(bhac)} fragment is essentially planar, barring an insignificant twisting [by 3.03(11)˚] of the phenyl ring plane (mean deviation 0.002 Å) with respect to the plane containing the rest of the atoms (Cu, O1, O2, N1, N2, C1–C6; mean deviation 0.033 Å). However, the dmpz plane (mean deviation 0.002 Å) has a deferent orientation with respect to the above mentioned plane. The dihedral angle between these two mean planes is 11.53(10)˚.

Table 2.2. Selected bond lengths (Å) for **[Cu(bhac)(dmpz)]** (**1**).

Cu-O(1)	1.912(2)	N(3)-C(14)	1.338(3)	N(3)-N(4)	1.358(3)
Cu-N(1)	1.915(2)	O(2)-C(6)	1.300(3)	N(4)-C(16)	1.333(3)
Cu-O(2)	1.916(2)	N(1)-C(4)	1.313(3)	C(2)-C(3)	1.363(4)
Cu-N(3)	1.998(2)	N(1)-N(2)	1.396(3)	C(3)-C(4)	1.422(4)
O(1)-C(2)	1.300(3)	N(2)-C(6)	1.304(3)	C(6)-C(7)	1.485(3)

Table 2.3. Selected bond angles (°) for **[Cu(bhac)(dmpz)]** (**1**).

O(1)-Cu-N(1)	93.75(8)	C(2)-O(1)-Cu	125.22(16)	C(14)-N(3)-Cu	137.1(2)
O(1)-Cu-O(2)	174.20(7)	C(6)-O(2)-Cu	110.39(16)	N(4)-N(3)-Cu	116.8(2)
N(1)-Cu-O(2)	81.66(8)	C(4)-N(1)-N(2)	117.4(2)	O(1)-C(2)-C(3)	125.3(2)
O(1)-Cu-N(3)	88.18(8)	C(4)-N(1)-Cu	127.90(17)	C(2)-C(3)-C(4)	127.4(2)
N(1)-Cu-N(3)	177.51(9)	N(2)-N(1)-Cu	114.54(15)	O(2)-C(6)-N(2)	124.4(2)
O(2)-Cu-N(3)	96.51(8)	C(6)-N(2)-N(1)	109.0(2)	N(2)-C(6)-C(7)	118.2(2)

2.3.4. Self-assembly

Very often in square-planar copper(II) complexes the metal ion is involved in weak interactions at the apical position with another atom of a neighbouring molecule, forming dimeric units or polymeric chains having equatorial-apical bridges.[12] The metal ion is also displaced towards the apical atom from the square base in these complexes. In the present complex, other than the four coordinating atoms, the nearest atom to the metal ion is the metal-coordinated pyrazole-N of another molecule and the distance separating them is 3.275(2) Å. Considering this distance, the essentially planar CuN_2O_2 fragment and the sp^2 character of the pyrazole-N already coordinated to another metal centre, any kind of weak interaction and hence dimerization or polymerization *via* equatorial-apical bridges can be ruled out. However, the [Cu(bhac)(dmpz)] (**1)** molecules form a one-dimensional assembly through π-π interactions. This one-dimensional arrangement in the crystal lattice is illustrated in Figure 2.5. Each square-planar molecule is involved in two types of π-π interactions with the two adjacent molecules. This results in alternating short and long Cu···Cu distances (Figures 2.5 and 2.6) in the chain-like arrangement of the metal ions. In the first type of interaction, the dmpz rings and the chelate rings of two molecules are involved in π-π interactions in a reciprocal manner. The Cu···Cu distance observed is 3.5952(8) Å in this dimeric unit. The interplanar distances between the five- and the six-membered chelate rings and the dmpz ring are 3.232 and 3.406 Å, respectively. The corresponding centroid-to-centroid distances are 3.555 and 3.595 Å, respectively. The pyrazole ring is not exactly parallel with either of the five- or the six-membered chelate rings. The dihedral angles are 13.72˚ and 11.49˚, respectively. In the second type of interaction, the dmpz rings of each of these dimeric units are overlapped with the dmpz rings of dimeric units on both sides and the interdimer Cu···Cu distance observed is 5.5960(12) Å (Figure 2.5). The interplanar and the centroid-to-centroid distances between the pyrazole rings are 3.356 and 3.732 Å, respectively. The dihedral angle [0.0(1)˚] between these pyrazole rings suggests that they are perfectly parallel.

There is no significant interchain interaction. Although the phenyl rings of the $bhac^{2-}$ moieties from two successive chains (Figure 2.5) are parallel [dihedral angle 0.0(1)˚] and the interplanar distance is 3.396 Å, a π-π interaction can be ruled out

considering the large (7.621 Å) centroid-to-centroid distance. The shortest C···C distance between two phenyl rings is 5.486(7) Å.

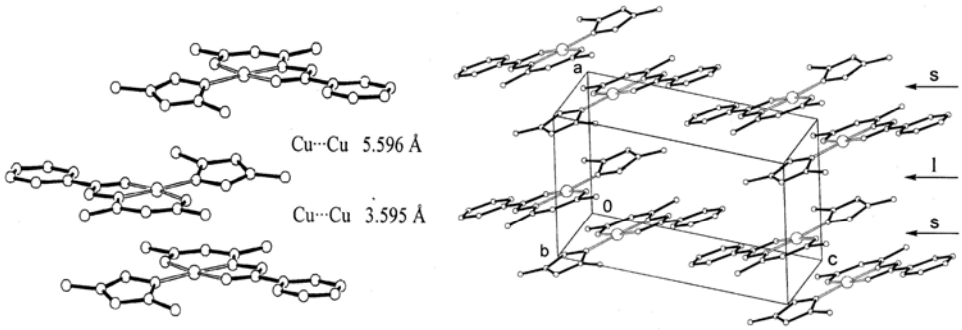

Figure 2.5. One-dimensional arrangement of π-stacked **[Cu(bhac)(dmpz)]** (**1**) molecules in the crystal lattice. The arrows indicate short (s) and long (l) Cu···Cu distances.

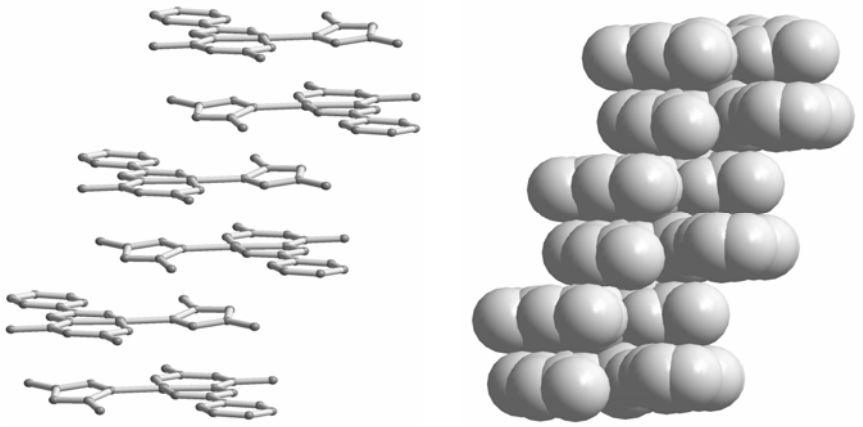

Figure 2.6. The ball-stick and space filling model of the one-dimensional arrangement of π–stacked **[Cu(bhac)(dmpz)]** (**1**) molecules in the crystal lattice.

To examine whether or not any other crystalline form of the complex exists we have collected the powder X-ray diffraction pattern of the complex and compared it with the simulated diffraction pattern generated from the unit cell and the molecular structure determined by single crystal X-ray crystallography.[20] The experimental and

simulated diffraction patterns are very similar with respect to the peak positions and the relative intensities (Figure 2.7). This similarity indicates that the complex crystallizes only in one form having a chain-like arrangement of molecules with alternating short and long Cu···Cu distances in the crystal lattice.

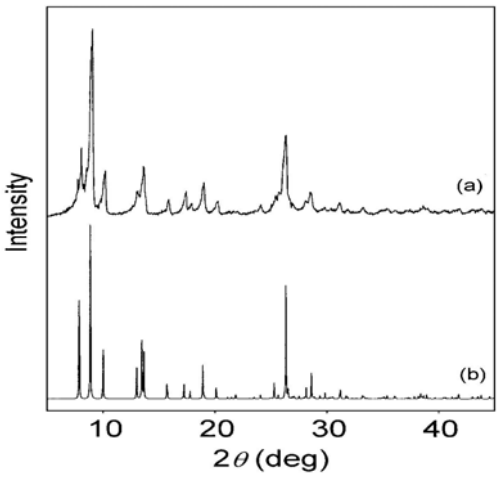

Figure 2.7. Powder X-ray diffraction pattern of **[Cu(bhac)(dmpz)]** (**1**): (a) experimental and (b) simulated.

2.3.5. Magnetic Properties

Magnetic susceptibility measurements on a powdered sample of [Cu(bhac)(dmpz)] (**1**) were performed in the temperature range of 10–300 K at a constant magnetic field of 5 kG. The effective magnetic moment (μ_{eff}) of the complex at 300 K is 1.94 μ_B. On cooling the moment gradually decreases. From 300 to 80 K the change in μ_{eff} is small. At 80 K the value of μ_{eff} is 1.87 μ_B. Below 80 K, the decrease in the value of μ_{eff} is relatively sharp, falling to 1.35 μ_B at 10 K. The nature of the curve obtained by plotting the moments against temperature (Figure 2.8) clearly indicates the antiferromagnetic behaviour of the complex. Considering the chain-like arrangement of the copper(II) centres with sequential long and short Cu···Cu distances in the solid state, we attempted to fit the data by using the alternating antiferromagnetic chain model.[21] The best least-squares[22] fit gave g = 2.207(3), J = −5.4(1) cm^{-1}, and α = 0.16(4) with a fixed TIP value of 60×10^{-6} emu

mol^{-1}, where J and J' are the antiferromagnetic coupling constants, $\alpha = J'/J$ and TIP is the temperature independent paramagnetism. Since these vaules suggest that J' is very small, the data were also fitted using the Bleany–Bowers expression.[23] The best least-squares fit was obtained with $g = 2.217(1)$, $J = 6.0(1)$ cm^{-1}, and TIP = 60×10^{-6} emu mol^{-1}. This fit is noticeably better than that obtained by using the alternating antiferromagnetic chain model (Figure 2.8).

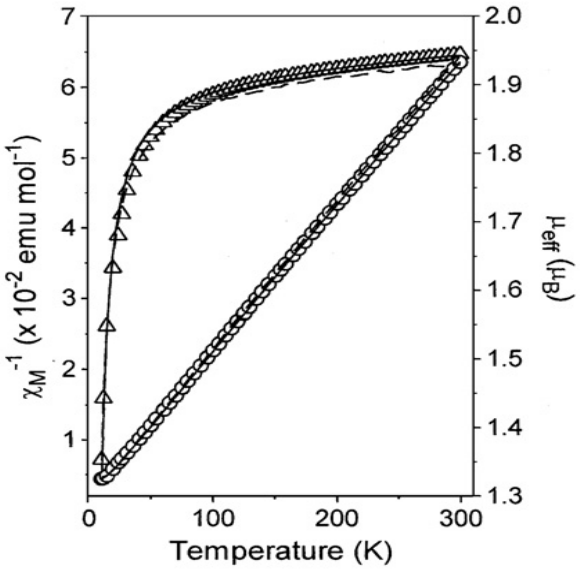

Figure 2.8. Inverse molar magnetic susceptibility (O) and effective magnetic moment (Δ) of **[Cu(bhac)(dmpz)]** (**1**) as a function of temperature. The solid and the dashed lines represent the quality of the least-squares fits using the Bleany–Bowers expression and the alternating antiferromagnetic chain model, respectively.

2.3.6. EPR spectral properties

The room temperature (298 K) X-band EPR spectral profile of the powdered complex is characteristic for a spin-coupled dicopper(II) species. A broad and strong asymmetric signal at $g = 2.08$ and a weak absorption at $g = 4.26$ are observed (Figure 2.9, trace a). The former is assigned to the $\Delta Ms = \pm 1$ transition and the latter to the $\Delta Ms = \pm 2$ transition.[24–26] Lowering the temperature to 110 K sharpens the $g = 2.08$

signal but decreases the intensity of the g = 4.26 signal, suggesting an antiferromagntically coupled system.

In solution, if the spin-coupled dicopper(II) species exists at room temperature a seven-line pattern at $g \sim 2$ is expected.[27] However, a $CHCl_3$–$C_6H_5CH_3$ (1:1) solution of the complex at 298 K gives a typical isotropic spectrum with a four-line pattern (g = 2.09, A = 88 G) for an uncoupled mononuclear copper(II) species.[24] In dilute conditions the nitrogen super-hyperfine lines are clearly visible on the high-field line.

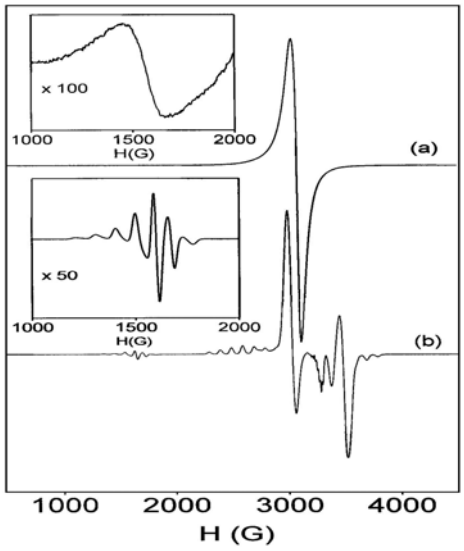

Figure 2.9. EPR spectra of **[Cu(bhac)(dmpz)]** (**1**): (a) in powder phase at 298 K, (b) in frozen (110 K) chloroform–toluene (1:1) solution (1.01×10^{-1} M). Insets: Magnified $\Delta Ms = \pm 2$ region for the powder phase (top) and that for the frozen solution (bottom).

The EPR spectra of frozen (110 K) $CHCl_3$–$C_6H_5CH_3$ (1:1) solutions of the complex having deferent concentrations have been recorded. The spectrum of the complex at the highest concentration is depicted in Figure 2.9, trace b. The spectral features are characteristic of two interacting copper(II) ions. The half-field transition is observed as a seven-line pattern with an average line spacing of 96 G at g = 4.39. The $\Delta Ms = \pm 1$ transitions are observed in the range of 2200–3750 G. Observation of two pairs of transitions in this range due to zero-field splitting are consistent with an

essentially axial symmetry. Seven copper hyperfine lines with an average line spacing of 99 G are readily apparent in the range of 2200–2850 G. Three absorptions with an average line separation of 96 G observed in the range of 3500–3800 G are assigned to the second seven-line pattern. The other four lines are presumably obscured by the preceding strong signal. These two seven-line patterns centered at 3458 and 2552 G are assigned to the parallel signals. The perpendicular components appear as two strong signals at 2984 and 3444 G. In between these two signals, two more signals are observed at ~3268 and ~3375 G. The signal at lower field is split by several lines. As the concentration decreases, the intensity of each of these two signals increases. On the other hand, there is a decrease in the intensities of the signals at 2984 and 3444 G, the seven-line patterns of the parallel components and the half-field signal. These decreasing signals are associated with the spin-coupled dicopper(II) species. Figure 2.10 depicts this concentration dependent change of the signals in the $\Delta Ms = \pm 1$ region. The major features in the spectrum of the complex at the lowest concentration (Figure 2.10, trace d) are typical for an axial spectrum of a mononuclear square-planar copper(II) complex.[24] The $g_{||}$ and $A_{\perp}$values are 2.19 and 212 G, respectively.

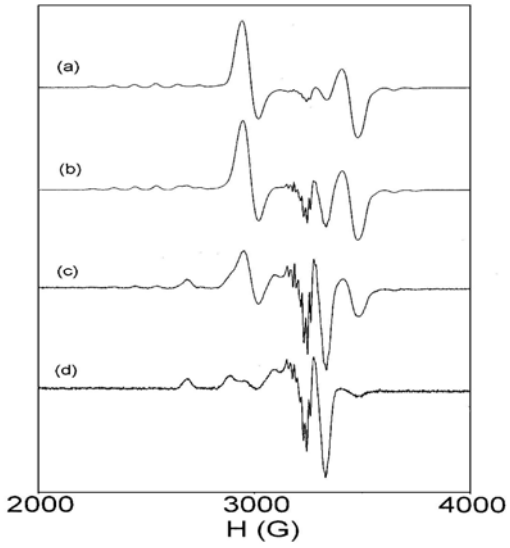

Figure 2.10. $\Delta Ms = \pm 1$ region in the EPR spectra of **[Cu(bhac)(dmpz)]** (**1**) in frozen (110 K) chloroform–toluene (1:1) solution: (a) 1.01×10^{-1} M, (b) 1.01×10^{-2} M, (c) 1.01×10^{-3} M, (d) 1.01×10^{-4} M.

The $g_{\perp}$ signal observed at 2.06 is split by several lines with an average line separation of 16 G. As the metal ion is coordinated to two deferent types of nitrogen atoms, nine nitrogen superhyperfine lines are expected. Eight lines are clearly visible in the $g_{\perp}$ signal. Two weak absorptions are observed at ~2950 and ~3480 G (Figure 2.10, trace d). Comparison of all the frozen solution spectra clearly suggests that these two weak absorptions are the perpendicular components of the $\Delta Ms = \pm 1$ transitions from a small amount of the dicopper(II) species. Similarly, the signals at ~3268 and ~3375 G in the spectrum (Figure 2.10, trace a) of the complex at the highest concentration indicate the presence of a small amount of uncoupled mononuclear copper(II) complex.

All the EPR spectra described above suggest that the spin-coupled dicopper(II) species exists not only in the solid state, but also in frozen solutions. The concentration dependent change of the spectral profiles clearly indicates the aggregation of [Cu(bhac)(dmpz)] molecules into a dimeric species at high concentrations. However, a small fraction of the molecules remains uncoupled. On the other hand, at low concentration, except for a small fraction most of the molecules remain uncoupled. The frozen solution EPR data can be used to calculate an approximate value for the Cu···Cu distance in the dicopper(II) species. In the $\Delta Ms = \pm 1$ region of the EPR spectrum, the spacing between the two parallel components is $2D_{||}$, where $D_{||}$ is the zero-field splitting parameter. According to our assignments of the signals in the frozen solution spectrum (Figure 2.10, trace a), the separation between the parallel components is 906 G. The value of $D_{||}$ (453 G = 0.041 cm^{-1}) is the sum of the zero-field splitting parameters due to dipole-dipole (D_{dd}) and pseudo-dipolar (D_{pd}) interactions. The magnitude of the pseudo-dipolar interaction depends on the extent of spin-exchange and magnetic anisotropy.[23,26] The relationship of D_{pd} with the spin-coupling constant J, $g_{||}$, and $g_{\perp}$ is as follows: $D_{pd} = 2J\{[(g_{||} - 2)^2/4] - (g_{\perp} - 2)^2\}/8$. From this relation the value of D_{pd} has been evaluated as -9.8×10^{-3} cm^{-1} using the values of J (-6.0 cm^{-1}), $g_{||}$ (2.19) and $g_{\perp}$ (2.05). Thus, D_{dd} is obtained as 0.051 cm^{-1} by subtraction of D_{pd} from $D_{||}$. Using these values of D_{dd} and $g_{||}$ in the equation[28] $R^3 = 0.65\ g_{||}^2 / D_{dd}$ the Cu···Cu distance (R) in the dicopper(II) species in frozen solution is evaluated as 3.94 Å.

2.4. Conclusion

The synthesis, structure and properties of a mixed-ligand square-planar copper(II) complex, [Cu(bhac)(dmpz)], have been described. In the solid state, each complex molecule is involved in reciprocal π-ovelapping of the chelate rings and dmpz rings with one neighbour (short Cu···Cu distance) and in another π-ovelapping of the dmpz rings only with the other neighbour (long Cu···Cu distance) (Figure 2.5) forming a chain-like arrangement of the metal complexes. Solid state variable temperature magnetic susceptibility measurements and the EPR spectra of the complex in powder phase as well as in frozen solution indicate a weakly coupled dicopper(II) species. The X-ray structure shows that there is no deviation of the metal centre from the square-plane formed by the four coordinating atoms. In addition, each molecule in the one-dimensional arrangement is laterally displaced with respect to its neighbouring molecules on both sides. Consequently, a direct Cu···Cu interaction can be ruled out as the origin of the observed weak antiferromagnetic interaction. Thus, the readily apparent pathway, at least in the solid state, for the observed antiferromagnetic spin-coupling is a superexchange *via* the electrons involved in the π-π interaction. The antiferromagnetic interaction between the more closely spaced metal ions is expected to be much stronger as the chelate rings containing these metal ions are involved in π-π interactions with the coordinated dmpz rings. Most likely this dimeric unit is reflected in the magnetic susceptibility and EPR data. Thus, the one-dimensional arrangement in the solid state can be viewed as the π-stacked assembly of this spin-coupled dimeric unit that itself is formed by π-π interactions. Within this chain of dimers, there is essentially no interdimer spin exchange.

Unlike in the solid state, existence of a typical dimeric Cu(II) species formed by mutual involvement of two molecules in equatorial-apical bridging through metal coordinated N or O atoms cannot be ruled out in frozen solution. However, the value of Cu···Cu distance (3.94 Å) calculated from the frozen solution EPR data is very close to the short Cu···Cu distance [3.5958(8) Å] observed in the one-dimensional arrangement of the molecules in the solid state. Thus, as observed in the solid state, formation of dimeric aggregates of [Cu(bhac)(dmpz)] molecules by π-overlapping is a distinct possibility in frozen solution. Similar π-stacking of organic ion radicals in solution phase was reported earlier.[29–31]

Magnetic exchange interactions *via* non-covalent weak intermolecular interactions such as van der Waals, hydrogen-bonding and π-stacking in supramolecular species formed by the same non-covalent intermolecular interactions is of considerable current interest.[32–36] Very few complexes are known in which magnetic exchange occurs solely through intermolecular π-π interactions involving the terminal aromatic ligands. To the best of our knowledge the present complex provides a unique example of metal ion spin-coupling in a square-planar copper(II) complex where π-overlapping of the chelate rings and unidentate heterocycles of two molecules helps to form a dimeric unit and provides the superexchange pathway. The only other example reported for copper(II) spin-exchange in a similar way is a dimeric aggregate of the non-planar anionic complex $[Cu(mnt)_2]^{2-}$, where mnt^{2-} is maleonitriledithiolate.[37]

References

1 Alcock, N. W.; Barker, P. R.; Haider, J. M.; Hannon, J. M.; Painting, C. L.; Pikramenou, Z.; Plummer, E. A.; Rissanen, K.; Saarenketo, P. *J. Chem. Soc., Dalton Trans.* **2000**, 1447.

2 Hunter, C. A.; Sanders, J. K. M. *J. Am. Chem. Soc.* **1990**, *112*, 5525.

3 Sigel, H.; Song, B. *Met. Ions Biol. Syst.* **1996**, *32*, 135.

4 Hatfield, W. E. In *Theory and Applications of Molecular Paramagnetism*; Boudreaux, E. A.; Mulay, L. N., Eds.; Wiley, New York, 1976; pp. 491.

5 North, A. C. T.;Philips, D. C.; Mathews, F. S. *Acta Crystallogr., Sect. A* **1968**, *24*, 351.

6 Farrugia, L. J. *J. Appl. Crystallogr.* **1999**, *32*, 837.

7 Sheldrick, G. M. SHELX-97 Structure Determination Software, University of Go¨ttingen, Go¨ttingen, Germany, 1997.

8 McArdle, P. *J. Appl. Crystallogr.* **1995**, *28*, 65.

9 Spek, A. L. Platon98 Molecular Graphics Software, University of Glasgow, UK, 1998.

10 Nakamoto, K. *Infrared and Raman Spectra of Inorganic and Coordination Compounds;* Wiley, New York, 1986; pp. 241–244.

11 Pal, S. N.; Pal, S. *J. Chem. Soc., Dalton Trans.* **2002**, 2102.

12 Sangeetha, N. R.; Pal, S. *Polyhedron* **2000**, *19*, 1593.

13 Pal, S. N.; Pal, S. *Inorg. Chem.* **2001**, *40*, 4807.

14 Sangeetha, N. R.; Pal, C. K.; Ghosh, P.; Pal, S. *J. Chem. Soc., Dalton Trans.* **1996**, 3293.

15 Sangeetha, N. R.; Baradi, K.; Gupta, R.; Pal, C. K.; Manivannan, V.; Pal, S. *Polyhedron* **1999**, *18*, 1425.
16 Clark, R.; Hall, D.; Waters, T. N. *J. Chem. Soc. A* **1969**, 823.
17 Sangeetha, N. R.; Pal, S. *J. Chem. Crystallogr.* **1999**, *29*, 287.
18 Mederos, A.; Medina, A.; Medina, E.; Manrique, F. G.; Nunez, P.; Rodriguez, M. L. *J. Coord. Chem.* **1987**, *15*, 393.
19 Elhert, M. K.; Rettig, S. J.; Storr, A.; Thompson, R. C.; Trotter, J. *Can. J. Chem.* **1992**, *70*, 2161.
20 Kraus, W.; Nolze, G. *PowderCell 2.3;* Federal Institute for Materials Research and Testing, Berlin, Germany, 1999.
21 Hatfield, W. E. *J. Appl. Phys.* **1981**, *52*, 1985.
22 Chandramouli, G. V. R.; Balagopalakrishna, C.; Rajasekharan, M. V.; Manoharan, P. T. *Comput. Chem.* **1996**, *20*, 353.
23 Bleany, B.; Bowers, K. D. *Proc. R. Soc. London, Ser. A* **1952**, *214*, 451.
24 Hasty, E. F.; Colburn, T. J.; Hendrickson, D. N. *Inorg. Chem.* **1973**, *12*, 2414.
25 Greenaway, A. M.; O'Connor, C. J.; Overman, J. W.; Sinn, E. *Inorg. Chem.* **1981**, *20*, 1508.
26 Costes, J.–P.; Dahan, F.; Laurent, J.-P. *Inorg. Chem.* **1985**, *24*, 1018.
27 Hasty, E. F.; Wilson, L. J.; Hendrickson, D. N. *Inorg. Chem.* **1978**, *17*, 1834.
28 Stevens, K. W. H. *Proc. R. Soc. London, Ser. A* **1952**, *214*, 237.
29 Zhong, C. J.; Kwan, W. S. V.; Miller, L. L. *Chem. Mater.* **1992**, *4*, 1423.
30 Benz, M. E.; Tabakovic, I.; Miller, L. L. *Chem. Mater.* **1994**, *6*, 351.
31 Miller, L. L.; Hashimoto, T.; Tabakovic, I.; Swanson, D. R.; Tomalia, D. A. *Chem. Mater.* **1995**, *7*, 9.
32 Kahn, O.; Pei, Y.; Journaux, Y. In *Inorganic Materials;* Bruce, D. W.; O'Hare, D., Eds.; Wiley, Chichester, 1992; pp. 59.
33 Kollmar, C.; Kahn, O. *Acc. Chem. Res.* **1993**, *26*, 259.
34 Miller, J. S.; Epstein, A. J. *Angew. Chem., Int. Ed. Engl.* **1994**, *33*, 385.
35 Wesolek, M.; Meyer, D.; Osborn, J. A.; De Cian, A.; Fischer, J.; Derory, A.; Legoll, P.; Drillon, M. *Angew. Chem., Int. Ed. Engl.* **1994**, *33*, 1592.
36 Amoroso, A. J.; Jeffery, J. C.; Jones, P. L.; McCleverty, J. A.; Thornton, P.; Ward, M. D. *Angew. Chem., Int. Ed. Engl.* **1995**, *34*, 1443.
37 Snaathorst, D.; Doesburg, H. M.; Perenboom, J. A. A. J.; Keijzers, C. P. *Inorg. Chem.* **1981**, *20*, 2526.

Chapter 3

Ternary copper(II) complexes with tridentate acetylacetone benzoylhydrazone and monodentate N–heterocycles[§]

This chapter deals with the synthesis, characterization and physical properties of three ternary copper(II) complexes of general formula [Cu(bhac)(hc)], with a tridentate Schiff base, acetylacetone benzoylhydrazone (H_2bhac) and monodentate heterocycles (hc = pyrazole, imidazole and pyridine). The O,N,O-donor $bhac^{2-}$ and the N-donor hc form an O_2N_2 square-plane around the metal ion in each complex. The whole molecule of none of the complexes is perfectly planar because of different orientations of the phenyl ring plane of $bhac^{2-}$ and the heterocyclic ring plane with respect to the plane containing rest of the molecule. In the solid state, the pyrazole and pyridine containing complexes exist as centrosymmetric dimeric species through weak apical coordination of the metal bound enolate-O. The complex of imidazole has no such apical coordination and exists as a monomer. In the crystal lattice, self-assembly of the molecules of these complexes via intermolecular non-covalent interactions lead to diverse varieties of supramolecular structures. The dimeric units of [Cu(bhac)(pyz)]·C_2H_5OH exist in a one-dimensional array due to intermolecular O–H···O and N–H···O hydrogen bonding and π···π interactions between the pyrazole rings. The roughly orthogonal C–H···π and N–H···N hydrogen bonding interactions assist to the formation of a two-dimensional sheet structure of the [Cu(bhac)(imd)] molecule. A three-dimesional network of [Cu(bhac)(py)] molecules is formed due to participation of the pyridine ring *meta*- and *para*-CH groups and the phenyl ring of $bhac^{2-}$ in C–H···π interactions. Cryomagnetic and EPR spectral measurements indicate weak antiferromagnetic spin-exchange in all the three complexes.

[§] This work has been published in *J. Mol. Struct.,* **2005***, 741,* 183-192.

3.1. Introduction

In the preceding chapter, we have described the low-dimensional π-stacked assembly of [Cu(bhac)(dmpz) (**1**) with its magnetic characteristics. To examine whether the self-assembly pattern and the magnetic properties observed for **1** is unique or general we have prepared three analogous complexes using three different N-donor heterocycles such as pyrazole (pyz), imidazole (imd) and pyridine (py). Interestingly, the packing pattern of none of these three complexes is akin to that of **1**. Both [Cu(bhac)(pyz)] (**2**) and [Cu(bhac)(py)] (**4**) exist as dimers due to weak apical coordination of the metal ion by the enolate-O of the acetylacetone fragment of the $bhac^{2-}$ in a reciprocal manner. In contrast, [Cu(bhac)(imd)] (**3**) does not form dimers through apical coordination. Dimeric units of **2** form a chain via intermolecular π–π interactions and solvent molecule (C_2H_5OH) assisted hydrogen bonds. On the other hand dimeric units of **4** form a three-dimensional network due to intermolecular C–H/π interactions. The monomeric **3** exists in a two-dimensional arrangement via intermolecular N–H/N hydrogen bonding and C–H/π interactions. Herein, we report the syntheses, characterization, X-ray structures, EPR spectroscopic and magnetic properties of **2**·C_2H_5OH, **3** and **4**.

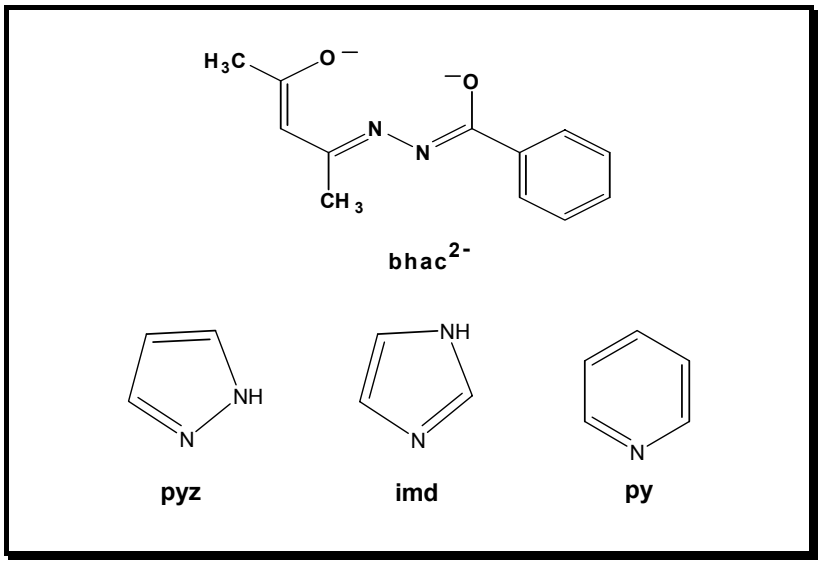

Figure 3.1.

3.2. Experimental section

3.2.1. Materials

The Schiff base, H_2bhac, was prepared from benzoylhydrazone and acetylacetone by following the procedure as described in the previous chapter. All other chemicals and solvents used in this work were of analytical grade available commercially and were used without further purification.

3.2.2. Physical measurements

Microanalytical (C, H, N) data were obtained with a Thermo Finnigon Flash EA1112 series elemental analyzer. Infrared spectra were collected by using KBr pellets on a Jasco-5300 FT-IR spectrophotometer. A Shimadzu 3101-PC UV/vis/NIR spectrophotometer was used to record the electronic spectra. Solution electrical conductivities were measured with a Digisun DI-909 conductivity meter. A CH-Instruments model 620A electrochemical analyzer was used for cyclic voltammetric experiments with acetonitrile solutions of the complexes containing tetrabutylammonium perchlorate (TBAP) as supporting electrolyte. The three electrode measurements were carried out at 298 K under a dinitrogen atmosphere with a platinum disk working electrode, a platinum wire auxiliary electrode and an Ag/AgCl reference electrode. Under identical conditions the $E_{1/2}$ value of Fc^+/Fc (Fc, ferrocene) couple was 0.48 V. The potentials reported in this work are uncorrected for junction contributions. EPR spectra were recorded on a Jeol JES-FA200 spectrometer. The variable temperature (18–300 K) magnetic susceptibility measurements with powdered samples of **2**, **3** and **4** were performed using the Faraday technique with a set-up comprising a George Associates Lewis coil force magnetometer, a CAHN microbalance and an Air Products cryostat. $Hg[Co(NCS)_4]$ was used as the standard. Diamagnetic corrections calculated from Pascal's constants[1] were used to obtain the molar paramagnetic susceptibilities.

3.2.3. Synthesis

[Cu(bhac)(pyz)]·C_2H_5OH (**2**·C_2H_5OH)

An ethanol solution (5 ml) of $Cu(O_2CCH_3)_2·H_2O$ (180 mg, 0.9 mmol) was added to another ethanol solution (5 ml) of H_2bhac (280 mg, 1.0 mmol) and the resulting mixture was stirred at room temperature for 2 h. The green solid separated was collected by filtration, washed with water and ethanol and transferred to 20 ml ethanol. To this suspension of green solid, an ethanol solution (15 ml) of pyrazole (82 mg, 1.2 mmol) was added and the resulting green solution was stirred at room temperature for 2 h. The mixture was then evaporated on a steam bath to 10 ml, cooled to room temperature and kept for slow evaporation in air. After 2–3 days the complex was precipitated as ethanol solvate (**2**·C_2H_5OH) in the form of deep brown crystalline material. This was collected by filtration, washed with cold ethanol and dried in air. Yield, 236 mg (75%). Anal. calcd. for $C_{17}H_{22}N_4O_3Cu$: C, 51.83; H, 5.63; N, 14.22; found: C, 51.58; H, 5.51; N, 14.03. Selected IR bands (cm^{-1}): 3310(m), 3057(w), 2918(w), 1597(s), 1568(m), 1510(s), 1491(s), 1412(s), 1271(s), 1168(m), 1037(s), 788(s), 686(s), 603(m), 472(w), 437(m). UV/Vis [$CHCl_3$; λ_{max}/nm (ε /dm^3 mol^{-1} cm^{-1})]: 568 (103), 375 (15040), 360sh (13730), 247 (22050).

[Cu(bhac)(imd)] (**3**)

Complex **3** was synthesized in 77% yield and isolated as brown crystalline solid by following the same procedure as described for **2** using imidazole instead of pyrazole. Anal. calcd. for $C_{15}H_{16}N_4O_2Cu$: C, 51.79; H, 4.63; N, 16.11; found: C, 51.61; H, 4.49; N, 16.02. Selected IR bands (cm^{-1}): 3144(w), 3056(w), 2921(w), 2852(w), 1589(s), 1506(s), 1406(s), 1290(m), 1143(w), 1066(s), 952(w), 823(m), 756(s), 704(s), 652(s), 617(w), 443(m), 416(w). UV/Vis [$CHCl_3$; λ_{max}/nm (ε /dm^3 mol^{-1} cm^{-1})]: 565 (102), 376 (14770), 361sh (12910), 249 (16650).

[Cu(bhac)(py)] (**4**)

Complex **4** was synthesized in 87% yield and isolated as green needles by following the same procedure as described for **2** using pyridine instead of pyrazole. Anal. calcd. for $C_{17}H_{17}N_3O_2Cu$: C, 56.89; H, 4.77; N, 11.71; found: C, 56.72; H, 4.70;

N, 11.59. Selected IR bands (cm^{-1}): 3078(w), 2916(w), 1591(s), 1531(s), 1506(s), 1487(s), 1398(s), 1282(s), 1219(s), 1066(s), 927(m), 788(m), 756(m), 702(s), 640(m), 569(w), 443(m), 416(m). UV/Vis [$CHCl_3$; λ_{max}/nm (ε /dm^3 mol^{-1} cm^{-1})]: 565 (112), 375 (17320), 361sh (16240), 251 (20390).

3.2.4. X-ray crystallography

Single crystals of all the complexes were collected directly from the products obtained from ethanolic reaction mixtures. Unit cell parameters and the intensity data for **2**·C_2H_5OH and **3** were obtained on a Bruker-Nonius SMART APEX CCD single crystal diffractometer, equipped with a graphite monochromator and a Mo $K\alpha$ fine-focus sealed tube (λ = 0.71073 Å) operated at 2.0 kW. The detector was placed at a distance of 6.0 cm from the crystal. Data were collected at 298 K with a scan width of 0.3º in ω and an exposure time of 10 sec/frame. The SMART software was used for data acquisition and the SAINT-Plus software was used for data extraction.[2] In each case, an empirical absorption correction was performed with the help of SADABS program.[3] Unit cell parameters for **4** were determined by the least-squares fit of 25 reflections having 2θ values in the range 18–22º on an Enraf-Nonius Mach-3 single crystal diffractometer using graphite monochromated Mo $K\alpha$ radiation (λ = 0.71073 Å). The data were collected by ω-scan method. The stability of the crystal was monitored by measuring the intensities of three check reflections after every 1.5 h during the data collection. No decay was observed during the 40 h exposure to X-ray. The ψ-scans[4] of 4 reflections having θ and χ values within 17–24º and 80–82º, respectively were used for an empirical absorption correction. The programs of the WinGX package[5] were used for data reduction and absorption correction. In each case, the structure was solved by direct methods and refined on F^2 by full-matrix least-squares procedures. All non-hydrogen atoms were refined with anisotropic thermal parameters. Hydrogen atoms were included in the structure factor calculation at idealized positions by using riding model, but not refined. The SHELX-97 programs[6] were used for structure solution and refinement. The ORTEX6a[7] and Platon packages[8] were used for molecular graphics. Significant crystallographic data for **2**·C_2H_5OH, **3** and **4** are summarized in Table 3.1.

Table 3.1 Crystallographic parameter for **2**·C_2H_5OH, **3** and **4**.

Complex	**2**·C_2H_5OH	**3**	**4**
Chemical formula	$CuC_{17}H_{22}N_4O_3$	$CuC_{15}H_{16}N_4O_2$	$CuC_{17}H_{17}N_3O_2$
Formula weight	393.93	347.86	358.88
Crystal system	Triclinic	Monoclinic	Monoclinic
Space group	$P\bar{1}$	$P2_1/c$	$P2_1/n$
T/K	298	298	298
a (Å)	7.7058(5)	14.5952(10)	13.0276(16)
b (Å)	10.7348(7)	5.6793(4)	10.707(2)
c (Å)	12.3684(9)	18.2721(13)	13.110(2)
α (°)	97.2330(10)	90	90
β (°)	104.0620(10)	93.1080(10)	116.975(12)
γ (°)	103.8180(10)	90	90
2θ(°) range	4.74–56.52	4.46–52.04	3.66–54.94
V (Å^3)	945.18(11)	1512.36(18)	1629.7(5)
Z	2	4	4
μ (mm^{-1})	1.178	1.456	1.352
N-collected	10339	14906	3927
N-unique	4215	2957	3719
N [$I \geq 2\sigma(I)$]	3860	2601	2989
Parameters	229	201	210
$R1$[a], $wR2$[b] [$I \geq 2\sigma(I)$]	0.0388, 0.1033	0.0296, 0.0860	0.0342, 0.0814
$R1$[a], $wR2$[b] [all data]	0.0415, 0.1060	0.0337, 0.0899	0.0495, 0.0879
GOF[c] on F^2	1.059	1.035	1.087
Largest peak and hole (*e* Å^{-3})	0.881, –0.511	0.301, –0.231	0.269, –0.385

[a] $R1 = \sum||F_o| - |F_c||/\sum|F_o|$. [b] $wR2 = \{\sum[(F_o^2 - F_c^2)^2]/\sum[w(F_o^2)^2]\}^{1/2}$.

[c] $GOF = \{\sum[w(F_o^2 - F_c^2)^2]/(n - p)\}^{1/2}$ where n is the number of reflections and p is the number of parameters refined; $w = 1/[\sigma^2(F_o^2) + (aP)^2 + bP]$.

3.3. Results and discussion

3.3.1. Synthesis and characterization

Reaction of one equivalent each of $Cu(O_2CCH_3)_2 \cdot H_2O$ and H_2bhac in ethanol initially produces an insoluble green solid which is most likely a dinuclear species similar to those commonly obtained with tridentate dibasic ligands.[9] On addition of the heterocycles this species becomes soluble and the mononuclear ternary square-planar complexes (**2**·C_2H_5OH, **3** and **4**) are isolated in 75–87% yields. Elemental analyses data for all the complexes are satisfactory with the Cu^{2+}:$bhac^{2-}$:hc ratio as 1:1:1. As expected the complexes are electrically non-conducting in acetonitrile solutions.

The infrared spectrum of **2**·C_2H_5OH displays a sharp band at 3310 cm^{-1}. This band is assigned to the pyrazole N–H group. Perhaps due to the participation of C_2H_5OH in hydrogen bonding (*vide infra*) no band assignable to the OH group is observed. In the spectrum of **3**, a weak band observed at 3144 cm^{-1} is most likely due to the imidazole N–H group. The significant lowering of the imidazole N–H stretching frequency in **3** compared to the pyrazole N–H stretching frequency in **2** is consistent with the participation of the former in strong intermolecular hydrogen bonds (*vide infra*). All the three complexes display several sharp but weak bands in the range 2850–3078 cm^{-1}. These are attributed to the C–H stretches. None of the complexes display the C=O (~1675 cm^{-1}) stretch of the amide functionality[10] observed for the free H_2bhac. A strong band observed in the range 1589–1597 cm^{-1} is attributed to the conjugated C=N–N=C moiety[11] of $bhac^{2-}$. Thus in each complex the metal ion is in +2 oxidation state and $bhac^{2-}$ coordinates the metal ion *via* the enolate-O, the imine-N and the deprotonated amide-O atoms. The fourth coordination site is satisfied by the imine-N atom of pyrazole, imidazole and pyridine in **2**, **3** and **4**, respectively. X-ray structures (*vide infra*) confirm this type of coordination of the metal ion by the monodentate heterocycles and the tridentate ligand in these complexes.

The electronic spectra of the complexes in chloroform solutions are very similar and comparable to that of **1**. A weak absorption observed near 565 nm is followed by several intense absorptions in the range 396–247 nm. The weak

absorption is assigned to d–d transition.[12] The higher energy absorptions are likely to be due to ligand–to–metal charge transfer and intraligand transitions.

3.3.2. Electrochemical properties

Redox properties of the complexes in acetonitrile solutions (0.1 M TBAP) have been investigated with the help of cyclic voltammetry. The complexes display an irreversible oxidation (Figure 3.2) in the potential range 0.59–0.63 V (vs. Ag/AgCl). The peak currents are comparable with known one-electron redox processes under identical conditions. The deprotonated $bhac^{2-}$ or the heterocycles do not display any such response under the same conditions. The iron(III) complex, $[Fe(bhac)_2]^-$, displays a metal centred oxidation at 0.40 V (vs. Ag/AgCl) in acetonitrile solution.[13] Considering all the above, the responses observed for [Cu(bhac)(hc)] have been assigned to copper(II) → copper(III) oxidation process.

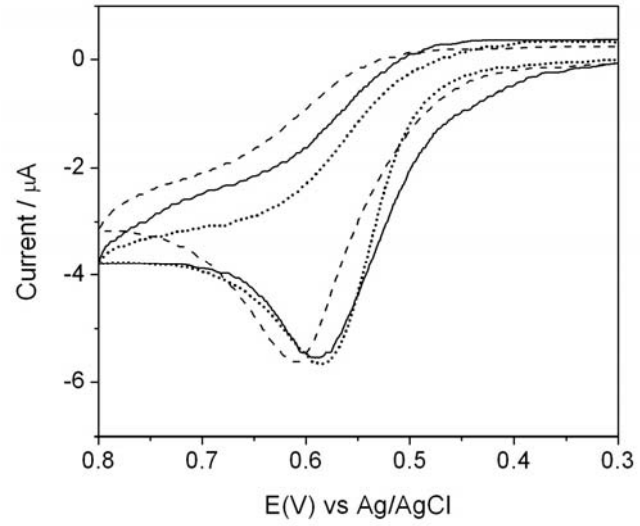

Figure 3.2. Cyclic voltammograms (scan rate 100 mVs^{-1}) of ~10^{-3} M solution of **2** (solid line), **3** (dashed line) and **4** (dotted line) in chloroform solutions (0.1 M TBAP) at platinum electrode (298 K).

3.3.3. Description of molecular structures

Complexes **2**, **3**, and **4** crystallize in $P\bar{1}$, $P2_1/c$ and $P2_1/n$ space groups, respectively. The asymmetric unit of **2** contains a molecule of [Cu(bhac)(pyz)] and a ethanol molecule. On the other hand, the asymmetric units of **3** and **4** contain a single molecule of [Cu(bhac)(hc)] (hc = imd and py). The molecular structures of **2**, **3**, and **4** are depicted in Figures 3.3, 3.4 and 3.5, respectively. Selected bond parameters are summarized in Tables 3.2, 3.3 and 3.4. In each case, the tridentate $bhac^{2-}$ coordinates the metal ion *via* the enolate-O, the imine-N and the deprotonated amide-O atoms forming a six- and a five-membered chelate ring. The C6–O2, C6–N2, C2–C3 and C2–O1 bond lengths are consistent with the enolate form of both amide and acetyacetone fragments of the tridentate ligand.[11,13] The imine-N of the heterocycle occupies the fourth coordination site. The maximum and minimum deviations from the O_2N_2 mean plane are in the ranges 0.12–0.07 Å and 0.10–0.04 Å, respectively. Thus the ligands form a satisfactory O_2N_2 square-plane around the metal centre in each complex. The deviations of the metal centre from this plane are in the range 0.04–0.08 Å. Thus there is no significant displacement of the metal centre from the O_2N_2 square-plane. However, none of the three complex molecules as a whole is planar. This is due to the twisting of the phenyl ring plane (mean deviations are in the range 0.005–0.008 Å) of $bhac^{2-}$ along the C6–C7 bond and that of the heterocycle plane (mean deviations are in the range 0.001–0.003 Å) along the Cu–N3 bond with respect to the plane containing rest of the molecule (Figures 3.3, 3.4 and 3.5). The dihedral angles between the phenyl ring plane and the plane constituted by O1, O2, N1, N2, C1–C6 atoms (mean deviations are in the range 0.04–0.08 Å) are 18.25(9)°, 19.53(10)° and 28.12(9)° for **2**, **3** and **4**, respectively. The dihedral angles between the heterocycle plane and the plane containing O1, O2, N1, N2, C1–C6 atoms are 10.67(11)°, 19.01(11)° and 11.31(15)° for **2**, **3** and **4**, respectively. Interestingly in **1** the dihedral angles formed by the phenyl ring plane and 3,5-dimethylpyrazole (dmpz) plane with the plane containing rest of the molecule are 3.03(11)° and 11.53(10)°, respectively. Thus the $bhac^{2-}$ is essentially planar in **1** but the same is not true for **2**, **3** and **4**. The Cu–O1(enolate) and Cu–N1(imine) bond lengths in **2**, **3** and **4** are similar and comparable to that observed for **1**. The Cu–O2(amide) bond lengths in **1**, **3** and **4** are also similar and in the range 1.9168(18)–1.9227(16) Å. However, the

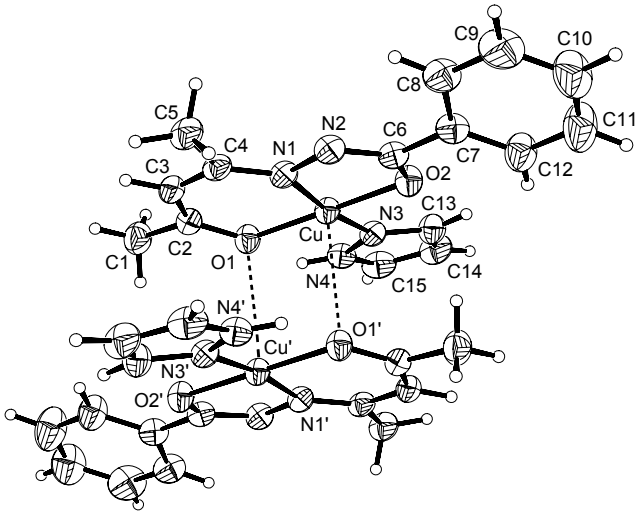

Figure 3.3. Structure of the dimeric unit of **[Cu(bhac)(pyz)]** (**2**) with the atom labeling scheme. All non-hydrogen atoms are represented by their 30% probability thermal ellipsoids.

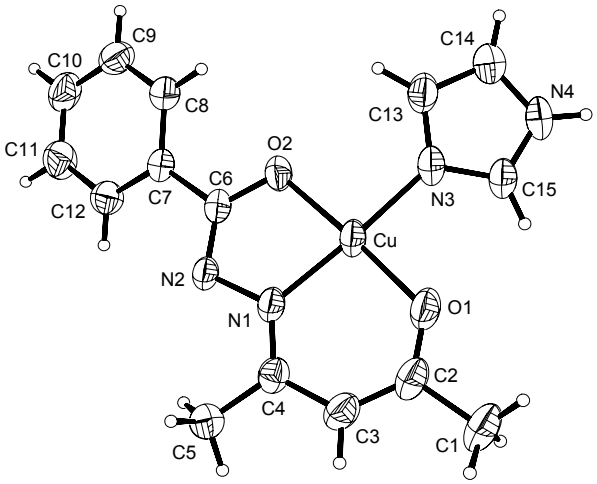

Figure 3.4. Molecular structure of **[Cu(bhac)(imd)]** (**3**) with the atom labeling scheme. All non-hydrogen atoms are represented by their 40% probability thermal ellipsoids.

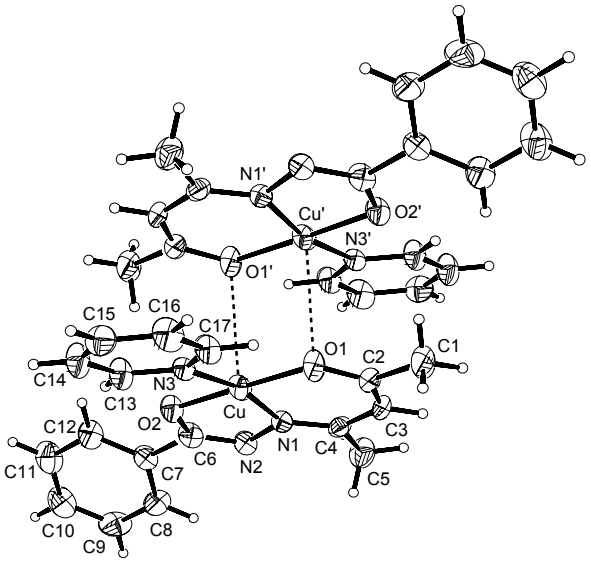

Figure 3.5. Dimeric structure of **[Cu(bhac)(py)]** (**4**) with the atom labeling scheme. All non-hydrogen atoms are represented by their 40% probability thermal ellipsoids.

Cu–O2(amide) bond is significantly longer [1.9503(13) Å] in **2** compared to that observed in the other complexes. This is most likely due to the involvement of O2 in hydrogen bonding with the ethanol molecule (*vide infra*) present in the crystal lattice of **2**. There is not much difference in the Cu–N3 bond lengths in **2** [1.9643(14) Å] and **3** [1.9581(17) Å]. On the other hand, the Cu–N3 bond is noticeably longer [2.0183(18) Å] in **4**. These bond lengths indicate that pyrazole and imidazole are similar and better donor than pyridine. Due to the presence of electron donating methyl groups, dmpz is expected to be a better donor than pyz and hence the Cu–N3 bond length should be shorter in **1** than that in **2**. However, Cu–N3 bond length is 1.998(2) Å in **1**. Possibly steric constraints imposed by the methyl substituents on dmpz cause the lengthening of this bond in **1**.

Table 3.2. Selected bond lengths (Å) and angles (°) for **[Cu(bhac)(pyz)]** (**2**).

Cu-N(1)	1.904(1)	O(2)-C(6)	1.302(2)	N(3)-C(13)	1.323(3)
Cu-O(1)	1.917(1)	O(3)-C(16)	1.362(5)	N(3)-N(4)	1.337(2)
Cu-O(2)	1.950(1)	N(1)-C(4)	1.306(2)	N(4)-C(15)	1.335(3)
Cu-N(3)	1.964(1)	N(1)-N(2)	1.398(2)	C(2)-C(3)	1.373(3)
O(1)-C(2)	1.299(2)	N(2)-C(6)	1.303(2)	C(3)-C(4)	1.413(3)
N(1)-Cu-O(1)	94.15(6)	C(2)-O(1)-Cu	123.52(12)	C(13)-N(3)-Cu	133.02(14)
N(1)-Cu-O(2)	82.15(6)	C(6)-O(2)-Cu	108.74(11)	N(4)-N(3)-Cu	121.16(12)
O(1)-Cu-O(2)	175.94(5)	C(4)-N(1)-N(2)	118.22(15)	O(2)-C(6)-C(7)	118.06(16)
N(1)-Cu-N(3)	172.25(6)	C(4)-N(1)-Cu	127.48(13)	N(2)-C(6)-C(7)	116.93(15)
O(1)-Cu-N(3)	89.68(6)	N(2)-N(1)-Cu	114.26(11)	O(3)-C(16)-C(17)	118.8(5)
O(2)-Cu-N(3)	94.19(6)	C(6)-N(2)-N(1)	109.65(14)		

Table 3.3. Selected bond lengths (Å) and angles (°) for **[Cu(bhac)(imd)]** (**3**).

Cu-O(1)	1.898(1)	O(2)-C(6)	1.289(2)	N(3)-C(13)	1.369(3)
Cu-N(1)	1.912(2)	N(1)-C(4)	1.309(2)	N(4)-C(15)	1.325(3)
Cu-O(2)	1.921(1)	N(1)-N(2)	1.410(2)	N(4)-C(14)	1.363(3)
Cu-N(3)	1.958(2)	N(2)-C(6)	1.313(3)	C(2)-C(3)	1.377(3)
O(1)-C(2)	1.286(3)	N(3)-C(15)	1.323(2)	C(3)-C(4)	1.420(3)
O(1)-Cu-N(1)	94.89(6)	C(4)-N(1)-Cu	126.85(13)	C(15)-N(3)-Cu	126.29(16)
O(1)-Cu-O(2)	176.75(6)	N(2)-N(1)-Cu	113.97(11)	C(13)-N(3)-Cu	127.70(13)
N(1)-Cu-O(2)	81.98(6)	C(6)-N(2)-N(1)	109.04(14)	N(1)-C(4)-C(3)	120.99(19)
O(1)-Cu-N(3)	90.71(7)	C(2)-O(1)-Cu	124.25(13)	N(1)-C(4)-C(5)	121.41(18)
N(1)-Cu-N(3)	171.95(7)	C(6)-O(2)-Cu	110.64(12)	O(2)-C(6)-N(2)	124.26(17)
O(2)-Cu-N(3)	92.31(6)	C(4)-N(1)-N(2)	118.92(16)	O(2)-C(6)-C(7)	116.28(17)

Table 3.4. Selected bond lengths (Å) and angles (°) for **[Cu(bhac)(py)]** (**4**).

Cu(1)-O(1)	1.901(2)	O(2)-C(6)	1.303(3)	N(3)-C(13)	1.332(3)
Cu(1)-N(1)	1.914(2)	O(1)-C(2)	1.300(3)	N(1)-C(4)	1.315(3)
Cu(1)-O(2)	1.922(2)	N(2)-C(6)	1.304(3)	C(2)-C(3)	1.365(3)
Cu(1)-N(3)	2.018(2)	N(2)-N(1)	1.401(2)	C(3)-C(4)	1.415(3)
O(1)-Cu(1)-N(1)	94.09(7)	C(6)-O(2)-Cu(1)	110.34(14)	N(2)-N(1)-Cu(1)	114.9(1)
O(1)-Cu(1)-O(2)	175.15(7)	C(2)-O(1)-Cu(1)	124.82(15)	O(1)-C(2)-C(3)	125.6(2)
N(1)-Cu(1)-O(2)	81.45(7)	C(6)-N(2)-N(1)	108.56(17)	C(2)-C(3)-C(4)	127.2(2)
O(1)-Cu(1)-N(3)	92.59(7)	C(13)-N(3)-Cu(1)	121.24(16)	N(1)-C(4)-C(3)	120.5(2)
N(1)-Cu(1)-N(3)	166.86(7)	C(4)-N(1)-N(2)	117.49(19)	C(3)-C(4)-C(5)	119.1(2)
O(2)-Cu(1)-N(3)	92.16(7)	C(4)-N(1)-Cu(1)	127.55(16)	O(2)-C(6)-N(2)	124.6(2)

3.3.4. Solid state packing patterns

Square-planar copper(II) complexes are known to form dimeric or polymeric one dimensional species containing equatorial-apical bridges due to the involvement of the metal ion in weak interactions with another atom of a neighbouring molecule at the apical position.[14] The complexes **2** and **4** are no exception to that observation. Both complex molecules form centrosymmetric dimeric units due to very weak apical coordination of the enolate-O in a reciprocal fashion (Figures 3.3 and 3.5). The Cu–O1' distances are 2.8736(16) Å and 2.8877(19) Å for **2** and **4**, respectively. The angles at the metal centre involving O1' at the apical site and the other coordinating atoms forming the square-base are in the ranges 84.57(6)–97.99(5)^{o} and 83.51(7)–108.36(6)^{o} for **2** and **4**, respectively. Thus in each complex the metal centre is in distorted square-pyramidal coordination environment. The Cu···Cu distance in the Cu_2O_2 core of **2** is 3.6021(4) Å and that in the **4** is 3.6322(7) Å. The Cu–O1–Cu' bridge angle are 95.43(6) and 96.49(7)^{o} for **2** and **4**, respectively. On the other hand, there is no such dimer formation for the molecules of **1** and **3** (Figure 3.4).

In the crystal lattice, the dimeric units of **2** exist in a one-dimensional arrangement. The ethanol molecules present in the crystal lattice participate in two types of hydrogen bonding interactions and act as bridges between these dimers to form the one-dimensional assembly (Figure 3.6). The O–H group of the ethanol is hydrogen bonded with the metal coordinated deprotonated amide-O of $bhac^{2-}$. The O···O distance and O–H···O angle are 3.012(4) Å and 157.5^{o}, respectively. The same ethanol O-atom also acts as a hydrogen bond acceptor involving the N–H group of the pyrazole moiety of an adjacent complex molecule. The N···O distance and N–H···O angle are 2.909(5) Å and 129.13^{o}, respectively. Thus two molecules are bridged by the two ethanol molecules and a dimeric unit is formed. The Cu···Cu distance in this dimeric unit is 5.4535(5) Å. Interestingly the pyrazole rings of these two molecules are also involved in π-π interaction (Figure 3.6). The dihedral angle between the mean planes containing the two pyrazole rings is 0.0(2)^{o}. The centroid(cg)-to-centroid(cg) and the interplanar distances are 3.767(4) and 3.285(3) Å, respectively. Thus each complex molecule in this one-dimensional arrangement is connected to the two adjacent molecules in two different ways. On one side there are two reciprocal Cu–O···Cu equatorial-apical interactions (*vide supra*) and on the other

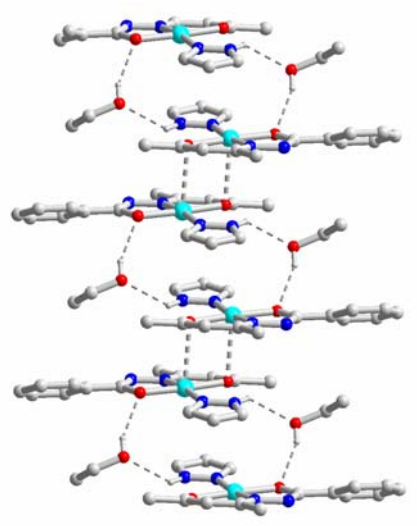

Figure 3.6. One-dimensional ordering of **[Cu(bhac)(pyz)]**·C_2H_5OH (**2**·C_2H_5OH) in the crystal lattice.

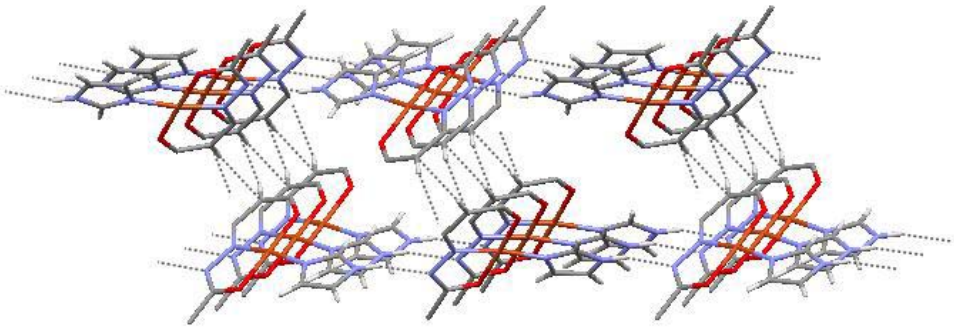

Figure 3.7. Two-dimensional double layered network of **[Cu(bhac)(imd)]** (**3**) in the crystal lattice.

side there are two reciprocal N–H···O–H···O interactions as well as π-π interaction between the metal coordinated pyrazole moieties (Figure 3.6). As a consequence there are sequential short [3.6021(4) Å] and long [5.4535(5) Å] Cu···Cu distances in the chain-like arrangement of the metal ions. There are no significant interchain short contacts or non-covalent interactions.

As mentioned before, the molecules of **3** do not form dimeric units via weak apical interactions. However, each molecule takes part in two types of hydrogen bonding interactions in the crystal lattice. The imidazole N–H group of one molecule and the uncoordinated amide N-atom of the adjacent molecule are involved in the first type of interaction and a one-dimensional assembly is formed (Figure 3.7). The N···N distance and N–H···N angle are 2.881(2) Å and 162.70°, respectively. The Cu···Cu distance in this chain is 9.1600(7) Å. Interestingly in each chain the C-atom (C3) of the methine group (–CH=) of each molecule is somewhat closer to the methine C-atoms of two symmetry related molecules belonging to the two adjacent chains. The C···C and H···C distances and the C–H···C angle are 3.983(3), 3.072 Å and 166.92°, respectively. These parameters perhaps indicate a weak non-covalent C–H···π interaction.[15,16] Thus the –CH= group of each molecule acts as donor as well as acceptor for the two C–H···C interactions with the two adjacent molecules. These interactions lead to the formation of a zigzag chain of the molecules (Figure 3.7). The Cu···Cu distance in this chain is 7.1077(5) Å. The C–H···C and the N–H···N interactions are roughly orthogonal to each other. As a result, an infinite two-dimensional crimped sheet structure is formed. There are no significant short contacts between the adjacent layers.

The molecule of **4** forms dimeric unit (*vide supra*) due to equatorial-apical bridging (Figure 3.5). Each molecule in these dimeric units are involved in two intermolecular C–H···π interactions involving the pyridine ring C–H groups and the phenyl ring of the tridentate ligand. The pyridine *meta*-CH of one neighbouring molecule participate in the first interaction on one side of the phenyl ring [H···cg distance, 2.900 Å; C–H···cg angle, 143.55°]. On the other side of the same phenyl ring, the pyridine *para*-CH of a second neighbouring molecule participate in the second interaction [H···cg distance, 2.896 Å; C–H···cg angle, 138.76°]. The H(*meta*)···cg···H(*para*) angle is 162.03° (Figure 3.8). These C–H···π interactions lead to a three-dimensional framework of the complex molecules in the crystal lattice.

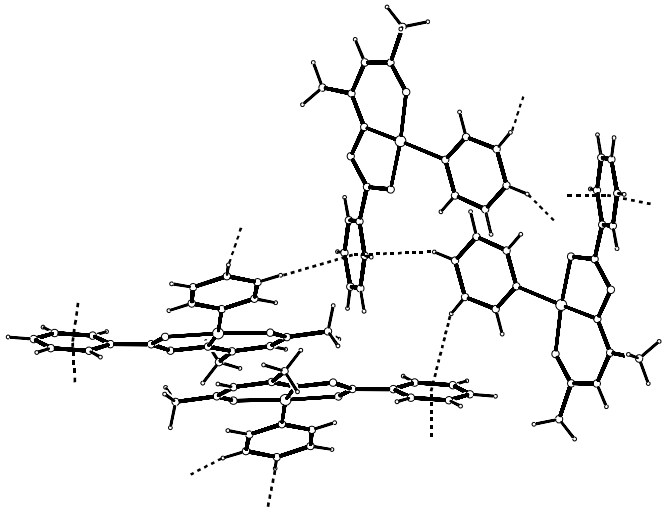

Figure 3.8. C–H···π interactions in the crystal lattice of **[Cu(bhac)(py)]** (**4**).

In each case, how the orientation of the phenyl ring plane present in $bhac^{2-}$ and that of the heterocycle ring plane with respect to the satisfactorily planar rest of the molecule are related with the self-assembly and the resulting supramolecular structure of a particular dimension is readily apparent. The dihedral angles between the heterocycle ring plane and the plane containing O1, O2, N1, N2, C1–C6 atoms are within 10.67(11)^o and 11.53(10)^o for **1**, **2** and **4**. The same for **3** is significantly larger [19.01(11)^o]. In **3**, the different orientation of the imidazole ring plane facilitates intermolecular hydrogen bonding involving the imidazole N–H group and dictates the self-organization motif of the molecules. The dihedral angles between the phenyl ring plane and the plane containing O1, O2, N1, N2, C1–C6 atoms are 18.25(9)^o and 19.53(10)^o for **2** and **3**, respectively. However, that for **4** is 28.12(9)^o. The participation of the phenyl ring as acceptor in the two intermolecular C–H···π interactions responsible for the formation of the three-dimensional framework of **4** is the most likely reason for the larger twist of it along the C6–C7 bond compared to the rest. The orientations of the heterocycle rings in **1**, **2** and **4** are very similar. But the twisting of the phenyl ring along C6–C7 in **1** is insignificant compared to that in **2** and **4**. The dihedral angle between the phenyl ring plane and the plane containing O1, O2, N1, N2, C1–C6 atoms is 3.03(11)^o for **1**. This difference in the orientation of the phenyl ring plane may perhaps be primarily responsible for the π-stacked one-

dimensional arrangement of **1** and dimer formation for **2** and **4** *via* weak apical interaction.

3.3.5. Magnetic Properties

Magnetic susceptibility measurements with powdered samples of all the three complexes were performed in the temperature range 18-300 K at a constant magnetic field of 5 kG. The effective magnetic moments (μ_{eff}) of the complexes at 300 K are 1.85, 1.86 and 1.82 μ_B for **2**·C_2H_5OH, **3** and **4**, respectively. On cooling the moments of **2**·C_2H_5OH and **4** gradually decreases. On the other hand, there is essentially no change in the moment for **3**. The μ_{eff} values at 18 K are 1.68, 1.85 and 1.69 μ_B for **2**·C_2H_5OH, **3** and **4**, respectively. The curves obtained by plotting the magnetic moments as a function of temperature are illustrated in Figure 3.9. The natures of the

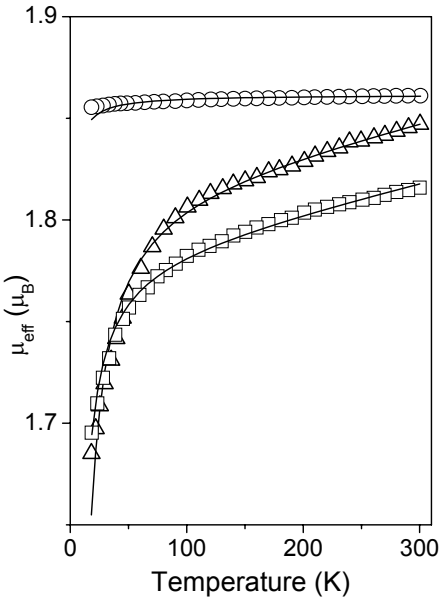

Figure 3.9. Effective magnetic moments of **[Cu(bhac)(Hpyrz)]**·C_2H_5OH (Δ), **[Cu(bhac)(Himdz)]** (O) and **[Cu(bhac)(py)]** (□) as a function of temperature. The solid lines represent the best least-squares fits using the parameters described in the text.

curves indicate the antiferromagnetic character of **2** and **4** and Curie paramagnetic behaviour of **3**. The Curie (C) and Weiss (θ) constants obtained by fitting the data of **3** using Curie-Weiss law are 0.43 and –0.24 K, respectively. The data of **2**·C_2H_5OH and **4** were fitted using the Bleany-Bowers expression[17] with a fixed temperature independent paramagnetism value of 60 x 10^{-6} emu mol^{-1}. The best least-squares fits were obtained with g = 2.097(1) and J = –3.8(1) cm^{-1} for **2**·C_2H_5OH and g = 2.059(1) and J = –2.3(1) cm^{-1} for **4**. Weak antiferromagnetic spin-exchange in similar dicopper(II) species containing two equatorial-apical chloro or acetato bridges are well known.[14]

3.3.6. EPR spectral properties

The room temperature (298 K) X-band EPR spectral profiles of **2** and **4** in powdered phase are very similar. In the g ≈ 2 region, a strong axial signal ($g_{||}$ = 2.14, $g_{\perp}$ = 2.05 for **2** and $g_{||}$ = 2.15, $g_{\perp}$ = 2.05 for **4**) typical of a square-planar or square-pyramidal copper(II) species is observed (Figure 3.10, trace a). On the other hand, a broad and strong asymmetric signal centered at g = 2.08 is observed for **3**. Interestingly all the three complexes display a weak signal (Figure 3.10, top inset) within g = 4.19–4.25. The higher field signal is assigned to the $\Delta M_S = \pm 1$ transition. The origin of the weak signal at the low-field region is perhaps the $\Delta M_S = \pm 2$ transition expected for weakly coupled dicopper(II) species.[18–21]

The EPR spectra of all the complexes in frozen (110 K) solutions have been recorded to examine the concentration dependence of the self-organization process to form exchange coupled species. The solubility of the complexes is such that solutions having maximum concentration of ~10^{-2} M can be prepared. The EPR spectrum of **2** in frozen (110 K) $CHCl_3$–$C_6H_5CH_3$ (1:1) solution (~10^{-2} M) displays a seven line pattern with an average line spacing of 97 G at g = 4.41 (Figure 3.10, bottom inset) due to the half-field transition. This feature is characteristic of two interacting copper(II) ions. The $\Delta M_S = \pm 1$ transitions are observed in the range 2200–3800 G. Two pairs of signals observed in this region (Figure 3.10, trace b) are due to zero-field splitting and indicate essentially an axial symmetry. Five weak copper hyperfine lines with the average line spacing of 98 G are readily apparent in the range 2200–2850 G. The remaining two lines are not observed due to the following strong

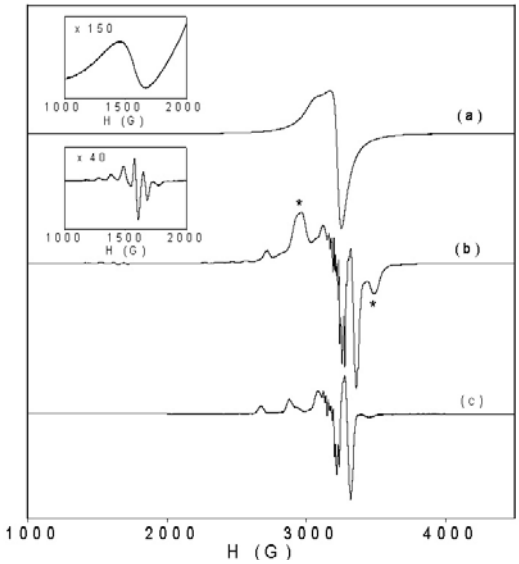

Figure 3.10. EPR spectra of **[Cu(bhac)(Hpyrz)]**·C_2H_5OH: (a) in powder phase at 298 K, (b) in frozen (110 K) chloroform-toluene (1:1) solution (~10^{-2} M), (c) in frozen (110 K) chloroform-toluene (1:1) solution (~10^{-4} M). Insets: Magnified $\Delta Ms = \pm 2$ region for the powder phase (top) and that for the frozen ~10^{-2} M solution (bottom).

signal. Three very weak absorptions with the average line separation of 95 G observed in the range 3500–3800 G are assigned to the second seven-line pattern. The other four lines expected are obscured by the preceding strong signal. These two seven-line patterns centered at ~3454 and ~2552 G are assigned to the parallel signals. The perpendicular components appear as two moderately strong signals (indicated by asterisks in Figure 3.10, trace b) at ~2935 and ~3460 G. In between these two signals, two more strong signals are observed at ~3200 and ~3320 G. The signal at lower field shows the nitrogen super-hyperfine structure. The intensities of these two signals increase with the decrease of the complex concentration. At the same time, as the concentration decreases the intensities of the signals at 2935 and 3460 G, the seven line patterns of the parallel components and the half-field signal decrease. These decreasing signals are associated with the spin-coupled dicopper(II) species. At the lowest concentration of **2** (~10^{-4} M) the spectral features are typical for an axial spectrum of a mononuclear square-planar copper(II) complex (Figure

3.10, trace c).[18] The $g_{||}$, $A_{||}$ and $g_{\perp}$ values are 2.18, 214 G and 2.04, respectively. As two different types of nitrogen atoms are coordinated to the metal ion, nine nitrogen superhyperfine lines are expected. The $g_{\perp}$ signal is split and eight lines with an average line separation of 14 G can be clearly seen.

The spectrum of **3** in frozen (110 K) $CHCl_3$–$C_6H_5CH_3$ (1:1) solution is very similar to the solid state spectrum observed at room temperature. Both the very weak signal at $g \approx 4$ and the strong asymmetric signal at $g \approx 2$ are devoid of any fine structure. However, in frozen (110 K) CH_3OH–C_2H_5OH (1:1) solution (10^{-2} M) of **3**, a seven line pattern at $g = 4.43$ with an average line spacing of 105 G is observed. The spectrum of **4** in frozen (110 K) $CHCl_3$–$C_6H_5CH_3$ (1:1) solution (~10^{-2} M) shows similar seven line pattern with an average line spacing of 98 G at the half field position ($g = 4.46$) as observed for **2** in the same solvent mixture. Although in frozen solutions the concentrations are very similar (10^{-2} M) the intensity of this half-field signal decreases in the order **2** > **4** > **3**. The spectrum of **2** at ~10^{-2} M concentration indicates the presence of spin-coupled dicopper(II) as well as mononuclear square-planar copper(II) species near $g \approx 2$ region (*vide supra*). On further dilution (~10^{-4} M) the spectrum suggests essentially mononuclear species. In contrast, the spectra of frozen solutions of both **3** and **4** having ~10^{-2} M concentrations although display the weak half-field signal but the signals corresponding to dicopper(II) species near $g \approx 2$ could not be identified. In this region, the spectral profiles are very similar to that observed for ~10^{-4} M solution of **2** and indicate the presence of predominantly mononuclear square-planar copper(II) species. The $g_{||}$, $A_{||}$ and $g_{\perp}$ values are 2.17, 207 G and 2.04 and 2.18, 215 G and 2.04 for **3** and **4**, respectively. As observed for **2**, the nitrogen super-hyperfine lines on the $g_{\perp}$ signal are clearly visible in both cases. With dilution the weak seven line pattern near $g \approx 4$ disappears for both **3** and **4**.

The solid state EPR spectral features suggest that the spin-coupled copper(II) species exist for all the three complexes. The solid state structures show dimeric units for both **2** and **4** having equatorial-apical O bridges and the cryomagnetic measurements also indicate weak antiferromagntically coupled dicopper(II) system. However, there is no equatorial-apical bridging for **3**. But the molecules of **3** are connected by N–H···N hydrogen bonds and C–H···π interactions (*vide supra*). Spin-exchange in copper(II) complexes through hydrogen bonds has been reported earlier.[22] It is very likely that spin-exchange is occurring in a similar fashion in **3**.

In frozen solutions, observation of the seven line pattern at $g \approx 4.4$ in each case indicates the presence of spin-coupled species. However, the differences in the intensities of this half-field signal and of the spectral profiles in the $g \approx 2$ region suggest that the concentration needed for the aggregation of the complex molecules increases in the order **2** < **4** < **3**. The nature of the spin-coupled species in frozen solution is not clear. Two possible ways for the formation of dimeric units are (a) mutual involvement of two molecules in equatorial-apical bridging via metal coordinated O atoms as observed in the solid state for both **2** and **4** and (b) π···π interactions between two molecules as observed for **1**.

3.4. Conclusion

Three new ternary mononuclear square-planar complexes having the general formula [Cu(bhac)(hc)] with a tridentate dibasic O,N,O-donor ligand ($bhac^{2-}$) and monodentate neutral sp^2 N donor heterocycles (hc = pyrazole, imidazole and pyridine) have been prepared and structurally characterized. The analogous complex, [Cu(bhac)(dmpz)] (**1**) (dmpz = 3,5-dimethylpyrazole), described in the previous chapter forms a one-dimensional assembly with alternate short and long Cu···Cu distances due to π-overlapping of the chelate rings and the heterocycle rings. One of the prerequisites for a π-stacked assembly is the planarity of the whole molecule.[23,24] However, there are subtle variations in the relative orientations of both the phenyl ring plane of $bhac^{2-}$ and the heterocycle ring plane with respect to the plane constituted by rest of the molecule and hence in the extent of non-planarity of the whole molecule in these square-planar complexes. As a result, the nature and the directionality of the intermolecular weak interactions and the ensuing supramolecular structures of these apparently very similar complexes differ drastically. Among all the four complexes only **1** is sufficiently planar to give a π-stacked one-dimensional arrangement. Although the solvated molecules of [Cu(bhac)(pyz)] (**2**·C_2H_5OH) form a similar one-dimensional array but in a different way. On the other hand, [Cu(bhac)(imd)] (**3**) and [Cu(bhac)(py)] (**4**) assemble to infinite two-dimensional and three-dimensional network, respectively. In the solid state as well as in frozen solution, weak antiferromagnetic spin exchange is operative in each complex presumably via the intermolecular weak interactions.

References

1 Hatfield, W. E. *Theory and Applications of Molecular Paramagnetism*; Boudreaux, E. A.; Mulay, L. N., Eds.; Wiley, New York, 1976; pp. 491.

2 *SMART*; 5.630, Eds.; *SAINTPLUS*; 6.45, Eds.; Bruker AXS, Inc.: Madison, WI, USA, 2003.

3 *SADABS*; 2.10, Eds.; Bruker AXS, Inc.: Madison, WI, USA, 2003.

4 North, A. C. T.;Philips, D. C.; Mathews, F. S. *Acta Crystallogr., Sect. A* **1968**, *24*, 351.

5 Farrugia, L. J. *J. Appl. Crystallogr.* **1999**, *32*, 837.

6 Sheldrick, G. M. SHELX-97 Structure Determination Software, University of Go¨ttingen, Go¨ttingen, Germany, 1997.

7 McArdle, P. *J. Appl. Crystallogr.* **1995**, *28*, 65.

8 Spek, A. L. Platon98 Molecular Graphics Software, University of Glasgow, UK, 1998.

9 Sangeetha, N. R.; Baradi, K.; Gupta, R.; Pal, C. K.; Manivannan, V.; Pal, S. *Polyhedron* **1999**, *18*, 1425.

10 Nakamoto, K. *Infrared and Raman Spectra of Inorganic and Coordination Compounds;* Wiley, New York, 1986; pp. 241–244.

11 Pal, S. N.; Pal, S. *J. Chem. Soc., Dalton Trans.* **2002**, 2102.

12 Maslen, H. S.; Waters, T. N. *Coord. Chem. Rev.* **1975**, *17*, 137.

13 Sangeetha, N. R.; Pal, C. K.; Ghosh, P.; Pal, S. *J. Chem. Soc., Dalton Trans.* **1996**, 3293.

14 Sangeetha, N. R.; Pal, S. *Polyhedron* **2000**, *19*, 1593.

15 Steiner, T. *J. Chem. Soc., Chem. Commun.* **1995**, 95.

16 Nishio, M. *CrystEngComm* **2004**, *6*, 130.

17 Bleany, B.; Bowers, K. D. *Proc. R. Soc. London, Ser. A* **1952**, *214*, 451.

18 Hasty, E. F.; Colburn, T. J.; Hendrickson, D. N. *Inorg. Chem.* **1973**, *12*, 2414.

19 Hasty, E. F.; Wilson, L. J.; Hendrickson, D. N. *Inorg. Chem.* **1978**, *17*, 1834.

20 Greenaway, A. M.; O'Connor, C. J.; Overman, J. W.; Sinn, E. *Inorg. Chem.* **1981**, *20*, 1508.

21 Costes, J.–P.; Dahan, F.; Laurent, J.-P. *Inorg. Chem.* **1985**, *24*, 1018.

22 Desplanches, C.; Ruiz, E.; Rodríguez-Fortea, A.; Alvarez, S. *J. Am. Chem. Soc.* **2002**, *124*, 5197.

23 Janiak, C. *J. Chem. Soc.*, *Dalton Trans.* **2000**, 3885.

24 Hunter, C. A.; Saunders, J. K. M. *J. Am. Chem. Soc.* **1990**, *112*, 5525.

Chapter 4

Ternary copper(II) complexes with tridentate salicylaldehyde benzoylhydrazone and monodentate N–heterocycles[§]

Synthesis, characterization and physical properties of four ternary copper(II) complexes having the general formula [Cu(bhs)(hc)], with a tridentate Schiff base, N-(benzoyl)-N′-(salicylidene)hydrazine (H_2bhs) and monodentate N-heterocycles (hc = 3,5-dimethylpyrazole, pyrazole, imidazole and pyridine) are described in this chapter. The crystal structures of all the complexes have been determined by X-ray crystallography. Cryomagnetic and EPR spectral measurements show weak antiferromagnetic spin-exchange in all four complexes. In the solid state, the complexes having 3,5-dimethylpyrazole, imidazole and pyridine as the heterocyclic ligand, exist as centrosymmetric dimeric species due to weak apical coordination of the metal bound phenolate-O. There are two independent molecules in the asymmetric unit of the complex with pyrazole. Only one of them forms the centrosymmetric dimeric species due to weak apical coordination of the metal bound amide-O. In the crystal lattice, due to various non-covalent intermolecular interactions such as π–π, C–H···π, C–H···N, O–H···N and N–H···O interactions involving the complex and the solvent molecules lead diverse one- and two-dimensional supramolecular structures for all the complexes.

4.1. Introduction

In the preceding two chapters, we have seen how minor variations in the molecular structures of very similar complex molecules, [Cu(bhac)(hc)], affect the self-assembly patterns and the crystal packing motifs. Copper(II) complexes of another tridentate Schiff base N-(benzoyl)-N'-(salicylidene) (H_2hbs, Figure 4.1) very similar to H_2bhac are reported to be potent inhibitors of DNA synthesis and cell

[§] This work has been published in *J. Mol. Struct.*, **2005**, *753*, 68-79.

growth.[1–5] This Schiff base is reported to have mild bacteriostatic activity.[6] A range of analogous compounds has been also investigated as potential oral iron-chelation drugs for genetic disorders such as thalassemia.[7,8] In this chapter, we have explored the intermolecular interactions in the solid state and the self-assembly patterns of ternary copper(II) complexes with H_2bhs and various N-donor heterocycles such as 3,5-dimethylpyrazole (dmpz), pyrazole (pyz), imidazole (imd) and pyridine (py). In addition we have also discussed the solution state behavior of all the complexes.

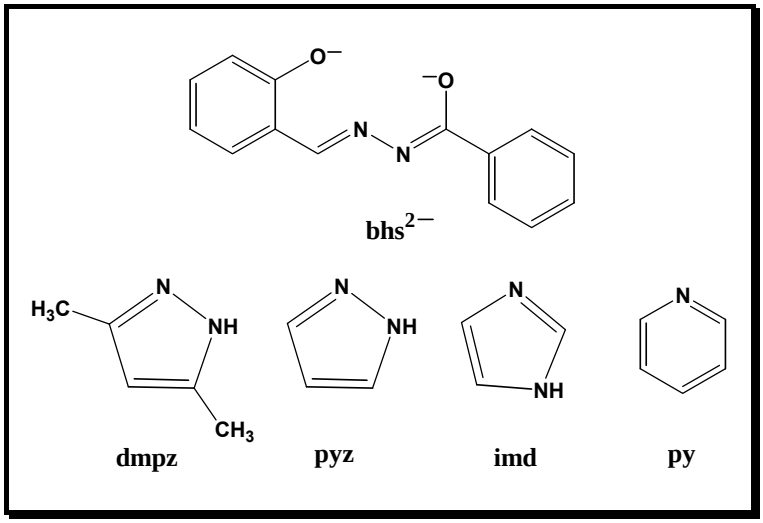

Figure 4.1.

4.2. Experimental section

4.2.1. Materials

The Schiff base, N-(benzoyl)-N'-(salicylidene)hydrazine (H_2bhs) was prepared in 80 % yield by the condensation of one mole equivalent of salicylaldehyde with one mole equivalent of benzoylhydrazine in boiling methanol. All other chemicals and solvents used in this work were of analytical grade available commercially and were used without further purification.

4.2.2. Physical measurements

Microanalytical data (C, H, N) were obtained with a Thermo Finnigon Flash EA1112 elemental analyzer. Infrared spectra were collected by using KBr pellets on a Jasco-5300 FT-IR spectrophotometer. A Shimadzu 3101-PC UV/vis/NIR spectrophotometer was used to record the electronic spectra. Solution electrical conductivities were measured with a Digisun DI-909 conductivity meter. EPR spectra were recorded on a Jeol JES-FA200 spectrometer. The variable temperature (18–300 K) magnetic susceptibility measurements with powdered samples of the complexes were performed using the Faraday technique with a set-up comprising a George Associates Lewis coil force magnetometer, a CAHN microbalance and an APD closed-cycle cryostat. $Hg[Co(NCS)_4]$ was used as the standard. Diamagnetic corrections calculated from Pascal's constants[9] were used to obtain the molar paramagnetic susceptibilities.

4.2.3. Synthesis

[Cu(bhs)(dmpz)] (**5**)

To a methanol solution (50 ml) of the Schiff base (H_2bhs) (0.240 g, 1.0 mmol) and 3,5-dimethylpyrazole (dmpz) (0.288 g, 3.0 mmol), a methanol solution (20 ml) of $Cu(O_2CCH_3)_2{\cdot}H_2O$ (0.199 g, 1 mmol) was added gradually with stirring over a period of 5 min. The resulting green solution was stirred at room temperature for an additional period of 2 h. The volume of the reaction mixture was reduced to 25 ml on a steam bath, cooled to room temperature and filtered. The filtrate was kept in air for slow evaporation. The greenish brown crystalline material that separated after about

3-4 days was collected by filtration, washed with ethanol and dried in air. Yield, 0.35 g (87%). Anal. calcd. for $CuC_{19}H_{18}N_4O_2$: C, 57.35; H, 4.56; N, 14.08. Found: C, 57.13; H, 4.44; N, 13.92. Selected IR bands (cm^{-1}): 3272(s), 3033(w), 2926(w), 1612(s), 1597(s), 1504(s), 1442(s), 1172(s), 1024(s), 786(s), 437(m). Electronic spectral data in $CHCl_3$ (λ_{max} (nm) (ε (M^{-1} cm^{-1}))): 571 (150), 398sh (14,500), 382 (16,400), 329 (15,200), 314(18,300), 302 (17,100), 291sh (14,800), 248 (22,500).

[Cu(bhs)(pyz)]·0.5H_2O (**6**·0.5H_2O)

This complex was synthesized in 77% yield from H_2bhs, $Cu(O_2CCH_3)_2·H_2O$ and pyrazole (1:1:4 mole ratio) using the same procedure as described for **5**. It was isolated in the form of a greenish brown crystalline material. Anal. calcd. for $CuC_{17}H_{15}N_4O_{2.5}$: C, 53.91; H, 3.99; N, 14.79. Found: C, 53.74; H, 4.03; N, 14.58. Selected IR bands (cm^{-1}): 3290(s), 3056(w), 2921(w), 1616(s), 1508(s), 1467(s), 1354(s), 1149(s), 1045(s), 754(s), 613(s), 462(w). Electronic spectral data in $CHCl_3$ (λ_{max} (nm) (ε (M^{-1} cm^{-1}))): 549 (140), 396sh (12,300), 382 (13,400), 329 (17,000), 314 (17,600), 298 (19,000), 288sh (18,300), 247 (26,600).

[Cu(bhs)(imd)]·CH_3OH (**7**·CH_3OH)

This complex was synthesized in 84% yield and isolated as greenish brown crystalline material in the same manner as detailed for **5** by reacting H_2bhs, $Cu(O_2CCH_3)_2·H_2O$ and imidazole (1:1:4 mole ratio) in methanol. Anal. calcd. for $CuC_{18}H_{18}N_4O_3$: C, 53.81; H, 4.52; N, 13.94. Found: C, 53.73; H, 4.31; N, 13.79. Selected IR bands (cm^{-1}): 3130(s), 3030(w), 2934(w), 1614(s), 1506(s), 1442(s), 1197(s), 850(s), 709(s), 453(s). Electronic spectral data in $CHCl_3$ (λ_{max} (nm) (ε (M^{-1} cm^{-1}))): 560 (160), 399sh (16,400), 388 (17,600), 330 (16,100), 315(17,200), 301 (15,100), 290sh (13,600), 263sh (18,600), 248 (21,500).

[Cu(bhs)(py)] (**8**)

Using H_2bhs, $Cu(O_2CCH_3)_2·H_2O$ and pyridine (1:1:4 mole ratio), synthesis of **8** was performed by following the procedure similar to that described for **5** in 85% yield. The complex was obtained as green crystalline solid. Anal. calcd. for $CuC_{19}H_{15}N_3O_2$: C, 59.91; H, 3.97; N, 11.03. Found: C, 59.84; H, 3.88; N, 10.95.

Selected IR bands (cm^{-1}): 3070(w), 3028(w), 1599(s), 1502(s), 1486(s), 1199(s), 758(s), 451(m). Electronic spectral data in $CHCl_3$ (λ_{max} (nm) (ε (M^{-1} cm^{-1}))): 562 (180), 398sh (16,900), 387 (17,900), 330(16,800), 315 (19,400), 302 (17,800), 291sh (15,900), 252 (52,000).

3.2.4. X-ray crystallography

Single crystals of all the complexes were collected directly from the products obtained from methanolic reaction mixtures. Unit cell parameters for **5**, **7** and **8** were determined by the least-squares fit of 25 reflections on an Enraf-Nonius Mach-3 single crystal diffractometer using graphite monochromated Mo Kα radiation (λ = 0.71073 Å). The intensity data were collected by ω-scan method at 298 K. The intensities of three check reflections were measured after every 1.5 h during the data collection and no decay was observed for any of the three crystals. In each case, the ψ -scans[10] of selected reflections were used for an empirical absorption correction. The programs of the WinGX package[11] were used for data reduction and absorption correction. Unit cell parameters and the intensity data for **6** were obtained on a Bruker-Nonius SMART APEX CCD single crystal diffractometer, equipped with a graphite monochromator and a Mo Kα fine-focus sealed tube (λ = 0.71073 Å) operated at 2.0 kW. The detector was placed at a distance of 6.0 cm from the crystal. Data were collected at 298 K with a scan width of 0.3º in ω and an exposure time of 10 sec/frame. The SMART software was used for data acquisition and the SAINT-Plus software was used for data extraction[12]. An absorption correction was performed with the help of SADABS program[13]. In each case, the structure was solved by direct methods and refined on F^2 by full-matrix least-squares procedures. All non-hydrogen atoms were refined anisotropically. The N–H protons of the heterocycles and the protons of the solvent molecules in **5**, **6** and **7** were located in the corresponding difference maps and refined with $U_{iso}(H) = 1.2U_{eq}(N)$ and $U_{iso}(H) = 1.5U_{eq}(O)$, respectively. Other hydrogen atoms in all the structures were included in the structure factor calculation at idealized positions by using a riding model. The SHELX-97 programs[14] were used for structure solution and refinement. The ORTEX6a[15] and Platon packages[16] were used for molecular graphics. Significant crystallographic data for **5**, **6**·0.5H_2O, **7**·CH_3OH and **8** are summarized in Table 4.1.

Table 4.1. Crystallographic parameter for **5**, **6**·0.5H_2O, **7**·CH_3OH and **8**.

Complex	**5**	**6**·0.5H_2O	**7**·CH_3OH	**8**
Chemical formula	$CuC_{19}H_{18}N_4O_2$	$CuC_{17}H_{15}N_4O_{2.5}$	$CuC_{18}H_{18}N_4O_3$	$CuC_{19}H_{15}N_3O_2$
Formula weight	397.91	378.87	401.90	380.88
Crystal system	Monoclinic	Monoclinic	Monoclinic	Triclinic
Space group	$P2_1/c$	$P2_1/n$	$P2_1/c$	$P\bar{1}$
T(K)	298	298	298	298
a (Å)	10.6027(11)	19.0475(13)	11.6683(19)	7.9056(18)
b (Å)	7.7087(10)	7.4712(5)	11.0176(9)	10.823(3)
c (Å)	21.9787(19)	24.3667(17)	13.771(3)	11.054(2)
α (°)	90	90	90	97.38(2)
β (°)	95.501(7)	112.7660(10)	91.835(18)	106.356(17)
γ (°)	90	90	90	109.49(2)
2θ(°)	3.72–54.94	3.46–56.60	3.50–54.98	3.96–54.94
V (Å^3)	1788.1(3)	3197.4(4)	1769.5(5)	829.4(3)
Z	4	8	4	2
μ (mm^{-1})	1.242	1.387	1.260	1.334
N-collected	4388	30468	4275	3805
N-unique	4077	7095	4053	3805
N [$I \geq 2\sigma(I)$]	2771	2885	3279	3326
Parameters	240	454	242	226
*R*1[a], *wR*2[b] [$I \geq 2\sigma(I)$]	0.0362, 0.0795	0.0550, 0.0701	0.0324, 0.1006	0.0332, 0.0851
*R*1[a], *wR*2[b] [all data]	0.0738, 0.0919	0.1663, 0.0891	0.0492, 0.1401	0.0403, 0.0894
GOF[c] on F^2	1.032	0.752	1.153	1.057
Largest peak and hole (*e* Å^{-3})	0.321, –0.272	0.504, –0.463	0.434, –0.570	0.354, –0.494

[a] $R1 = \sum||F_o| - |F_c||/\sum|F_o|$. [b] $wR2 = \{\sum[(F_o^2 - F_c^2)^2]/\sum[w(F_o^2)^2]\}^{1/2}$.

[c] $GOF = \{\sum[w(F_o^2 - F_c^2)^2]/(n - p)\}^{1/2}$ where n is the number of reflections and p is the number of parameters refined; $w = 1/[\sigma^2(F_o^2) + (aP)^2 + bP]$.

4.3. Results and discussion

4.3.1. Synthesis and characterization

All four complexes have been synthesized in good yields by reacting one mole equivalent each of H_2bhs and $Cu(O_2CCH_3)_2{\cdot}H_2O$ and 3-4 mole equivalents of the corresponding heterocycle in methanol. In each case, the metal ion solution was added to the solution of a mixture of H_2bhs and an excess amount of heterocycle compared to the stoichiometric amount required to prevent the precipitation of the insoluble dimeric species commonly obtained with similar tridentate dibasic ligands.[17,18] The elemental analyses data are consistent with the proposed empirical formulae given in the experimental section. The complexes are electrically non-conducting in acetonitrile solutions.

Infrared spectra of **5**, **6**·0.5H_2O and **7**·CH_3OH display a medium to strong band at 3272, 3290 and 3130 cm^{-1}, respectively. This band is most likely associated with the dmpz N–H group for **5** and the heterocycle (pyz and imd) N–H and the solvent O–H group for **6**·0.5H_2O and **7**·CH_3OH. The spectrum of **8** is devoid of any such band in this region. A series of bands observed in the range 3030–2800 cm^{-1} in all the spectra is attributed to the C–H stretches. None of the spectra displays any band assignable to the C=O group of the amide functionality present in the tridentate Schiff base.[19] This observation is consistent with the deprotonation and the enolate form of the amide functionality in each complex. A strong band observed within 1616–1599 cm^{-1} is assigned to the conjugated –N=C–C=N– fragment.[20]

The electronic spectra of the complexes have been recorded in chloroform solutions. Electronic spectral data for all the complexes are given in the experimental section. The spectral profiles are very similar. A weak absorption is observed within 571–549 nm and several intense absorptions appear in the range 398–247 nm Electronic spectrum of [Cu(bhs)(dmpz)] has depicted in Figure 4.2. The weak absorption is assigned to the d–d transition.[21] The higher energy strong absorptions are attributed to the ligand–to–metal charge transfer and the intraligand transitions.

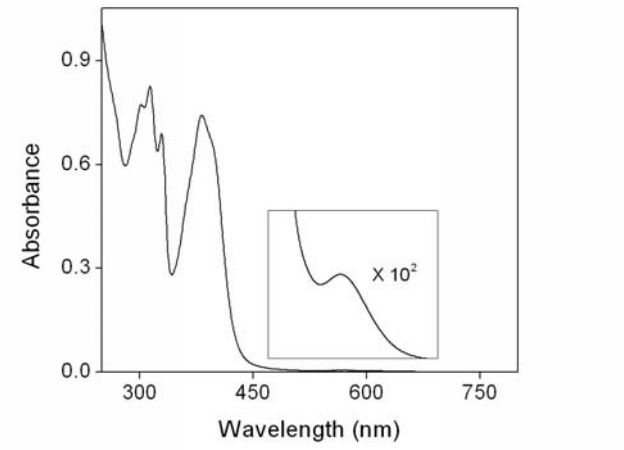

Figure 4.2. Electronic absorption spectrum of **[Cu(bhs)(dmpz)]** (**5**) in chloroform solution. Inset: Magnified d−d transition.

4.3.2. Description of molecular structures

Complexes **5**, **6**·0.5H_2O, **7**·CH_3OH and **8** crystallize in the space groups $P2_1/c$, $P2_1/n$, $P2_1/c$ and $P\bar{1}$, respectively. The asymmetric unit of each of **5** and **8** contains a molecule of the complex and that of **7** contains a complex molecule and a methanol molecule. On the other hand, the asymmetric unit of **6** contains two complex molecules and a water molecule. The bond parameters of both complex molecules in the asymmetric unit of **6** are essentially identical. The structure of **6**·0.5H_2O having the same $P2_1/n$ space group has been reported earlier.[22] Interestingly both structures were determined at room temperature and the unit cell contents are same but there are significant differences in the *c*-axis lengths and hence in the unit cell volumes. In the previously reported structure[22], the bond lengths associated with the metal ions are also unusually longer compared to analogous copper(II) species.

The structures of the complexes are illustrated in Figures 4.3–4.6. The selected bond parameters are listed in Tables 4.2–4.5. In each complex, the metal ion is coordinated to the phenolate-O, the imine-N and the deprotonated amide-O atoms of bhs^{2-} and the imine-N atom of the neutral heterocycle. The C–O and C–N bond lengths in the amide functionality of the tridentate ligand are within 1.286(3)–1.301(4) and 1.311(5)–1.323(5) Å, respectively. These values are consistent

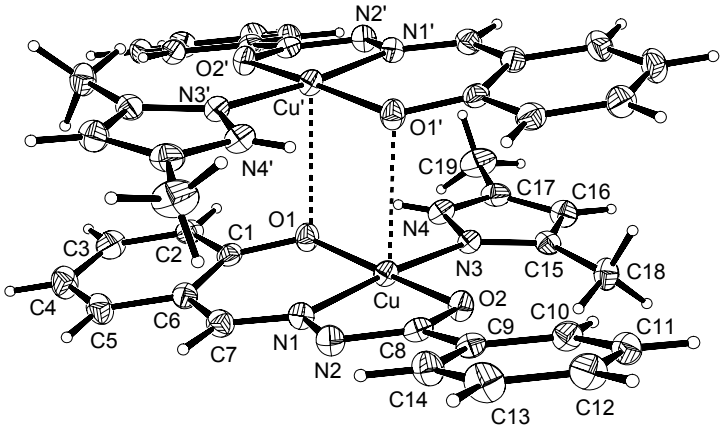

Figure 4.3. Dimeric structure of **[Cu(bhs)(dmpz)]** (**5**) with the atom-labeling scheme. All non-hydrogen atoms are represented by their 25% probability thermal ellipsoids.

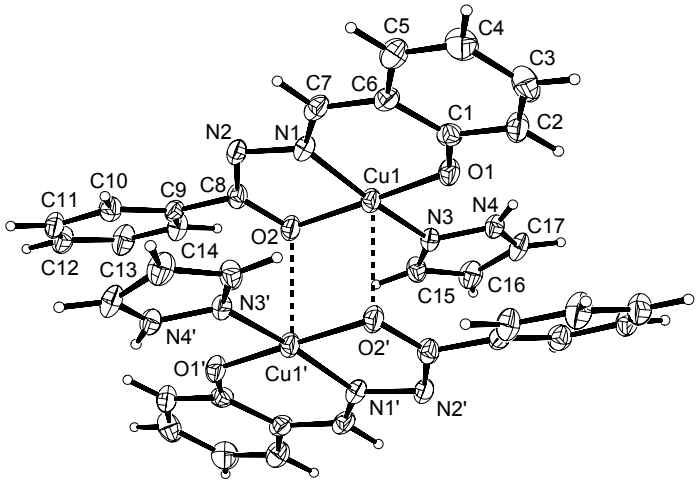

Figure 4.4. Dimeric form of one of the two molecules of **[Cu(bhs)(pyz)]** (**6**) in the asymmetric unit. All non-hydrogen atoms are represented by their 30% probability thermal ellipsoids.

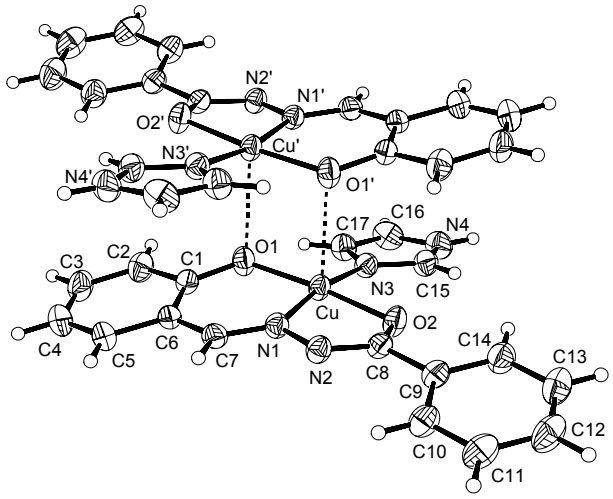

Figure 4.5. Dimeric structure of **[Cu(bhs)(imd)]** (**7**) with the atom-labeling scheme. All non-hydrogen atoms are represented by their 40% probability thermal ellipsoids.

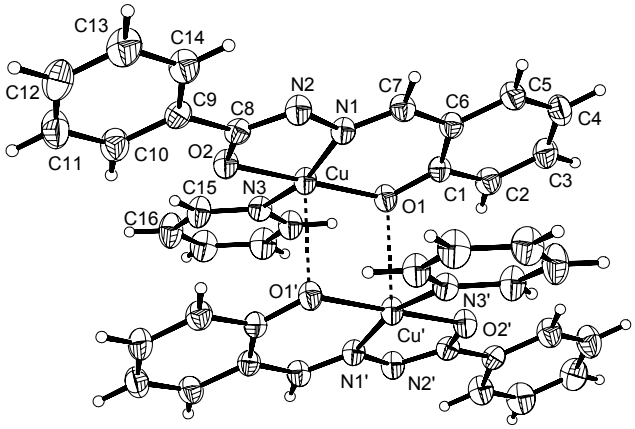

Figure 4.6. Structure of the dimeric form of **[Cu(bhs)(py)]** (**8**) with the atom-labeling scheme. All non-hydrogen atoms are represented by their 35% probability thermal ellipsoids.

with the enolate form of the amide functionality.[23] The Cu–O(phenolate) (1.865(3)–1.9129(15) Å) and Cu–N(imine) (1.888(3)–1.9250(16) Å) bond lengths (Tables 4.2−4.5) are comparable to the bond lengths observed in copper(II)

complexes having the same coordinating atoms.[24,25] The Cu–O(amide) bond lengths are in the range 1.9188(17)–1.950(2) Å. These values are similar to the values reported for deprotonated amide-O coordinated copper(II) complexes[23] and shorter than the values observed in complexes having copper(II) coordinated to O-atom of protonated amide functionality.[24] The Cu–N(heterocycle) bond lengths in all four complexes are unexceptional.[17,18] In each complex, the ligands form a satisfactory O_2N_2 square plane (mean deviations are in the range 0.05–0.15 Å) around the metal ion. There is no significant displacement (0.01–0.09 Å) of the metal centre from this O_2N_2 square-plane. However, none of the four complex molecules as a whole is planar. This is due to the twisting of the phenyl ring plane (mean deviations are in the range 0.003–0.009 Å) of the benzoyl fragment in bhs^{2-} along the C6–C7 bond and that of the heterocycle plane (mean deviations are in the range 0.0005–0.01 Å) along the Cu–N3 bond with respect to the plane containing rest of the molecule (Figures 4.3−4.6). The dihedral angles between the phenyl ring plane and the plane constituted by O1, O2, N1, N2, C1–C8 atoms (mean deviations are in the range 0.05–0.14 Å) are 16.25(12), 8.41(13) and 2.89(15)^o for **5**, **7** and **8**, respectively. The values of this angle in the two molecules present in the asymmetric unit of **6** are 28.59(11) and 23.57(14)^o. Thus the bhs^{2-} is essentially planar in **8** but the same is not true for **5**, **6** and **7**. The dihedral angles between the heterocycle plane and the plane containing O1, O2, N1, N2, C1–C8 atoms are 11.55(12)^o, 11.72(11)^o and 19.72(11)^o for **5**, **7** and **8**, respectively. The values of this dihedral angle are 23.65(16) and 21.75(17)^o for the two molecules of **6**.

Square-planar copper(II) complexes are known to form dimeric species containing equatorial-apical bridges due to the involvement of the metal ion in weak interactions with another atom of a neighbouring molecule at the apical position.[26,27] The molecules of **5**, **7** and **8** form centrosymmetric dimeric units due to weak apical coordination of the phenolate-O in a reciprocal fashion (Figures 4.3, 4.5 and 4.6). The Cu–O1′ distances are 2.857(2), 2.611(3) and 2.523(2) Å for **5**, **7** and **8**, respectively. In the Cu_2O_2 core, the Cu–O1–Cu′ bridge angle and the Cu···Cu′ distance are 89.09(7)^o and 3.4077(7) Å, 94.35(10)^o and 3.3488(10) Å and 96.26(6)^o and 3.3283(8) Å for **5**, **7** and **8**, respectively. Interestingly for **6**, only one of the two molecules present in the asymmetric unit forms this type of dimeric units. However, the amide-O participates in the equatorial-apical bridging instead of the phenolate-O (Figure

4.4). In this Cu_2O_2 core, the Cu1–O2′ and the Cu1···Cu1′ distances are 2.812(3) and 3.3193(10) Å, respectively. The Cu1–O2–Cu1′ bridge angle is 86.78(10)°.

Table 4.2. Selected bond lengths (Å) and angles (°) for **[Cu(bhs)(dmpz)]** (**5**).

Cu-O(1)	1.903(2)	O(1)-C(1)	1.332(3)	N(2)-C(8)	1.321(3)
Cu-O(2)	1.919(2)	O(2)-C(8)	1.286(3)	N(3)-C(15)	1.337(3)
Cu-N(1)	1.925(2)	N(1)-C(7)	1.292(3)	N(3)-N(4)	1.363(3)
Cu-N(3)	1.986(2)	N(1)-N(2)	1.402(3)	N(4)-C(17)	1.326(4)
O(1)-Cu-O(2)	171.15(9)	N(1)-Cu-N(3)	175.27(9)	N(2)-N(1)-Cu	114.86(16)
O(1)-Cu-N(1)	92.57(8)	C(1)-O(1)-Cu	127.11(17)	C(8)-N(2)-N(1)	107.9(2)
O(2)-Cu-N(1)	81.04(8)	C(8)-O(2)-Cu	110.86(16)	C(15)-N(3)-Cu	138.96(18)
O(1)-Cu-N(3)	89.11(8)	C(7)-N(1)-N(2)	117.3(2)	N(4)-N(3)-Cu	116.05(17)
O(2)-Cu-N(3)	97.74(8)	C(7)-N(1)-Cu	127.79(19)	O(2)-C(8)-N(2)	124.6(2)

Table 4.3. Selected bond lengths (Å) and angles (°) for **[Cu(bhs)(pyz)]** (**6**).

Cu(1)-O(1)	1.865(3)	N(2)-C(8)	1.323(5)	O(3)-C(18)	1.322(5)
Cu(1)-N(1)	1.902(3)	N(3)-C(15)	1.317(5)	O(4)-C(25)	1.299(5)
Cu(1)-O(2)	1.929(3)	N(3)-N(4)	1.333(4)	N(5)-C(24)	1.275(5)
Cu(1)-N(3)	1.962(3)	N(4)-C(17)	1.329(5)	N(5)-N(6)	1.399(4)
O(1)-C(1)	1.318(5)	Cu(2)-O(3)	1.875(3)	N(6)-C(25)	1.311(5)
O(2)-C(8)	1.301(4)	Cu(2)-N(5)	1.888(3)	N(7)-C(32)	1.322(5)
N(1)-C(7)	1.284(5)	Cu(2)-O(4)	1.929(3)	N(7)-N(8)	1.338(5)
N(1)-N(2)	1.395(4)	Cu(2)-N(7)	1.963(4)	N(8)-C(34)	1.321(5)
O(1)-Cu(1)-N(1)	95.45(13)	C(7)-N(1)-Cu(1)	126.0(3)	N(5)-Cu(2)-O(4)	81.96(13)
O(1)-Cu(1)-O(2)	176.6(1)	N(2)-N(1)-Cu(1)	115.3(3)	O(3)-Cu(2)-N(7)	90.28(14)
N(1)-Cu(1)-O(2)	81.64(13)	C(8)-N(2)-N(1)	108.7(3)	N(5)-Cu(2)-N(7)	172.8(1)
O(1)-Cu(1)-N(3)	89.71(13)	C(15)-N(3)-N(4)	104.9(4)	O(4)-Cu(2)-N(7)	93.31(14)
N(1)-Cu(1)-N(3)	168.3(1)	C(15)-N(3)-Cu(1)	131.7(3)	C(18)-O(3)-Cu(2)	126.4(3)
O(2)-Cu(1)-N(3)	93.47(12)	N(4)-N(3)-Cu(1)	122.2(3)	C(25)-O(4)-Cu(2)	109.7(3)
C(1)-O(1)-Cu(1)	125.6(3)	O(2)-C(8)-N(2)	123.8(4)	C(24)-N(5)-Cu(2)	126.9(3)
C(8)-O(2)-Cu(1)	110.3(3)	O(3)-Cu(2)-N(5)	94.71(13)	N(6)-N(5)-Cu(2)	115.3(3)
C(7)-N(1)-N(2)	118.7(3)	O(3)-Cu(2)-O(4)	175.5(1)	N(8)-N(7)-Cu(2)	123.9(3)

Table 4.4. Selected bond lengths (Å) and angles (°) for **[Cu(bhs)(imd)]** (**7**).

Cu-O(1)	1.908(2)	O(2)-C(8)	1.289(3)	N(3)-C(15)	1.325(4)
Cu-N(1)	1.915(2)	O(3)-C(18)	1.397(5)	N(3)-C(17)	1.376(4)
Cu-N(3)	1.949(2)	N(1)-C(7)	1.287(3)	N(4)-C(15)	1.331(4)
Cu-O(2)	1.950(2)	N(1)-N(2)	1.392(3)	N(4)-C(16)	1.354(5)
O(1)-C(1)	1.323(3)	N(2)-C(8)	1.314(3)	C(8)-N(2)-N(1)	108.8(2)
O(1)-Cu-N(1)	93.25(9)	N(3)-Cu-O(2)	92.84(8)	C(15)-N(3)-Cu	126.6(2)
O(1)-Cu-N(3)	92.67(9)	C(1)-O(1)-Cu	125.09(19)	N(1)-C(7)-C(6)	124.0(3)
N(1)-Cu-N(3)	169.8(1)	C(8)-O(2)-Cu	109.85(17)	O(2)-C(8)-N(2)	124.6(3)
O(1)-Cu-O(2)	173.94(8)	C(7)-N(1)-N(2)	117.7(2)	O(2)-C(8)-C(9)	117.6(2)
N(1)-Cu-O(2)	80.94(8)	C(7)-N(1)-Cu	127.3(2)		

Table 4.5. Selected bond lengths (Å) and angles (°) for **[Cu(bhs)(py)]** (**8**).

Cu-O(1)	1.913(2)	O(1)-C(1)	1.324(2)	N(3)-C(19)	1.332(3)
Cu-N(1)	1.925(2)	O(2)-C(8)	1.290(2)	N(3)-C(15)	1.335(3)
Cu-O(2)	1.940(2)	N(1)-C(7)	1.285(3)	N(2)-C(8)	1.313(3)
Cu-N(3)	2.022(2)	N(1)-N(2)	1.393(2)	C(6)-C(7)	1.434(3)
O(1)-Cu-N(1)	92.67(7)	O(2)-Cu-N(3)	94.39(7)	N(2)-N(1)-Cu	115.08(12)
O(1)-Cu-O(2)	171.92(6)	C(1)-O(1)-Cu	126.12(12)	C(19)-N(3)-Cu	121.26(14)
N(1)-Cu-O(2)	80.95(7)	C(8)-O(2)-Cu	110.36(12)	C(15)-N(3)-Cu	121.31(14)
O(1)-Cu-N(3)	93.00(7)	C(7)-N(1)-N(2)	117.49(16)	O(2)-C(8)-N(2)	124.78(18)
N(1)-Cu-N(3)	165.12(7)	C(7)-N(1)-Cu	127.04(13)	O(2)-C(8)-C(9)	117.85(17)

4.3.3. Intermolecular interactions and self-assembly

[Cu(bhs)(dmpz)] (**1**)

In the crystal lattice, the dimeric units of **5** are involved in two types of non-covalent intermolecular interactions such as π–π and C–H···π (Figure 4.7). Two dmpz rings of each dimeric unit are involved in π–π interactions with the dmpz rings of the two adjacent neighbours. The dihedral angle (0.007(2)°) between these overlapping dmpz ring planes indicates that they are parallel to each other. The inter-planar and the centroid-to-centroid distances are 3.1853(13) and 3.7198(15) Å, respectively. The difference in these two distances indicates that the dmpz rings are slipped. The slip

angle (angle between the normal to the planes and the centroid-centroid vector) is 31.1°.[25] The interdimer Cu···Cu distance is 5.4324(9) Å. Thus in this π-stacked

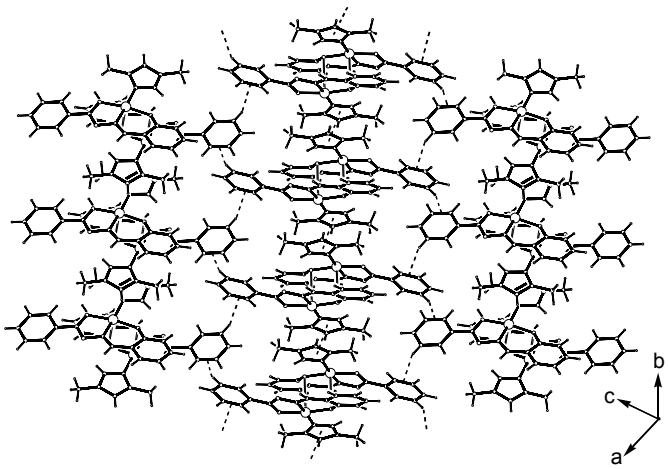

Figure 4.7. Two-dimensional network of **[Cu(bhs)(dmpz)]** (**5**) in the crystal lattice.

chain-like arrangement of **5**, there are alternate short (3.4077(7) Å) and long (5.4324(9) Å) Cu···Cu distances. Both phenyl rings of each dimeric unit in this chain are involved in C–H···π interactions[28] with the phenyl rings of neighbouring dimers belonging to the adjacent chains. Each phenyl ring participates in two C–H···π interactions as donor and also as acceptor. The H13···C10 and H13···C11 distances are 2.904 and 2.835 Å, respectively. The H13···π_C (centre of the C10–C11 bond) and the C–H···π_C angle are 2.786 Å and 155.5°, respectively. Thus the parallel chains of dimers formed by the π–π interactions between the dmpz rings are connected by these C–H···π interactions and an infinite two-dimensional sheet structure is formed (Figure 4.7).

[Cu(bhs)(pyz)]·0.5H_2O (**6**·0.5H_2O)

In case of **6**, one of the two molecules present in the asymmetric unit forms dimeric units due to equatorial-apical bridging (*vide supra*). Each of these dimeric units is involved in the π–π interactions with the neighbouring dimers on both sides.

As a result, they form a one-dimensional structure. Here the chelate rings and the benzene ring of the salicylaldimine fragment are involved in π–π interactions (Figure 4.8). Inter-planar distances between the five- and six-membered chelate rings, the five-membered chelate ring and the benzene ring and two six-membered chelate rings are 3.324(1), 3.456(1) and 3.340(1) Å, respectively. The corresponding centroid-to-centroid distances are 3.7036(5), 3.7774(4) and 3.4929(5) Å, respectively. The five-

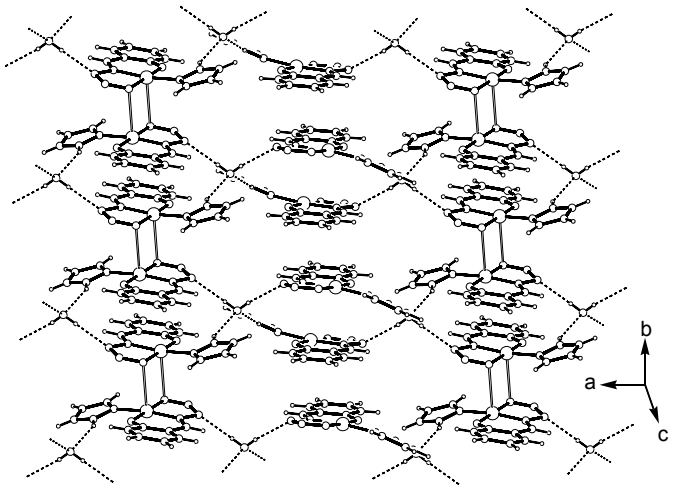

Figure 4.8. Two-dimensional network of **[Cu(bhs)(pyz)]**·0.5H_2O (**6**·0.5H_2O) in the crystal lattice. For clarity the phenyl ring of the benzoyl fragment of the tridentate ligand in each molecule is not shown.

membered chelate ring plane is not exactly parallel with either of the six-membered chelate ring plane or the benzene ring plane. The corresponding dihedral angles are 4.72 and 9.16°, respectively. However, the dihedral angle (0.04°) between the two overlapping six-membered chelate rings suggests that they are essentially parallel to each other. The interdimer Cu···Cu distance is 4.3898(10) Å. Thus as in **5**, there are alternating short and long Cu···Cu distances in the chain formed by the π-stacking of the dimers of **6**.

The other molecule of **6** in the asymmetric unit, that does not form dimer through equatorial-apical bridging, is also involved in π–π interactions with the two

adjacent molecules and a second one-dimensional assembly is formed (Figure 4.8). The π–π interactions are operative in different ways on both sides of each molecule and as a consequence alternating short (4.3165(15) Å) and long (6.6421(13) Å) Cu···Cu distances are observed in this chain-like arrangement of these molecules. On one side of each molecule, both the chelate rings and the benzene ring of the salicylaldimine moiety are overlapping with the six-membered chelate ring and the benzene ring of the salicylaldimine moiety of one neighbour. The inter-planar distances and the dihedral angles between the five- and the six-membered chelate rings, the five-membered chelate ring and the benzene ring and two six-membered chelate rings are 3.337(1) Å and 3.80°, 3.325(1) Å and 5.88° and 3.368(1) Å and 0.0°, respectively. The corresponding centroid-to-centroid distances are 3.337(1), 3.325(1) and 3.368(1) Å, respectively. Between these two molecules the Cu···Cu distance is 4.3165(15) Å. On the other side of the same molecule, the two chelate rings are overlapping with the six-membered chelate ring and the benzene ring of the salicylaldimine moiety of the second neighbour. The inter-planar distances, the centroid-to-centroid distances and the dihedral angles between the five-membered chelate ring and the benzene ring, six-membered chelate ring and the benzene ring and two six-membered chelate rings are 3.460(1), 3.777(4) Å and 5.88°; 3.408(1), 3.563(3) Å and 2.37° and 3.462(1), 4.022(3) Å and 0.0°, respectively. Here the Cu···Cu distance is 6.6421(13) Å.

In the crystal lattice of **6**·0.5H_2O, these two π-stacked one-dimensional structures are roughly parallel to each other. The water molecules sit in between these alternating columns of the dimers and the monomers of **6**. These columns are connected to each other by hydrogen bonding interactions between the water molecules, pyrazole N–H groups and the deprotonated and uncoordinated amide N-atoms of the complex molecules. Due to these hydrogen bonds an infinite two-dimensional layered structure is formed (Figure 4.8). The hydrogen bonding parameters are listed in Table 4.6. Each water molecule is involved in four hydrogen bonds and performs the role of a bridge between four molecules. It acts as donor to the two amide N-atoms of two complex molecules belonging to the two adjacent columns and as acceptor from the N–H groups of two pyrazole ligands from two other complex molecules belonging to the same two columns (Figure 4.8).

Table 4.6. Intermolecular hydrogen bond distances (Å) and angles (°).

Complex	Interaction	*d* (Å)	*D* (Å)	*θ* (°)
6·0.5H_2O	O(5)–H(5B)···N(6)	2.23(5)	2.948(5)	170(6)
	O(5)–H(5A)···N(2)[a]	2.19(5)	3.012(5)	174(5)
	N(4)–H(4P)···O(5)	2.37(4)	3.021(5)	143(4)
	N(8)–H(8P)···O(5)[b]	2.34(4)	3.003(5)	141(4)
7·CH_3OH	N(4)–H(4I)···O(3)	1.90(4)	2.729(4)	170(4)
	O(3)–H(3A)···N(2)[c]	1.90(5)	2.779(3)	175(5)

Symmetry transformations used to generate equivalent atoms: a = 1 – x, 1 – y, –z; b = 2 – x, 1 – y, –z and c = x, 1 + y, z.

[Cu(bhs)(imd)]·CH_3OH (**7**·CH_3OH)

In the crystal lattice, the self-assembly of the dimeric units of **7** and the methanol molecules due to hydrogen bonding interactions leads to a one-dimensional array of the solvated species. The hydrogen bonding parameters are given in Table 4.6. Each methanol molecule participates in two hydrogen bonds whereas each dimer participates in four hydrogen bonds and the chain-like arrangement is formed (Figure 4.9). On one side the O–H group of the methanol acts as a donor to the uncoordinated and deprotonated amide-N atom of one dimer and on the other side it acts as an acceptor from the imidazole N–H group of another dimer. Two methanol molecules bridge two dimers in a reciprocal fashion with respect to the donor-acceptor behavior. There are no significant short contacts or non-covalent interactions between the adjacent chains.

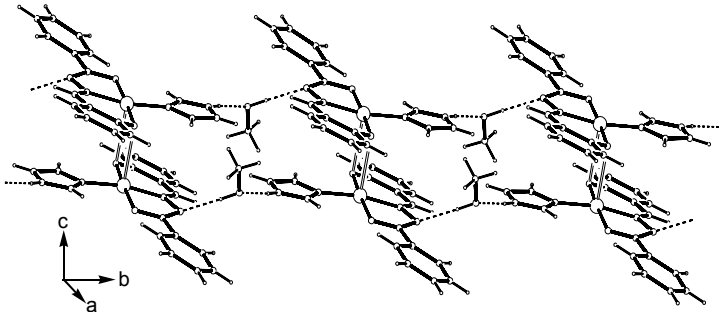

Figure 4.9. One-dimensional ordering of **[Cu(bhs)(imd)]**·CH_3OH (**7**·CH_3OH) in the crystal lattice.

[Cu(bhs)(py)] (**8**)

As observed for **5** and **6**, the dimeric units of **8** also form a π-stacked one-dimensional structure. On both sides of each dimer the six-membered chelate rings and the salicyaldimine benzene rings are involved in π–π interactions with the salicyaldimine benzene rings and the six-membered chelate rings of the adjacent dimers (Figure 4.10). The dihedral angle between the overlapping six-membered chelate ring and the salicyaldimine benzene ring is 3.87°. The inter-planar and the centroid-to-centroid distances are 3.202(1) and 3.731(1) Å, respectively. The shorter

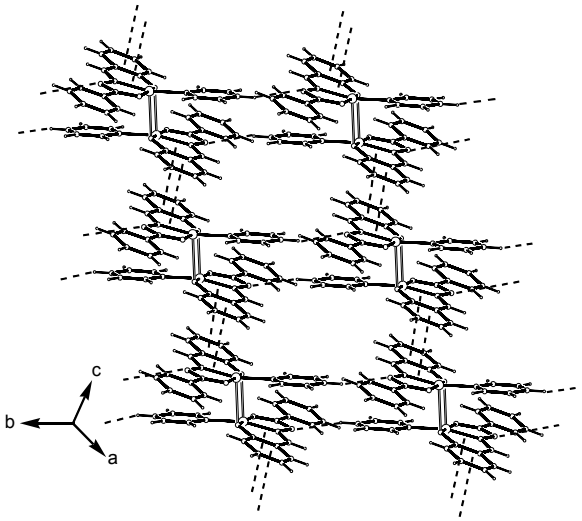

Figure 4.10. Two-dimensional layered structure of **[Cu(bhs)(py)]** (**8**) in the crystal lattice.

inter-planar distance indicates that the overlapping rings are slipped. The slip angle is 30.9°. In addition to the above, the *para*-CH of the metal coordinated pyridine of one dimer is somewhat closer to the uncoordinated sp^2 amide N-atom of another dimer. The H17···N2 (2.68 Å) and C17···N2 (3.599(3) Å) distances and the C17–H17···N2 angle (169.4°) perhaps indicate a weak C–H···N interaction.[29] These interactions between the two adjacent dimers are operative in a reciprocal way and are roughly orthogonal to the π–π interactions. As a result the parallel π-stacked one-dimensional

structures are connected by these interactions and an infinite two-dimensional layered structure is assembled (Figure 4.10).

4.3.4. Magnetic Properties

Magnetic susceptibilities of all the complexes in powdered form have been measured in the temperature range 20–300 K at a constant magnetic field of 5 kG. The effective magnetic moments at 300 K are in the range 1.78–1.99 μ_B. These values are consistent with the spin-only moments expected for d^9 systems. On cooling there is no significant change in the moment values. At 20 K the moments are in the range 1.73–1.89 μ_B. In each case, a linear plot is obtained when the inverse molar susceptibilities are plotted against temperature (Figure 4.11) with a small negative

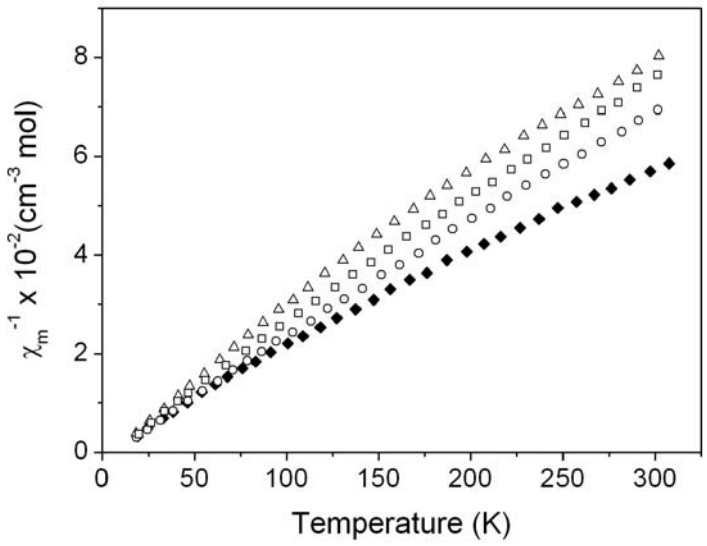

Figure 4.11. The inverse molar magnetic susceptibility of **[Cu(bhs)(dmpz)]**·(**5**) [♦], **[Cu(bhs)(pyz)]**·0.5H_2O (**6**) [Δ], **[Cu(bhs)(imd)]**·CH_3OH (**7**) [O] and **[Cu(bhs)(py)]** (**8**) [□] as a function of temperature.

intercept on the temperature axis. The data were fit using the expression for Curie-Weiss law. The Curie (C) and Weiss (θ in K) constants are 0.51 and –9.8, 0.45 and –9.6, 0.48 and –3.4, and 0.40 and –4.8 for **5**, **6**·0.5H_2O, **7**·CH_3OH and **8**, respectively.

The values of the Weiss constants indicate a weak antiferromagnetic interaction between the copper(II) centres in these complexes.

4.3.5. EPR spectral properties

X-band EPR spectral profiles of polycrystalline **5** and **7**·CH_3OH at 300 K are very similar. A strong axial signal ($g_{||}$ = 2.16, $g_{\perp}$ = 2.04 for **1** and $g_{||}$ = 2.17, $g_{\perp}$ = 2.04 for **7**·CH_3OH) is observed near $g \approx 2$ (Figure 4.12, trace (a)). However, a broad and strong asymmetric signal centred at $g \approx 2$ is observed for both **6**·$0.5H_2O$ and **8**. Such EPR spectra are typical for square-planar or square-pyramidal copper(II) species.[30–33] Interestingly all the complexes display a weak signal within g = 4.18–4.29 (Figure 4.12, inset (i)). The origin of this weak signal is perhaps the $\Delta M_S = \pm 2$ transition expected for weakly coupled dicopper(II) species.[32,33]

EPR spectra of all the complexes in frozen (110 K) chloroform-toluene (1:1) solutions were recorded. The solubility of the complexes allowed to prepare solutions having maximum concentration of ~10^{-2} M. All the spectra display a seven-line pattern within g = 4.44–4.49 with an average line spacing in the range 89–98 G due to the $\Delta M_S = \pm 2$ transition (Figure 4.12, inset (ii)). This seven-line pattern is typical of spin-coupled dicopper(II) systems and confirms the existence of such species in frozen solutions of all four complexes.[34–36] Although in frozen solutions the concentrations are very similar (~10^{-2} M) the intensity of this half-field signal decreases in the order **5** > **6**·$0.5H_2O$ > **8** > **7**·CH_3OH. For all four complexes the intensity of this signal diminishes with dilution.

For **5** the more prominent features near $g \approx 2$ region (Figure 4.12, trace (b)) indicate the characteristic axial spectrum ($g_{||}$ = 2.20, $A_{||}$ = 207 G and $g_{\perp}$ = 2.05) of a mononuclear square-planar copper(II) species.[31–35] As two different types of N-atoms are coordinated to the metal ion, nine nitrogen super-hyperfine lines are expected. The $g_{\perp}$ signal is split into six lines with an average line separation of 15 G. A close scrutiny of the 2200–3850 G range in the spectrum of **5** reveals the presence of weak signals assignable to the $\Delta M_S = \pm 1$ transitions for a spin-coupled dicopper(II) species (Figure 4.12, trace (b)). Two pairs of signals observed in this region are due to the zero-field splitting and suggest an axial symmetry.[36–40] Five weak copper hyperfine lines with the average line spacing of 89 G are readily apparent in the range 2150–2600 G (Figure 4.12, inset (iii)). The remaining two lines are not observed due

to the following strong signal. Four more weak absorptions with the average line separation of 86 G are observed in the range 3550–3850 G (Figure 4.12, inset (iv)). These are likely to be the part of the second seven-line pattern.[41–43] These two seven-line patterns centered at g = 2.66 and 1.79 are assigned to the parallel signals. The perpendicular components appear as two weak signals (indicated by asterisks in Figure 4.12, trace (b)) at g = 2.20 and 1.93. The intensities of these signals and the half-field signal associated with the spin-coupled dicopper(II) species decrease with the decrease of the complex concentration in frozen solution.[44,45] The spectrum of **5** at ~10^{-4} M concentration does not indicate the presence of any dicopper(II) species and only the axial spectrum of a mononuclear square-planar copper(II) species is observed (Figure 4.12, trace (c)).

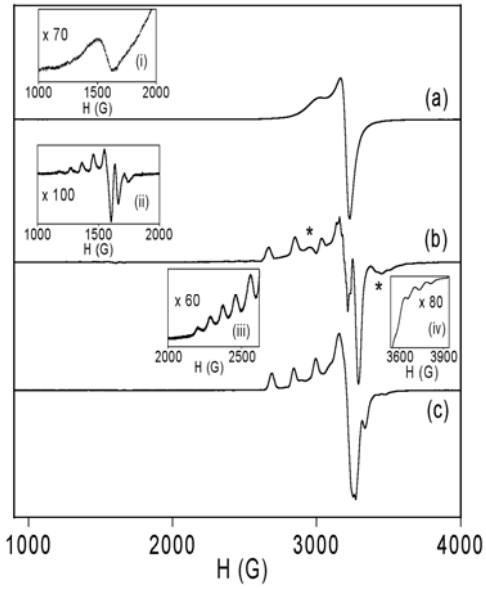

Figure 4.12. EPR spectra of **[Cu(bhs)(dmpz)]** (**5**): (a) in powder form at 300 K, (b) ~10^{-2} M and (c) ~10^{-4} M frozen (110 K) chloroform-toluene (1:1) solutions. Insets: (i) and (ii) magnified $\Delta Ms = \pm 2$ region for the powder and frozen ~10^{-2} M solution, respectively. (iii) and (iv) magnified parallel components in the $\Delta Ms = \pm 1$ region for the frozen ~10^{-2} M solution.

Like **5** the frozen solution (~10^{-2} M) of **6**·0.5H_2O shows the axial spectrum ($g_{||}$ = 2.21, $A_{||}$ = 202 G and $g_{\perp}$ = 2.06) indicating predominantly mononuclear copper(II) species. The signals due to the $\Delta M_S = \pm 1$ transitions associated with the dicopper(II) species are observed but the intensities are very low compared to that observed for **5** having the similar concentration. Here the perpendicular components are relatively more visible than the parallel components. In contrast to **5** and **6**·0.5H_2O, both **7**·CH_3OH and **8** in frozen solutions having ~10^{-2} M concentrations although display the weak half-field signal but do not show the signals corresponding to the dicopper(II) species near $g \approx 2$. In this region, the spectral profiles are very similar to that observed for ~10^{-4} M solutions of **5** and **6**·0.5H_2O indicating the presence of essentially mononuclear square-planar copper(II) species. The $g_{||}$, $A_{||}$ and $g_{\perp}$ values are 2.18, 221 G and 2.04 and 2.21, 202 G and 2.05 for **7**·CH_3OH and **8**, respectively. However, in contrast to **5**, the nitrogen super-hyperfine lines on the $g_{\perp}$ signal are not observed for **6**·0.5H_2O, **7**·CH_3OH and **8**.

4.4. Conclusion

Four ternary square-planar complexes having the general formula [Cu(bhs)(hc)] with the tridentate O,N,O-donor Schiff base N-(benzoyl)-N′-(salicylidene)hydrazine (H_2bhs) and monodentate neutral sp^2 N-donor heterocycles (hc = 3,5-dimethylpyrazole (dmpz), pyrazole (pyz), imidazole (imd) and pyridine (py)) have been synthesized and structurally characterized. As a whole none of the complex molecules is planar due to different orientations of both the phenyl ring plane of bhs^{2-} and the heterocycle ring plane with respect to the plane constituted by rest of the molecule. There are subtle variations in the relative orientations of these planes and hence in the extent of non-planarity of these complex molecules. The [Cu(bhs)(hc)] molecules form dimeric units due to equatorial-apical bridging involving the phenolate-O when hc is dmpz, imd and py. Whereas in the case of [Cu(bhs)(pyz)], the amide-O participates in the equatorial-apical bridging to form the dimer for one of the two complex molecules present in the asymmetric unit. In the crystal lattice, self-assembly *via* intermolecular non-covalent interactions leads to two-dimensional layered structure for the dimers of both [Cu(bhs)(dmpz)] and [Cu(bhs)(py)]. These interactions are π–π and C–H···π for [Cu(bhs)(dmpz)] and π–π and C–H···N for [Cu(bhs)(py)]. The complex with pyz ([Cu(bhs)(pyz)]·0.5H_2O) also forms two-

dimensional layered structure but through intermolecular π–π interactions and H_2O assisted O–H···N and N–H···O hydrogen bonds. In contrast, dimers of [Cu(bhs)(imd)] are connected by only O–H···N and N–H···O hydrogen bonds involving the CH_3OH molecules present in the crystal lattice and a one-dimensional structure is formed. Cryomagnetic and EPR measurements suggest weak antiferromagnetic spin-exchange in each complex.

References

1 Johnson, D. K.; Murphy, T. B.; Rose, N. J.; Goodwin, W. H.; Pickart, L. *Inorg. Chim. Acta* **1982**, *67*, 159.

2 Pickart, L.; Goodwin, W. H.; Burgua, W.; Murphy, T. B.; Johnson, D. K. *Biochem. Pharmacol.* **1983**, *32*, 3868.

3 Polzin, G. M.; Burstyn, J. N. *Metal Ions in Biological Systems*; Marcel Dekker: New York, 2001; pp 104-143.

4 Gallagher, J.; Zelenko, O.; Walts, A. D.; Sigman, D. S. *Biochemistry* **1998**, *37*, 2096.

5 Samasundaram, I.; Kommiya, M. K.; Palaniandavar, M. *J. Chem. Soc., Dalton Trans.* **1991**, 2083.

6 Offe, H. A.; Siefken, W.; Domagk, G. *Naturforsch., Teil B* **1952**, *7*, 446.

7 Richardson, D.; Barker, E.; Ponka, P.; Wilairat, P.; Vitolo, M. L.; Webb, J. In *Thalassemia: Pathophysiology and Management*, Part B; Fucharoen, S.; Rowley, P. T.; Paul, N. W., Eds.; Alan R. Liss, New York, 1988; pp. 81.

8 Arapov, O. V.; Alferva, O. F.; Levocheskaya, E. I.; Krasil'nikov, I. *Radiobiologiya* **1987**, *27*, 843.

9 Hatfield, W. E. *Theory and Applications of Molecular Paramagnetism*; Boudreaux, E. A.; Mulay, L. N., Eds.; Wiley, New York, 1976; pp. 491.

10 North, A. C. T.;Philips, D. C.; Mathews, F. S. *Acta Crystallogr., Sect. A* **1968**, *24*, 351.

11 Farrugia, L. J. *J. Appl. Crystallogr.* **1999**, *32*, 837.

12 *SMART*; 5.630, Eds.; *SAINTPLUS*; 6.45, Eds.; Bruker AXS, Inc.: Madison, WI, USA, 2003.

13 *SADABS*; 2.10, Eds.; Bruker AXS, Inc.: Madison, WI, USA, 2003.

14 Sheldrick, G. M. *SHELX-97* Structure Determination Software, University of Go¨ttingen, Go¨ttingen, Germany, 1997.

15 McArdle, P. *J. Appl. Crystallogr.* **1995**, *28*, 65.

16 Spek, A. L. *Platon98* Molecular Graphics Software, University of Glasgow, UK, 1998.

17 Chan, S. C.; Koh, L. L.; Leung, P. –H.; Ranford, J. D.; Sim, K. Y. *Inorg. Chim. Acta* **1995**, *236*, 101.
18 Iskander, M. F.; Khalil, T. E.; Werner, R.; Haase, W.; Svoboda, I.; Fuess, H. *Polyhedron* **2000**, *19*, 1181.
19 Nakamoto, K. *Infrared and Raman Spectra of Inorganic and Coordination Compounds;* Wiley, New York, 1986; pp. 241–244.
20 Sangeetha, N. R.; Baradi, K.; Gupta, R.; Pal, C. K.; Manivannan, V.; Pal, S. *Polyhedron* **1999**, *18*, 1425.
21 Lever, A. B. P., *Inorganic Electronic Spectroscopy; Elsevier, Amsterdam*, 1984.
22 Iskander, M. F.; Khalil, T. E.; Haase, W.; Werner, R.; Svoboda, I.; Fuess, H. *Polyhedron* **2001**, *20*, 2787.
23 Sigel, H.; Martin, R. B. *Chem. Rev.* **1982**, *82*, 385.
24 Sangeetha, N. R.; Pal, S. *J. Chem. Crystallogr.* **1999**, *29*, 287.
25 Sangeetha, N. R.; Pal, S. N.; Anson, C. E.; Powell, A. K.; Pal, S. *Inorg. Chem. Commun.* **2000**, *3*, 394.
26 Sangeetha, N. R.; Pal, S. *Polyhedron* **2000**, *19*, 1593.
27 Antosik, S.; Brown, N. M. D.; McConnell, A. A.; Porte, A. L. *J. Chem. Soc., A* **1969**, 545.
28 Nishio, M. *CrystEngComm* **2004**, *6*, 130.
29 Reddy, D. S.; Ovchinnikov, Y. E.; Shishkin, O. V.; Struchkov, Y. T.; Desiraju, G. R. *J. Am. Chem. Soc.* **1996**, *118*, 4085.
30 Reddy, P. A. N.; Nethaji, M.; Chakravarty, A. K. *Eur. J. Inorg. Chem.* **2003**, 2318.
31 Hasty, E. F.; Colburn, T. J.; Hendrickson, D. N. *Inorg. Chem.* **1973**, *12*, 2414.
32 Sartoris, R. P.; Ortigoza, L.; Casado, N. M. C.; Calvo, R.; Castellano, E. E.; Piro, O. E. *Inorg. Chem.* **1999**, *38*, 3598.
33 Gutierrez, L.; Alzuet, G.; Borras, J.; Castineiras, A.; Rodriguez-Fortea, A.; Ruiz, E. *Inorg. Chem.* **2001**, *40*, 3089.
34 Valko, M.; Morris, H.; Mazur, M.; Telser, J.; Mclnnes, E. J. L.; Mabbs, F. E. *J. Phys. Chem. B* **1999**, *103*, 5591.
35 Koolhaas, G. J. A. A.; Driessen, W. L.; Reedijk, J.; van der Plas, J. L.; de Graaff, R. A. G.; Gatteschi, D.; Kooijman, H.; Spek, A. L. *Inorg. Chem.* **1996**, *35*, 1509.
36 Bill, E.; Muller, J.; Weyhermuller, T.; Wieghardt, K. *Inorg. Chem.* **1999**, *38*, 5795.
37 Mondal, A.; Li, Y.; Khan, M. A.; Ross, J. H. Jr.; Houser, R. P. *Inorg. Chem.* **2004**, *43*, 7075.

38 Maher, J. P.; Rieger, P. H.; Thornton, P.; Ward, M. D. *J. Chem. Soc., Dalton Trans.* **1992**, 3353.
39 Acevedo-Chaves, R.; Costas, M. E.; Escudero, R. *Inorg. Chem.* **1996**, *35*, 7530.
40 Manikandan, P.; Justin, K. R.; Periakaruppan, T.; Manoharan, T. *J. Chem. Soc., Dalton Trans.* **2000**, 2779.
41 Malek, K.; Vala, M.; Swiatek-Kozlowska, J.; Proniewicz, L. M. *New J. Chem.* **2004**, *28*, 477.
42 Casassas, E.; Izquierdo-Ridorsa, A.; Tauler, R. *J. Chem. Soc., Dalton Trans.* **1990**, 2341.
43 Larin, G. M.; Zvereva, G. A. *Mendeleev Commun.* **2001**, 104.
44 Lai, C. K.; Wang, K. –W.; Lin, R. *J. Mater. Chem.* **1998**, 2379.
45 Gilbert, B. C.; Silvester, S.; Walton, P. H.; Whitwood, A. C. *J. Chem. Soc., Perkin Trans. 2* **1999**, 1891.

Chapter 5

Non-oligomeric zipper structure from plate like ternary copper(II) complexes

Two copper(II) complexes with monoanionic N,N,O-donor deprotonated Schiff base 2-*N*-(picolinylidene)phenol (Hpyp) and halide as an ancillary ligand having the formula [Cu(pyp)X] (where X^- = Cl^- and Br^-) have been synthesized and characterized. The pseudo-polymorphism that arises from cocrystallization of these complexes with solvent molecules has been discussed. Two cases have been investigated: (i) the quantitative preparation of dihydrated species by very slow evaporation of aqueous methanol solution of the complexes {[Cu(pyp)Cl]·$2H_2O$ (**9a**) and [Cu(pyp)Br·$2H_2O$ (**10a**)} and (ii) the quantitative isolation of corresponding mono methanolic forms by fast crystallization from dry methanol solution of the complexes {[Cu(pyp)Cl]·MeOH (**9b**) and [Cu(pyp)Br·MeOH (**10b**)}. In the context of structural features, both chloro and bromo analogues are isomorphic. In order to investigate the crystal compositions and packing features, single crystal X-ray diffraction measurements as well as thermogravimetry and differential scanning calorimetry have been carried out. The water interspersed form shows closed zipper like infinite chain structure through hydrogen bonding with the water molecules and π···π interactions. The parallel zippers are again connected to each other through hydrogen bonding between the water molecules to give a 2D crimped sheet. In contrast, the methanol recognized forms demonstrate π-stacked columnar structure.

5.1. Introduction

The formation of multi-stranded complexes by self-assembly of comparatively lower strands is very common structural motif in biological systems. Biological zipper motif is of fundamental importance for self-replication, fiber behavior and formation of functional multi-component complexes.[1–5] In the past decade, chemists have prepared synthetic zipper systems from oligomeric nucleic acid derivatives,[6]

polypeptides or amides,[7,8] steroid derivatives,[9] metalloporphyrins[10] and coordination polymers.[11–16] Such zippers are nevertheless architecturally conventional. More unconventional are the elegant non-oligomeric supramolecular zipper systems of small organic molecules or metal-organic building blocks. The self-assembly of non-oligomeric building blocks into a double-stranded zipper-like structure is thus more akin to the closure or the interlocking of the teeth of a man-made zipper (Figure 5.1, trace (a)). Such supramolecular zippers will undoubtedly be harder to design than oligomeric ones. In particular, self reorganization through hydrogen bonding poses the lack of interpenetration among the molecular teeth (Figure 5.1, trace (b)). On the other hand, molecular teeth possessing stacking motifs can be well interpenetrated (Figure 5.1, trace (c)). Metal coordination complexes containing 2,2'-bipyridine, 1,10-phenanthroline or terpyridine are well known to form zipper structures through "aryl embrace" or multiple π-stacking interactions.[12-14] The extended zipper structure of non-oligomeric components with non-coordinating backbones are very rare in the literature. In the following account, we will present the hydrated forms of a pair of isomorphous complexes which form closed zipper network architecture. However, the isomorphous complexes interspersed with methanol are diverted from the perfect one-dimensionality to asymmetric columnar packing. In addition, due to the lesser number of hydrogen bond donor sites in methanol compared to the water, the methanol included complexes fail to form the zipper structure.

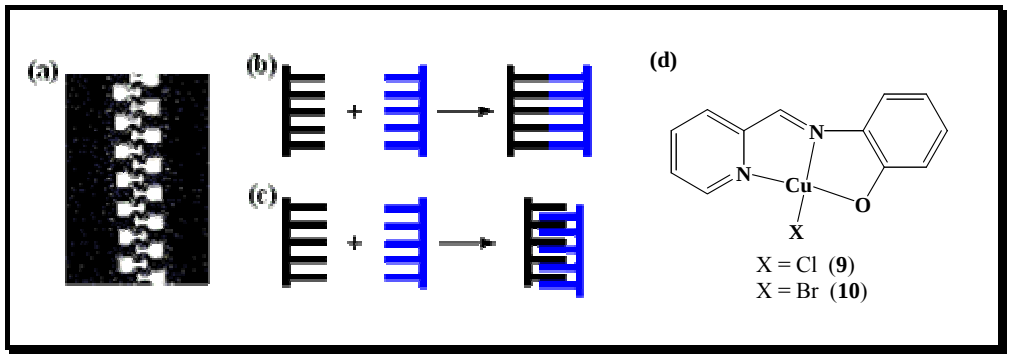

Figure 5.1.

5.2. Experimental section

5.2.1. Materials

The Schiff base (Hpyp) was prepared in ~80 % yield by the condensation of one mole equivalent each of 2-pyridinecarboxaldehyde and 2-aminophenol in boiling methanol. All other chemicals and solvents used in this work were of analytical grade available commercially and were used without further purification.

5.2.2. Physical measurements

Microanalytical (C, H, N) data were obtained with a Thermo Finnigon Flash EA1112 elemental analyzer. The infrared spectra were recorded by using a KBr pellet on a Jasco-5300 FT-IR spectrophotometer. Solutions electrical conductivities were measured with a Digisun DI-909 conductivity meter. A Shimadzu 3101-PC UV/vis/NIR spectro-photometer was used to record the electronic spectra. DSC was performed on a Mettler Toledo DSC 822e module and TGA was performed on a Mettler Toledo TGA/SDTA 851e module. The typical sample size is 4-6 mg for DSC and 9-12 mg for TGA. A SQUID magnetometer was used for the magnetic susceptibilities measurements in the temperature range 2–300 K. Diamagnetic correction calculated from Pascal's constants,[17] were used to obtain the molar paramagnetic susceptibilities.

5.2.3. Synthesis

[Cu(pyp)Cl]·$2H_2O$ (**9a**)

A methanol solution (15 ml) of $CuCl_2·2H_2O$ (17.0 mg, 0.1 mmol) was added to a methanol solution (30 ml) of KOH (6.0 mg, 0.1 mmol) and Hpyp (20.0 mg, 0.1 mmol). The mixture was stirred in air at room temperature for 30 min. The red solution was then refluxed for 10 min. and left at room temperature for slow evaporation. Red-brown crystals formed after 2-3 days were collected by filtration. Yield: 74 %. Anal. calcd. for $CuC_{12}H_{13}N_2O_3Cl$: C, 43.38; H, 3.94; N, 8.43. Found: C, 43.35; H, 3.89; N, 8.01. UV/Vis [$CHCl_3$; λ_{max}/nm (ε /dm^3 mol^{-1} cm^{-1})]: 547 (7840), 363 (8830), 306sh (9240), 285 (9960).

[Cu(pyp)Br]·2H_2O (**10a**)

This complex was prepared from $CuBr_2$, Hpyp and KOH (1:1:1 mole ratio) by following the same procedure as described for **9a**. Yield: 77 %. Anal. calcd. for $CuC_{12}H_{13}N_2O_3Br$: C, 38.26; H, 3.48; N, 7.44. Found: C, 38.24; H, 3.37; N, 7.27. UV/Vis [$CHCl_3$; λ_{max}/nm (ε /dm^3 mol^{-1} cm^{-1})]: 551 (7570), 363 (8770), 289 (13290).

[Cu(pyp)Cl]·MeOH (**9b**)

The compound **9a** was dissolved in dry methanol and kept at 35ºC for over night. Brown colored needle shaped crystals deposited were collected by filtration. Yield: 63 %. Anal. calcd. for $CuC_{13}H_{13}N_2O_2Cl$: C, 47.57; H, 3.99; N, 8.53. Found: C, 47.51; H, 3.87; N, 8.43. UV/Vis [$CHCl_3$; λ_{max}/nm (ε /dm^3 mol^{-1} cm^{-1})]: 547 (7910), 363 (8950), 306sh (9370), 285 (10060).

[Cu(pyp)Br]·MeOH (**10b**)

Crystals of **10b** were obtained by following the same procedure as described for **9b**. Yield: 69 %. Anal. calcd. for $CuC_{13}H_{13}N_2O_2Br$: C, 41.89; H, 3.52; N, 7.52. Found: C, 41.89; H, 3.47; N, 7.39. UV/Vis [$CHCl_3$; λ_{max}/nm (ε /dm^3 mol^{-1} cm^{-1})]: 551 (7640), 363 (8870), 289 (13410).

5.2.4. X-ray crystallography

Unit cell parameters and the intensity data for **9a** and **10a** were obtained on a Bruker-Nonius SMART APEX CCD single crystal diffractometer, equipped with a graphite monochromator and a Mo Kα fine-focus sealed tube (λ = 0.71073 Å) operated at 2.0 kW. The detector was placed at a distance of 6.0 cm from the crystal. Data were collected at 100 K with a scan width of 0.3º in ω and an exposure time of 10 sec/frame. The SMART software was used for data acquisition and the SAINT-Plus software was used for data extraction.[18] In each case, an absorption correction was performed with the help of SADABS program.[19] X-ray data for **9b** and **10b** were collected on an Enraf-Nonius Mach-3 single crystal diffractometer using graphite monochromated Mo Kα radiation (λ = 0.71073 Å) by ω-scan method at 298 K. In each case, the ψ-scans[20] of selected reflections were used for an empirical absorption correction. The programs of the WinGX[21] package were used for data reduction and absorption correction. The structures were solved by direct methods and refined on F^2 by full-matrix least-squares procedures. All non-hydrogen atoms were refined anisotropically. The protons of the solvent molecules in all the cases were located in the corresponding difference maps and refined with $U_{iso}(H) = 1.5U_{eq}(O)$. Other hydrogen atoms in all the structures were included in the structure factor calculation at idealized positions by using a riding model. The SHELX-97[22] programs were used for structure solution and refinement. The ORTEX6a[23] and Platon[24] packages were used for molecular graphics. Significant crystallographic data are summarized in Table 5.1.

Table 5.1. Crystallographic parameters for **9a**, **10a**, **9b** and **10b**.

Complex	**9a**	**10a**	**9b**	**10b**
Chemical formula	$CuC_{12}H_{13}N_2O_3Cl$	$CuC_{12}H_{13}N_2O_3Br$	$CuC_{13}H_{13}N_2O_2Cl$	$CuC_{13}H_{13}N_2O_2Br$
Formula weight	332.23	378.87	328.24	372.70
Crystal system	Monoclinic	Monoclinic	Triclinic	Triclinic
Space group	$P2_1/m$	$P2_1/m$	$P\bar{1}$	$P\bar{1}$
T(K)	100	100	298	298
a (Å)	9.5269(7)	9.5793(8)	6.9205(17)	6.8991(17)
b (Å)	6.4027(5)	6.4040(5)	9.2257(9)	9.3473(9)
c (Å)	10.5813(8)	10.7646(9)	10.4996(14)	10.6527(15)
α (°)	90	90	100.529(10)	100.277(10)
β (°)	99.913(1)	100.5340(10)	97.798(17)	98.699(15)
γ (°)	90	90	92.593(13)	91.912(13)
2θ range	3.90–56.46	3.84–56.54	3.98–59.94	3.94–54.94
V (Å^3)	635.80(8)	649.23(9)	651.29(19)	666.9(2)
Z	2	2	2	2
μ (mm^{-1})	1.932	4.763	1.879	4.631
N-collected	7385	7574	3781	3045
N-unique	1627	1706	3781	3045
N [$I \geq 2\sigma(I)$]	1533	1528	2975	2658
Parameters	121	121	176	176
$R1$[a], $wR2$[b] [$I \geq 2\sigma(I)$]	0.0340, 0.0824	0.0285, 0.0695	0.0308, 0.0734	0.0325, 0.0919
$R1$[a], $wR2$[b] [all data]	0.0367, 0.0840	0.0334, 0.0722	0.0478, 0.0797	0.0398, 0.1036
GOF[c] (F^2)	1.099	1.061	1.039	1.188
Largest peak and hole (e Å^{-3})	0.738, –0.351	0.905, –0.399	0.319, –0.315	0.581, –0.859

[a] $R1 = \sum||F_o| - |F_c||/\sum|F_o|$. [b] $wR2 = \{\sum[(F_o^2 - F_c^2)^2]/\sum[w(F_o^2)^2]\}^{1/2}$.

[c] $GOF = \{\sum[w(F_o^2 - F_c^2)^2]/(n - p)\}^{1/2}$ where n is the number of reflections and p is the number of parameters refined; $w = 1/[\sigma^2(F_o^2) + (aP)^2 + bP]$.

5.3. Results and discussion

5.3.1. Synthesis and some properties

The complexes have been prepared in moderate yields, by reacting the corresponding copper(II) halide, Hpyp and KOH with 1:1:1 mole ratio in methanol. The elemental analyses data are satisfactory for all the solvated species. None of the complexes are electrically conducting in methanol solutions. The room temperature magnetic moments of all the complexes are consistent with an s = ½ ground state of the metal ions.

5.3.2. Infrared and electronic spectral features

The free Schiff base (Hpyp) displays a medium intensity band near 3360 cm^{-1} due to the phenolic-OH. The absence of this band in the spectra of the solvated complexes indicates deprotonation and coordination of the phenolic-O. However, the solvated species display a broad band centered at ~3460 cm^{-1} possibly due to solvent –OH group stretching.[25] The C=N stretch for the complexes is observed near 1585 cm^{-1}. The low energy shift (by ~39 cm^{-1}) of this band compared to that of Hpyp indicates metal coordination by the N-atom of the –CH=N fragment of pyp^{-}.

The electronic spectra of the complexes have been recorded in chloroform solutions. Electronic spectral profiles of the corresponding bromo and chloro analogues are very similar. A strong absorption is observed within 547–552 nm and several closely spaced intense absorptions appear in the range 370–280 nm. Electronic spectrum of $[Cu(pyp)Cl]\cdot 2H_2O$ has been depicted in Figure 5.2. The lower energy absorptions is most likely due to the ligand to metal charge transfer (LMCT), where as the higher energy bands are due to intraligand charge transfers (LLCT).[26] We have also examined the change of the band profile in terms of their relative position and intensity, in a range of solvents having different polarity. The LMCT band has shown a blue shift with the increase of the polarity of the solvent (Figure 5.2). It may be noted that the LLCT bands are almost unaffected. The polarity of the complex molecule is expected to change with the change of molecular conformation from perfectly planar to a varying degree of non-planarity. The variation of solvent polarity may cause such conformation change of complex molecules in solution and as a result there could be variation in the energies of the ground as well excited states

causing a shift of the LMCT band. It is also likely that the solvent molecules can coordinate the metal ion at the axial sites. The coordination ability is expected to vary with the change of the solvent polarity. As a result the energies of the ground and excited states may vary with polarity of the solvent in such a way that there is a blue shift of the LMCT band.

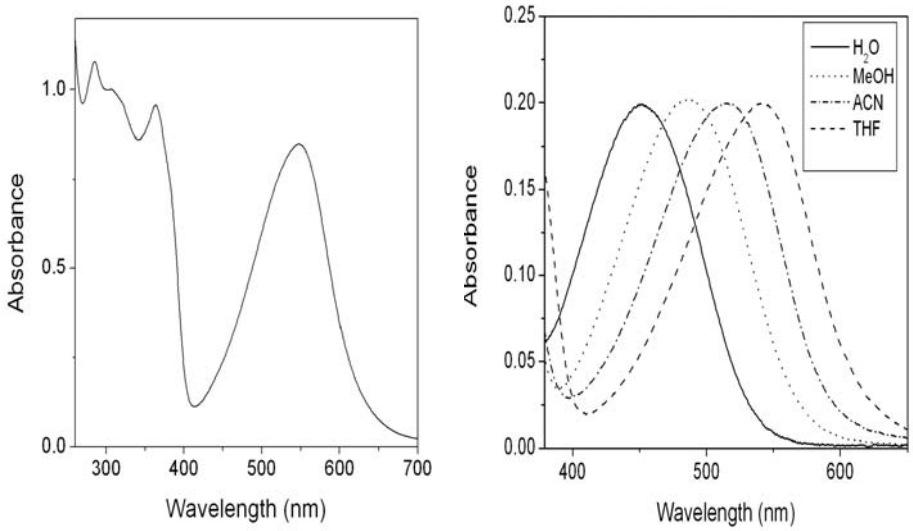

Figure 5.2. Electronic spectrum of **9a** in chloroform solution (left) and the shift of LMCT band in a range of solvents (right).

5.3.3. Description of molecular structures

The Complexes **9a** and **10a** crystallize in the space group $P2_1/m$. In each case, the asymmetric unit contains half of [Cu(pyp)X)] {X = Cl (**9a**) and Br (**10a**)} molecule and a water molecule. The complex molecule is in crystallographic mirror plane. In contrast, the methanol interspersed isomorphous pair **9b** and **10b** crystallizes in the space group $P\bar{1}$. The asymmetric units contain a full molecule of [Cu(pyp)X] and a methanol molecule. The molecular structure of **9a** is depicted in Figure 5.3 and the selected bond parameters of all the complexes are summarized in Table 5.2. In each case, the tridentate pyp^- coordinates the metal ion *via* the phenolate-O, the imine-N and the pyridine-N atoms forming two five-membered chelate rings. The halide ion occupies the fourth coordination site. Thus the ligands form an ON2X

square-plane around the metal center in each complex. Complexes **9a** and **10a** are perfectly square-planar, whereas **9b** and **10b** are slightly deviated from the square-planar geometry. The maximum deviations from the ON_2X mean plane are in the ranges 0.032–0.031 Å. The Cu–O1(phenolate), Cu–N1(imine) and Cu–N2(pyridine) bond lengths (Table 5.2) in all the structures are very similar. The Cu–N2(pyridine) bond lengths are little bit longer than the Cu–N1(imine). This difference may be due to the combined effect of better π-back bonding in the Cu–N(imine) bond than in Cu–N(pyridine) bond, rigidity of the tridentate ligand and *trans* effect of the phenolate-O.[27] The Cu–Cl and Cu–Br bond lengths are unexceptional. The chelate bite angles for the five-membered rings formed by pyp^- are in the range of 80.29–83.39°.

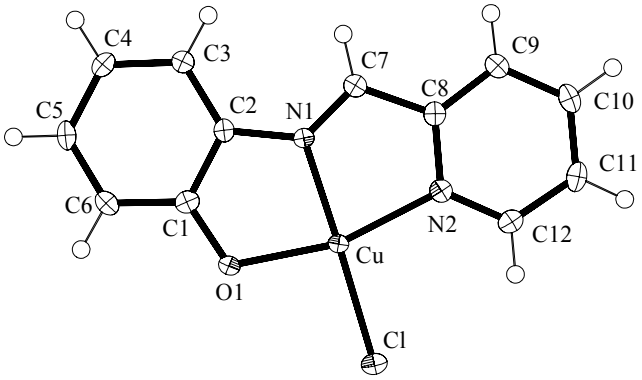

Figure 5.3. Structure of **[Cu(pyp)Cl]** (**9a**) with the atom-labeling scheme. All non-hydrogen atoms are represented by their 50% probability thermal ellipsoids.

Table 5.2. Selected bond lengths (Å) and angles (°) for **9a**, **9b**, **10a** and **10b**.

	9a	**9b**	**10a**	**10b**
Cu-O(1)	1.945(2)	1.9537(14)	1.947(2)	1.950(2)
Cu-N(1)	1.946(2)	1.9483(16)	1.958(3)	1.945(2)
Cu-N(2)	2.019(3)	2.0257(16)	2.016(3)	2.028(2)
Cu-Cl	2.1973(8)	2.1927(6)	- - - - -	- - - - -
Cu-Br	- - - - -	- - - - -	2.3355(5)	2.3333(5)
O(1)-C(1)	1.337(3)	1.323(2)	1.334(4)	1.332(3)
N(1)-C(7)	1.284(4)	1.278(2)	1.280(4)	1.284(4)
N(1)-C(6)	1.399(4)	1.397(2)	1.392(4)	1.397(4)
N(2)-C(12)	1.330(4)	1.333(3)	1.328(4)	1.331(3)
N(2)-C(8)	1.353(4)	1.349(2)	1.359(4)	1.358(4)
C(7)-C(8)	1.473(4)	1.462(3)	1.462(4)	1.463(4)
O(1)-Cu-N(1)	83.23(9)	83.39(6)	83.31(10)	83.29(9)
O(1)-Cu-N(2)	164.07(10)	163.64(6)	164.39(10)	163.91(9)
N(1)-Cu-N(2)	80.84(10)	80.29(7)	81.09(11)	80.67(9)
O(1)-Cu-Cl	95.18(7)	97.24(5)	- - - - -	- - - - -
N(1)-Cu-Cl	178.41(7)	177.88(5)	- - - - -	- - - - -
N(2)-Cu-Cl	100.74(8)	99.11(5)	- - - - -	- - - - -
O(1)-Cu-Br	- - - - -	- - - - -	94.57(7)	96.66(6)
N(1)-Cu-Br	- - - - -	- - - - -	177.87(7)	178.25(6)
N(2)-Cu-Br	- - - - -	- - - - -	101.04(8)	99.41(7)
C(1)-O(1)-Cu	112.08(18)	111.69(12)	111.90(19)	111.49(17)
C(7)-N(1)-C(6)	128.9(3)	129.08(17)	130.4(3)	128.9(2)
C(7)-N(1)-Cu	117.4(2)	117.42(14)	116.4(2)	117.39(19)
C(6)-N(1)-Cu	113.66(19)	113.36(12)	113.2(2)	113.57(18)
C(8)-N(2)-Cu	112.5(2)	112.64(13)	112.3(2)	112.13(19)
N(1)-C(7)-C(8)	114.9(3)	115.40(17)	116.0(3)	115.3(2)
N(2)-C(8)-C(7)	114.3(3)	122.26(19)	114.2(3)	114.4(2)

5.3.4. Architectural studies

The complexes described in this chapter have perfect or near perfect square-planar geometry. Such complexes with sufficient π–electron are very good candidates to form supramolecular architectures through stacking interactions.[28] Since stacking interactions results into slipped assembly of the molecules, formation of either stair-case type or columnar type structural motifs are very common.[29] By incorporating other functionalities on the molecule which can participate in additional non-covalent interactions with themselves or with the incorporated solvent molecules, can lead to interesting architectural motifs. The molecules of [Cu(pyp)X] possess hydrogen bond acceptor sites such as phenolate-O, which can be involved in further interactions along with the stacking if some donor groups are available in close proximity. In the following subsections, we have discussed the molecular assemblies of $[Cu(pyp)X]\cdot 2H_2O$ and $[Cu(pyp)X]\cdot CH_3OH$ with respect to their topological recognitions.

5.3.4.1. Zipper motif

In the isomorphous complexes **9a** and **10a**, the molecules are on the crystallographic mirror planes. The guest water molecules are connected to the phenolate-O of the complex molecule and to another water molecule through strong hydrogen bonding. The phenolate-O of each complex molecule is serving as a hydrogen bond acceptor for two water molecule on its both sides. Consequently a water dimer is trapped in between two complex molecules. All the hydrogen bonding parameters are given in Table 5.3. Thus alternate water dimer and the planar complex molecule forms a single strand zipper structure, where the distance between the parallel teeth are 6.473 Å and 6.404 Å for **9a** and **10a**, respectively. Due to the dimeric water spacer, there is enough space between the teeth for self-recognition of a similar strand through stacking of the planar complex molecules. As a result, an infinite closed zipper structure has been formed along the crystallographic *b*-axis (Figure 5.4). The inter-planar distances between the two inversely stacked teeth are 3.236 Å and 3.202 Å for **9a** and **10a**, respectively. The Cu···Cu distances in these linear arrangements are 6.058 Å (**9a**) and 6.050 Å (**10a**). Due to less electronic repulsion between the molecules of the bromide analogue (**10a**) has packed more closely than the corresponding chloride one (**9a**), which is reflected in their inter-planar distances. The

shortest Cg···Cg distance involves the phenolate benzene ring and the chelate ring formed by the imine-N and pyridine-N. These distances are 3.327 and 3.319 Å for **9a** and **10a**, respectively. The parallel zippers are again connected by hydrogen bonds involving water molecules and a 2D sheet is formed which is parallel to the crystallographic *ab*-plane (Figure 5.4). As a result, a zig-zag infinite water chain has been trapped in between the 1D stacked columns of the complexes.

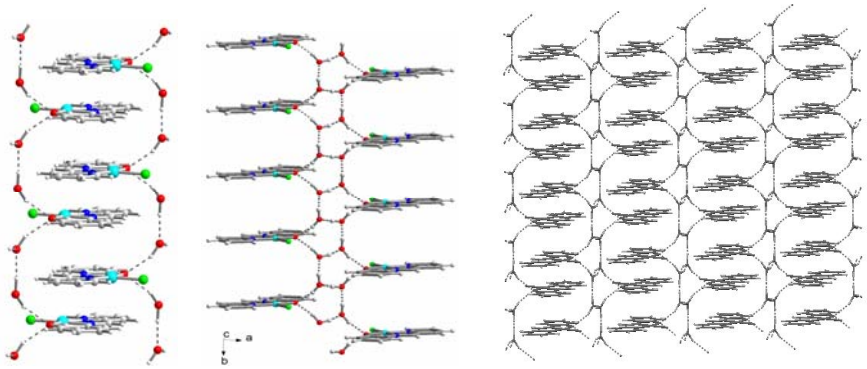

(a) **(b)** **(c)**

Figure 5.4. The zipper motif of **9a:** (a) double strand, (b) two single strands connected by hydrogen bonds and (c) parallel zippers as a 2D sheet.

5.3.4.2. Asymmetrical columnar packing

Fast crystallization of the complexes from dry methanol provides thermodynamically less stable methanol interspersed species **9b** and **10b**. As expected the zipper structure observed for **9a** and **10a** has been terminated due to inclusion of less symmetric guest molecule in **9b** and **10b**. Instead of continuous hydrogen bonded single stranded zipper (**9a** and **10a**), the reduction of the symmetry and the hydrogen bond donor arm of the guest molecule resulted in distinct dimerization through O–H···O and C–H···O hydrogen bonds for **9b** and **10b**. Both hydrogen bonding interactions involve the methanol molecule. The metal coordinated phenolate-O atom and the azomethine (–CH=N–) group act as the acceptor and donor in these O–H···O and C–H···O interactions, respectively. The hydrogen bonding parameters are given in Table 5.3. The isolated dimeric units are stacked in 1D columnar fashion with alternating short and long inter planer distances. Mainly the

five-membered chelate rings and the phenolate benzene ring are participating in the stacking interactions. The interplanar distances in the solvent mediated dimeric unit are 3.338 and 3.323 Å, whereas the same for the stacked shorter sides are 3.239 and 3.238 Å, for the **9b** and **10b**, respectively. The corresponding Cu···Cu distances are 4.473 and 6.082 Å for **9b** and that for **10b** are 4.500 and 6.069 Å. The packing diagrams of both **9a** and **10b** are depicted in Figure 5.5.

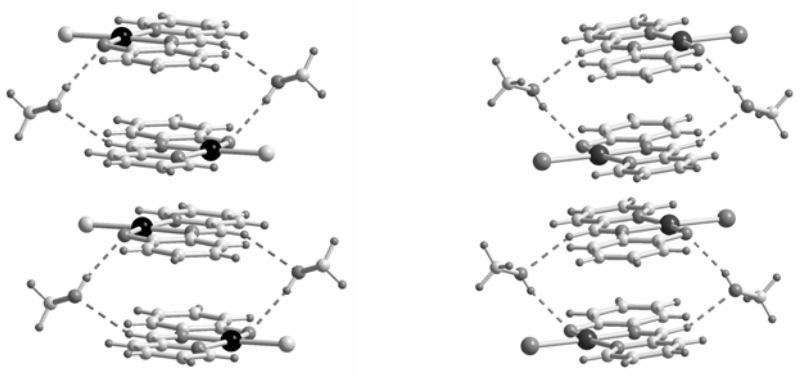

(a) **(b)**

Figure 5.5. The columnar packing of (a) [Cu(pyp)Cl]·CH_3OH (**9b**) and (b) [Cu(pyp)Cl]·CH_3OH (**10b**).

Table 5.3. The hydrogen bonding parameters.

Complex	Interaction	d (Å)	D (Å)	θ (°)
9a	[a]O−H···O	1.871	2.814	169
	[a]O−H···O	1.798	2.737	166
	[b]O−H···O	1.887	2.738	147
10a	[a]O−H···O	1.922	2.847	162
	[a]O−H···O	1.809	2.747	166
	[b]O−H···O	1.912	2.737	142
9b	O−H···O	2.052	2.812	172
	[c]C−H···O	2.483	3.313	155
10b	O−H···O	2.105	2.825	164
	[d]C−H···O	2.331	3.302	157

a = x, 3/2-y, z; b = -x, -1/2+y, 1-z; c = 1-x, -y, -z; d = 1-x, 1-y, -z.

5.3.5. Thermal analysis

The TGA measurements of all the solvate species under flowing nitrogen gas have been performed in the temperature range 30 to 400º C. Compounds **9b** and **10b** showed that, the endothermic desolvation starts at ~51º to 55º C and is completed at 96º to 99º C, whereas for **9a** and **10a** it starts at 54º to 57º C and is completed at 99º to 112º C. The observed weight losses of 10.69 %, 9.33 %, 9.61 % and 8.32 % correspond well to the calculated values of 10.84 %, 9.56 %, 9.76 % and 8.60 % for the two water and single methanol molecules per formula unit of **9a**, **10a**, **9b** and **10b**, respectively. Upon further heating up to 180º C, the insolated residue decomposes in two overlapping steps. The decomposition continued beyond 400º C. The differential scanning calorimetric measurements also correspond well with the TGA data.

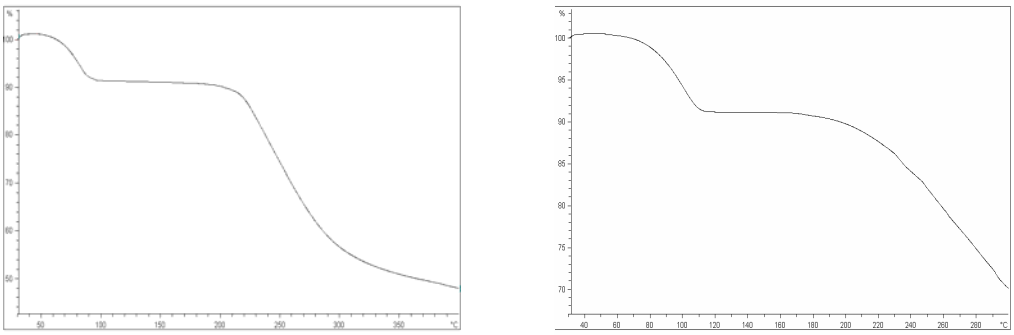

Figure 5.6. The thermal gravimetric plot of **9b** (left) and **10a** (right).

5.3.6. Magnetic and EPR spectral properties

Magnetic susceptibilities of **9a** and **10a** in powdered form have been measured in the temperature range 2–300 K at a constant magnetic field of 5 kG. The effective magnetic moments at 300 K are 1.79 and 1.80 μ_B for **9a** and **10a**, respectively. These values are consistent with the spin-only moments expected for d^9 systems. On cooling there is no significant change in the moment values. At 2 K the moments are ~1.76 μ_B. In each case, a linear plot is obtained when the inverse molar susceptibilities are plotted against temperature with a small negative intercept on the temperature axis (Figure 5.7). The data were fit using the expression for Curie-Weiss law. The Curie (C) and Weiss (θ in K) constants are very similar for both the species (0.41 and –0.1

for **9a** and 0.40 and –0.1 for **10a**). These values of the Weiss constants clearly indicate essentially the Curie-paramagnetic nature of both **9a** and **10a**.

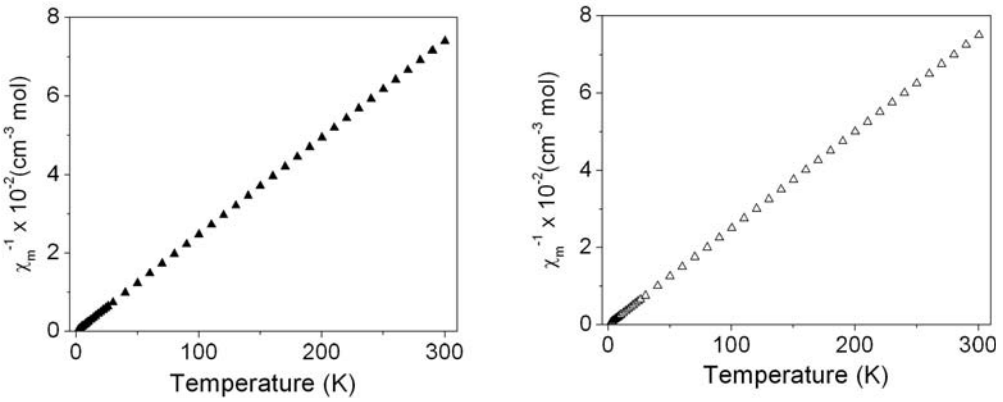

Figure 5.7. The inverse molar magnetic susceptibility of **9a** [▲] (left) and **10a** [Δ] (right) as a function of temperature.

The room temperature (298 K) X-band EPR spectral profiles of **9a** and **10a** in powdered phase are very similar. In the $g \approx 2$ region, a strong axial signal ($g_{||} = 2.21$, $g_{\perp} = 2.05$ for **9a** and $g_{||} = 2.18$, $g_{\perp} = 2.04$ for **10a**) typical of a square-planar copper(II) species is observed (Figure 5.8). Interestingly both the complexes display a very weak signal within $g = 4.20$–4.22 (Figure 5.8, inset). The higher field strong signal is assigned to the $\Delta M_S = \pm 1$ transition. The origin of the weak signal at the low-field region is perhaps the $\Delta M_S = \pm 2$ transition expected for very weakly coupled dicopper(II) species.[30,31]

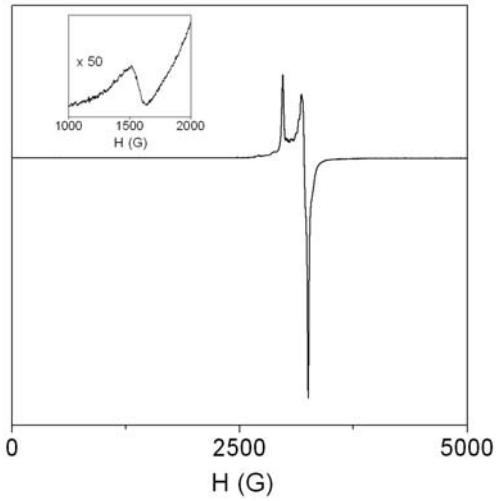

Figure 5.8. EPR spectra of **9a** in powder form at 300 K, the insets is the magnified $\Delta Ms = \pm 2$ region for the powder.

5.4. Conclusion

In conclusion, the perfectly planar $[Cu(pyp)X]\cdot 2H_2O$ (X = Cl and Br) species and closed to perfectly planar $[Cu(pyp)X]\cdot CH_3OH$ (X = Cl and Br) species form one-dimensional π-stacked supramolecular structures. In case of the hydrated species, a zipper like motif is formed due to the participation of the water molecules in hydrogen bonding interactions with itself and with the square-planar complexes molecules. It may be noted that the zipper like structure from the hydrogen bonded water chain and π-stacked flat motifs that are hydrogen bonded to the water chain is not common in literature. On the other hand, methanol containing species form a 1D columnar structure. This contrast arises primarily due to the less number of hydrogen bond sites in methanol compared to that in water.

Reference

1 Horton, R. H.; Moran, L. A.; Ochs, R. S.; Rawn, D. J.; Scrimgeour, G. K. *Principles of Biochemistry*; Prentice Hall International, Inc.: London, 1992.

2 Po¨rschke, D. *Biopolymers* **1971**, *10*, 1989.

3 Amirikyan, B. R.; Vologodskii, A. V.; Lyubchenko, Y., L. *Nucleic Acids Res.* **1981**, *9*, 5469.

4 Wendt, H.; Baici, A.; Bosshard, H. R. *J. Am. Chem. Soc.* **1994**, *116*, 6973.

5 O'Neil, K. T.; Hoess, R. H.; Degrado, W. F. *Science* **1990**, *249*, 774.

6 Kubota, M.; Ono, A. *Tetrahedron Lett.* **2004**, *45*, 5755.

7 Bisson, A. P.; Carver, F. J.; Eggleston, D. S.; Haltiwanger, R. C.; Hunter, C. A.; Livingstone, D. L.; McCabe, J. F.; Rotger, C.; Rowan, A. E. *J. Am. Chem. Soc.* **2000**, *122*, 8856.

8 Bisson, A. P.; Hunter, C. A. *Chem. Commun.* **1996**, *15*, 1723.

9 Munro, O. Q.; du Toit, K.; Drewes, S. E.; Crouch, N. R.; Mulholland, D. A. *New J. Chem*. **2006**, *30*, 197.

10 Plater, M. J.; Aiken, S.; Bourhill, G. *Tetrahedron Lett.* **2001**, *42*, 2225.

11 Zhang, J. P.; Lin, Y. Y.; Huang, X. C.; Chen, X. M. *Chem. Commun.* **2005**, 1258.

12 Chen, X. M.; Liu, G. F. *Chem.–Eur. J.* **2002**, *8*, 4811.

13 Barboiu, M.; Petit, E.; Vaughan, G. *Chem.–Eur. J.* **2004**, *10*, 2263.

14 Zheng, Y. Q.; Sun, J.; Lin, J. L. *Z. Anorg. Allg. Chem.* **2000**, *626*, 1501.

15 Ang, S. G.; Sun, B. W. *Cryst. Growth Des.* **2005**, *5*, 383.

16 Zhou, Z. H.; Yang, J. M.; Wan, H. L. *Cryst. Growth Des.* **2005**, *5*, 1825.

17 Hatfield, W. E. *Theory and Applications of Molecular Paramagnetism*; Boudreaux, E. A.; Mulay, L. N., Eds.; Wiley, New York, 1976; pp. 491.

18 *SMART*; 5.630, Eds.; *SAINTPLUS*; 6.45, Eds.; Bruker AXS, Inc.: Madison, WI, USA, 2003.

19 *SADABS*; 2.10, Eds.; Bruker AXS, Inc.: Madison, WI, USA, 2003.

20 North, A. C. T.;Philips, D. C.; Mathews, F. S. *Acta Crystallogr., Sect. A* **1968**, *24*, 351.

21 Farrugia, L. J. *J. Appl. Crystallogr.* **1999**, *32*, 837.

22 Sheldrick, G. M. *SHELX-97* Structure Determination Software, University of Go¨ttingen, Go¨ttingen, Germany, 1997.

23 McArdle, P. *J. Appl. Crystallogr.* **1995**, *28*, 65.

24 Spek, A. L. *Platon98* Molecular Graphics Software, University of Glasgow, UK, 1998.

25 Nakamoto, K. *Infrared and Raman Spectra of Inorganic and Coordination Compounds;* Wiley, New York, 1986; pp. 241–244.

26 Lever, A. B. P., *Inorganic Electronic Spectroscopy; Elsevier, Amsterdam*, 1984.

27 Pal, S. N.; Pal, S. *Inorg. Chem.* **2001**, *40*, 4807.

28 Alcock, N. W.; Barker, P. R.; Haider, J. M.; Hannon, M. J.; Painting, C. L.; Pikramenou, Z.; Plummer, E. A.; Rissanen, K.; Saarenketo, P. *J. Chem. Soc., Dalton Trans.* **2000**, 1447.

29 Janiak, C. *J. Chem. Soc., Dalton Trans.* **2000**, 3885.

30 Hasty, E. F.; Colburn, T. J.; Hendrickson, D. N. *Inorg. Chem.* **1973**, *12*, 2414.
31 Sartoris, R. P.; Ortigoza, L.; Casado, N. M. C.; Calvo, R.; Castellano, E. E.; Piro, O. E. *Inorg. Chem.* **1999**, *38*, 3598.

Chapter 6

A Family of copper(II) complexes with the substituted derivatives of 2-N-(picolinylidene)phenol: Self-assembly and supramolecular architecture

Ten copper(II) complexes of mono substituted monoanionic N,N,O-donor deprotonated Schiff base 2-*N*-(picolinylidene)phenol (n-R-Hpyp) (where n = 3, 4, 5 and 6, when R = Me; n = 4 when R = Cl) with halide as an ancillary ligand having the formula [Cu(n-R-pyp)X] (where X^- = Cl^- or Br^-) have been synthesized and characterized. Single crystal X-ray structural analyses, of all the complexes show square-planar, distorted square-pyramidal and trigonal-bipyramidal coordination geometries around the metal ions. In this family of ten complexes, we have gradually shifted the methyl substitution position on the phenolate ring. For comparison we have also prepared one choloro substituted ligand and its complexes. In coordinatively unsaturated complexes such as square-planar species, metal ion can interact with some bound electronegative atom at the apical site. We have studied the nature of the apical interaction along with the relative position of the substituent on the phenolate ring. Finally we have analyzed the supramolecular architectures that have been adopted by this set of complexes by considering the various non-covalent interactions which play important roles in holding the molecular building blocks. This set of ten copper(II) complexes can be described in terms of four major supramolecular architectures based on Cu···X, O–H···O, C–H···O, C–H···X and π···π interactions. These are stair case structure, ladder motif, brick wall and square-grid. The analogous chloride and bromide ligated complexes show similar structural features.

6.1. Introduction

The molecular self-assembly via non-covalent interactions, such as hydrogen bonds, π···π and C–H···π interactions, has emerged as an attractive approach in crystal engineering for the design and fabrication of new compounds not only for their

potential properties as functional solid materials but also for their intriguing and often complicated solid state architectures and topologies.[1–9] Discrete transition metal complexes can also form extended network structures through supramolecular interactions, such as hydrogen bonding involving donor or acceptor groups appended to the ligands, π···π stacking interactions, or combinations of interactions.[10–15] The metal bound halides having suitable geometric position and preference have the tendency to get involve in some interactions with the coordinatively unsaturated metal ions. We have focused on the use of weak apical interaction of metal ion with the halide bound to metal ion to hold the overall supramolecular structural pattern along with other intermolecular interactions. In this chapter, the crystal structures and packing features of a family of ten copper(II) complexes are analyzed and correlated with the 1D and 2D net architecture. These ten complexes can be described in terms of four major two-dimensional networks based on weak intermolecular apical interaction of metal with bound halide and the strong and/or weak hydrogen bonding between the functional parts of molecular units and the solvent incorporated as a guest molecule in the crystal lattice. We have varied the position of the methyl group on the phenolate ring of our ligand to study and compare the structural variations with the change of position of the substituent.

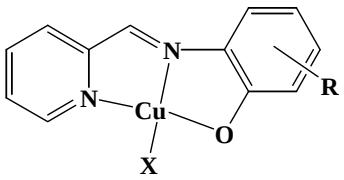

R = 3-Me, X = Cl (**11**) R = 3-Me, X = Br (**12**)
R = 4-Me, X = Cl (**13**) R = 4-Me, X = Br (**14**)
R = 5-Me, X = Cl (**15**) R = 5-Me, X = Br (**16**)
R = 6-Me, X = Cl (**17**) R = 6-Me, X = Br (**18**)
R = 4-Cl, X = Cl (**19**) R = 4-Cl, X = Br (**20**)

Figure 6.1.

6.2. Experimental section

6.2.1. Materials

The Schiff bases were prepared in ~80 % yield by the condensation of one mole equivalent each of 2-pyridinecarboxaldehyde and appropriate substituted 2-aminophenol in methanol. All other chemicals and solvents used in this work were of analytical grade available commercially and were used without further purification.

6.2.2. Physical measurements

Microanalytical (C, H, N) data were obtained with a Thermo Finnigon Flash EA1112 elemental analyzer. The infrared spectra were recorded by using a KBr pellet on a Jasco-5300 FT-IR spectrophotometer. Solution electrical conductivities were measured with a Digisun DI-909 conductivity meter. A Shimadzu 3101-PC UV/vis/NIR spectro-photometer was used to record the electronic spectra. The fluorescence spectra were recorded on a Spex FluoroMax-3 spectrofluorimeter. The magnetic susceptibility of the complexes was measured using a Sherwood Scientific balance. Diamagnetic correction calculated from Pascal's constants,[16] were used to obtain the molar paramagnetic susceptibilities.

6.2.3. Synthesis

All the complexes are prepared by following very similar procedures. Details are therefore given below for a representative case.

[Cu(3-Me-pyp)Cl] (11)

A methanol solution (15 ml) of $CuCl_2{\cdot}2H_2O$ (17.0 mg, 0.1 mmol) was added to a methanol solution (30 ml) of KOH (6.0 mg, 0.1 mmol) and 3-Me-Hpyp (22.0 mg, 0.1 mmol). The mixture was stirred in air at room temperature for 30 min. The red solution was then refluxed for 10 min. and left at room temperature for slow evaporation. Red-brown crystals formed after 2-3 days were collected by filtration. Yield: 62%. Anal. calcd. for $CuC_{13}H_{11}N_2OCl$: C, 50.33; H, 3.57; N, 9.03. Found: C, 49.96; H, 3.41; N, 8.67. Selected IR bands (cm^{-1}): 3047(w), 2928(w), 1560(s), 1467(s), 1282(s), 763(s), 489(w).

[Cu(3-Me-pyp)Br] (**12**)

Yield: 64%. Anal. calcd. for $CuC_{13}H_{11}N_2OBr$: C, 44.02; H, 3.13; N, 7.90. Found: C, 43.92; H, 3.02; N, 6.91. Selected IR bands (cm^{-1}): 3063(w), 2932(w), 1614(w), 1564(s), 1469(s), 1282(s), 763(s), 489(w).

[Cu(4-Me-pyp)Cl]·CH_3OH (**13**·CH_3OH)

Yield: 78%. Anal. calcd. for $CuC_{14}H_{15}N_2O_2Cl$: C, 49.13; H, 4.42; N, 8.18. Found: C, 47.74; H, 4.03; N, 8.16. Selected IR bands (cm^{-1}): 3418(br), 3061(w), 2927(w), 1649(w), 1597(s), 1489(s), 1253(s), 1018(m), 823(s), 515(m).

[Cu(4-Me-pyp)Br]·H_2O (**14**·H_2O)

Yield: 76%. Anal. calcd. for $CuC_{13}H_{13}N_2O_2Br$: C, 41.89; H, 3.52; N, 7.52. Found: C, 41.74; H, 3.49; N, 7.21. Selected IR bands (cm^{-1}): 3462(br), 3037(w), 2967(w), 1641(w), 1599(s), 1489(s), 1251(s), 1018(m), 821(s), 516(w).

[Cu(5-Me-pyp)Cl] (**15**)

Yield: 72%. Anal. calcd. for $CuC_{13}H_{11}N_2OCl$: C, 50.33; H, 3.57; N, 9.03. Found: C, 50.17; H, 3.46; N, 8.83. Selected IR bands (cm^{-1}): 3042(w), 2996(w), 1605(s), 1591(s), 1454(s), 1249(s), 765(m), 518(w).

[Cu(5-Me-pyp)Br] (**16**)

Yield: 73%. Anal. calcd. for $CuC_{13}H_{11}N_2OBr$: C, 44.02; H, 3.13; N, 7.90. Found: C, 43.89; H, 3.07; N, 7.61. Selected IR bands (cm^{-1}): 3039(w), 2997(w), 1606(w), 1591(s), 1454(s), 1155(s), 765(m), 518(w).

[Cu(6-Me-pyp)Cl] (**17**)

Yield: 68%. Anal. calcd. for $CuC_{13}H_{11}N_2OCl$: C, 50.33; H, 3.57; N, 9.03. Found: C, 50.21; H, 3.51; N, 8.61. Selected IR bands (cm^{-1}): 3037(w), 2995(w), 1603(s), 1592(s), 1541(s), 1201(s), 781(s), 493(m).

[Cu(6-Me-pyp)Br] (**18**)

Yield: 68%. Anal. calcd. for $CuC_{13}H_{11}N_2OBr$: C, 44.02; H, 3.13; N, 7.90. Found: C, 43.94; H, 3.12; N, 7.53. Selected IR bands (cm^{-1}): 3041(w), 2995(w), 1602(w), 1591(s), 1541(s), 1201(s), 740(s), 493(m).

[Cu(4-Cl-pyp)Cl] (**19**)

Yield: 82%. Anal. calcd. for $CuC_{12}H_8N_2OCl_2$: C, 43.59; H, 2.44; N, 8.47. Found: C, 43.24; H, 2.37; N, 7.97. Selected IR bands (cm^{-1}): 3062(br), 2994(w), 1606(m), 1531(m), 1477(s), 1454(s), 1165(s), 765(s), 51(m).

[Cu(4-Cl-pyp)Br] (**20**)

Yield: 85%. Anal. calcd. for $CuC_{12}H_8N_2OClBr$: C, 38.42; H, 2.15; N, 7.47. Found: C, 38.24; H, 2.12; N, 7.12. Selected IR bands (cm^{-1}): 3052(br), 2991(w), 1606(m), 1537(m), 1454(s), 1277(s), 1165(s), 765(s), 511(w).

6.2.4. X-ray crystallography

Unit cell parameters and the intensity data for the crystal of all the complexes are obtained on a Bruker-Nonius SMART APEX CCD single crystal diffractometer, equipped with a graphite monochromator and a Mo Kα fine-focus sealed tube (λ = 0.71073 Å) operated at 2.0 kW. The detector was placed at a distance of 6.0 cm from the crystal. Data are collected at 298 K with a scan width of 0.3º in ω and an exposure time of 10 sec/frame. In each case, the SMART software was used for data acquisition and the SAINT-Plus software was used for data extraction.[17] An absorption correction was performed with the help of SADABS program.[18] All the structures were solved by direct methods and refined on F^2 by full-matrix least-squares procedures. All non-hydrogen atoms were refined anisotropically. The protons of the solvent molecules in all the cases were located in the corresponding difference maps and refined with $U_{iso}(H) = 1.5U_{eq}(O)$, respectively. Other hydrogen atoms were included in the structure factor calculation at idealized positions by using a riding model. The SHELX-97[19] programs were used for structure solution and refinement. The ORTEX6a[20] and Platon[21] packages were used for molecular graphics. Significant crystallographic data are summarized in Tables 6.1–6.3.

Table 6.1. Crystallographic parameters for **11**, **12** and **13**·CH_3OH.

Complex	**11**	**12**	**13**·CH_3OH
Chemical formula	$CuC_{13}H_{11}N_2OCl$	$CuC_{13}H_{11}N_2OBr$	$CuC_{14}H_{15}N_2O_2Cl$
Formula weight	310.23	354.69	328.24
Crystal system	Triclinic	Triclinic	Triclinic
Space group	$P\bar{1}$	$P\bar{1}$	$P\bar{1}$
T(K)	298	298	298
a (Å)	8.0018(14)	8.0925(6)	6.8596(8)
b (Å)	8.9751(16)	8.9871(6)	9.1017(10)
c (Å)	9.8273(17)	10.0195(7)	11.4779(13)
α (°)	82.139(3)	84.576(1)	99.314(2)
β (°)	74.182(3)	73.831(1)	92.079(2)
γ (°)	64.184(2)	64.165(1)	94.296(2)
2θ range	4.30−52.42	4.24−56.44	3.60−52.16
V (Å^3)	611.14(19)	629.62(8)	704.32(14)
Z	2	2	2
μ (mm^{-1})	1.992	4.894	1.738
N-collected	6336	7114	7281
N-unique	2419	2865	2782
N [$I \geq 2\sigma(I)$]	2122	2508	2553
Parameters	164	164	186
*R*1[a], *wR*2[b] [$I \geq 2\sigma(I)$]	0.0370, 0.0831	0.0243, 0.0651	0.0329, 0.0926
*R*1[a], *wR*2[b] [all data]	0.0441, 0.0860	0.0291, 0.0673	0.0354, 0.0946
GOF[c] (F^2)	1.072	1.075	1.098
Largest peak and hole (*e* Å^{-3})	0.533, −0.270	0.490, −0.333	0.558, −0.519

Table 6.2. Crystallographic parameters for **14**·H_2O, **15**, **16** and **17**.

Complex	**14**·H_2O	**15**	**16**	**17**
Chemical formula	$CuC_{13}H_{13}N_2O_2Br$	$CuC_{13}H_{11}N_2OCl$	$CuC_{13}H_{11}N_2OBr$	$CuC_{13}H_{11}N_2OCl$
Formula weight	372.70	310.23	354.69	310.23
Crystal system	Triclinic	Monoclinic	Monoclinic	Orthorhombic
Space group	$P\bar{1}$	$P2_1/c$	$P2_1/c$	Pbca
T(K)	298	298	298	298
a (Å)	6.801(3)	11.1656(9)	11.1310(7)	14.7920(9)
b (Å)	8.900(4)	15.1860(12)	15.4597(9)	8.8261(5)
c (Å)	12.299(5)	7.0365(6)	7.1193(4)	18.8617(11)
α (°)	101.273(7)	90	90	90
β (°)	98.612(7)	94.862(1)	94.482(1)	90
γ (°)	110.387(7)	90	90	90
2θ range	3.48−50.00	3.66−52.04	3.68−52.02	4.32−52.20
V (Å^3)	664.9(5)	1188.8(2)	1221.4(1)	2462.5(3)
Z	2	4	4	8
μ (mm^{-1})	4.645	2.048	5.046	1.977
N-collected	6260	12156	12432	23919
N-unique	2336	2348	2402	2446
N [$I \geq 2\sigma(I)$]	1545	1593	2122	2112
Parameters	179	164	164	164
$R1$[a], $wR2$[b] [$I \geq 2\sigma(I)$]	0.0613, 0.1423	0.0456, 0.0818	0.0254, 0.0631	0.0467, 0.1118
$R1$[a], $wR2$[b] [all data]	0.0976, 0.1611	0.0775, 0.0890	0.0305, 0.0660	0.0547, 0.1166
GOF[c] (F^2)	0.960	0.908	1.048	1.071
Largest peak & hole(e Å^{-3})	1.172, −0.756	0.586, −0.295	0.483, −0.273	0.578, −0.991

Table 6.3. Crystallographic parameters for **18**, **19** and **20**.

Complex	**18**	**19**	**20**
Chemical formula	$CuC_{13}H_{11}N_2OBr$	$CuC_{12}H_8N_2OCl_2$	$CuC_{12}H_8N_2OClBr$
Formula weight	354.69	330.65	375.10
Crystal system	Orthorhombic	Monoclinic	Orthorhombic
Space group	Pbca	$P2_1/c$	Pbca
T(K)	298	298	298
a (Å)	15.267(2)	6.8709(6)	7.4359(6)
b (Å)	8.7840(13)	15.2190(12)	14.7997(11)
c (Å)	18.868(3)	23.5710(19)	22.4087(17)
α (°)	90	90	90
β (°)	90	94.2920(10)	90
γ (°)	90	90	90
2θ range	4.32−52.10	3.18−52.10	3.64−52.06
V (Å^3)	2530.3(6)	2457.9(4)	2466.1(3)
Z	8	4	8
μ (mm^{-1})	4.872	2.197	5.214
N-collected	13285	24411	23729
N-unique	2495	4765	2426
N [$I \geq 2\sigma(I)$]	1630	3775	1780
Parameters	164	325	163
*R*1[a], *wR*2[b] [$I \geq 2\sigma(I)$]	0.0447, 0.1012	0.0374, 0.0873	0.0515, 0.0994
*R*1[a], *wR*2[b] [all data]	0.0842, 0.1214	0.0498, 0.0942	0.0767, 0.1098
GOF[c] (F^2)	1.011	1.010	1.072
Largest peak and hole (*e* Å^{-3})	0.672, −1.103	1.263, −0.281	0.504, −0.395

[a] $R1 = \sum||F_o| - |F_c||/\sum|F_o|$. [b] $wR2 = \{\sum[(F_o^2 - F_c^2)^2]/\sum[w(F_o^2)^2]\}^{1/2}$.

[c] $GOF = \{\sum[w(F_o^2 - F_c^2)^2]/(n - p)\}^{1/2}$ where n is the number of reflections and p is the number of parameters refined; $w = 1/[\sigma^2(F_o^2) + (aP)^2 + bP]$.

6.3. Results and discussion

6.3.1. Synthesis and some properties

All the Complexes have been synthesized in moderate yield by reacting copper(II) halide with the appropriate Schiff base in presence of base in methanol. The elemental analyses data are satisfactory with the formulae given. All the complexes are electrically nonconducting in methanol solutions.

The infrared spectra of the free Schiff bases display a medium intensity band near 3364 cm^{-1}. This band is assigned to the phenolic-OH group. There is no such band in the spectra of the unsolvated complexes. Thus in the complexes the tridentate Schiff base is deprotonated and the phenolic-OH is coordinated to the metal ion. The solvated complexes display a broad band centred at ~3460 cm^{-1}, due to the stretching of the solvent OH group. The low energy shift (by ~20 cm^{-1}) of the imine band in the spectra of the complexes compared to that (~1626 cm^{-1}) of the free Schiff bases indicates coordination of the metal ion by the imine-N.[22] Thus the copper(II) centre in each of all the ten complexes is bound to the pyridine-N, the imine-N and the phenolate-O of the tridentate ligand. The remaining fourth coordination site is satisfied by the halide.

6.3.2. Absorption and emission spectral properties

The electronic absorption spectral features of the complexes in acetonitrile solutions are very similar. One broad absorption in the range 515−545 nm and three relatively sharp bands in the range 355−217 nm have been observed (Table 6.4). The broad lower energy band is assigned to the ligand to metal charge transfer band (LMCT), where as the relatively sharp higher energy bands are attributed to the ligand to ligand charge transfer (LLCT) transitions. The LLCT band positions are almost same for all the complexes. However, the LMCT band shows some shift with the position of the methyl group on the ligand (Table 6.5). The LMCT absorption for the chloride containing complexes with the methyl substitution at 3 or 5 positions has the band position at ~516 nm. This band shifts to lower energy (~526 nm) for 6-methyl and 4-chloro substituted complexes and the band gets further shifted to around 540 nm for the 4-methyl substituted species (Figure 6.2). The corresponding LLCT bands remain almost unaffected with the substituent position. The analogous bromide

containing complexes show similar trend in the absorption profiles. This LMCT band is also sensitive to the polarity of the solvent. It shows blue shift with the increase of the polarity of the solvent. While going from tetrahydrofuran (THF) to water the LMCT band has shown blue shift by almost 90 nm (Table 6.5). The shift of the LMCT band of [Cu(4-Me-pyp)Cl] (**13**) with the change of solvent polarity is shown in Figure 6.2. The bromide containing complexes display the similar blue shift of the LMCT band with the change of solvent polarity.

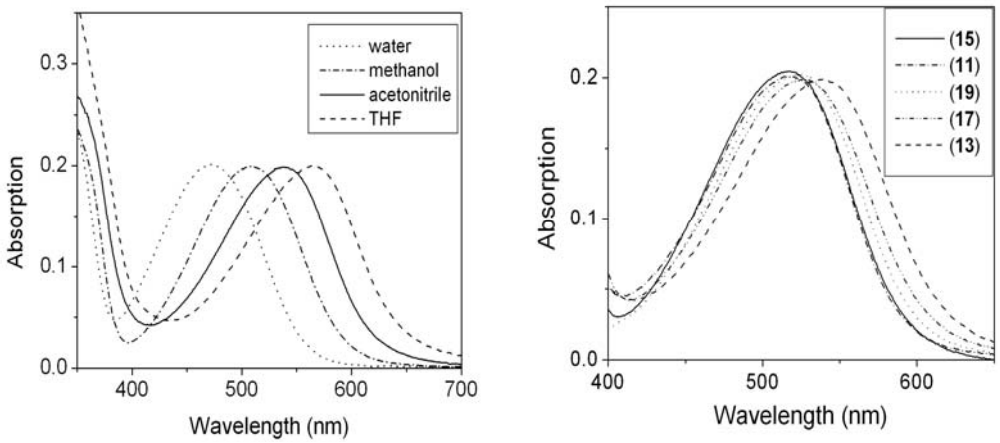

Figure 6.2. The variation of LMCT band position with the change of solvent for **[Cu(4-Me-pyp)Cl]** (**13**) (left) and the LMCT bands of all the five chloride containing complexes in acetonitrile solutions (right).

Table 6.4. The electronic absorption spectral data in acetonitrile solvent.

Complex	λ_{max} (nm) (ε ($M^{-1}cm^{-1}$))
11	517(2700), 355(4600), 300sh(9000), 286(9700), 235(15100)
12	510(2200), 351(4000), 300sh(8700), 293(93000), 220(14000)
13	541(5600), 348sh(7400), 297(12000), 236(20900)
14	534(5200), 348(7100), 297(10300), 217(23200)
15	519(4900), 355(5900), 305sh(8200), 296(8300), 235(14100)
16	514(4800), 353(6100), 304sh(8100), 298(8100), 218(25600)
17	527(6000), 357(7900), 301sh(10800), 292(11100), 237(21800)
18	522(4800), 354(6500), 302sh(10800), 291(12400), 219(23000)
19	525(6300), 338sh(7100), 291(12000), 238(19100)
20	521(5000), 338sh(6400), 292(15500), 219(26800)

Table 6.5. The wavelength (nm) of the LMCT band of all the ten complexes in water, methanol (MeOH), acetonitrile (MeCN) and tetrahydrofuran (THF).

Solvent	**11**	**12**	**13**	**14**	**15**	**16**	**17**	**18**	**19**	**20**
Water	453	452	472	471	453	454	465	463	466	467
MeOH	490	489	508	508	488	489	511	511	499	499
MeCN	517	510	541	534	519	514	527	522	525	521
THF	536	547	565	570	535	547	551	558	550	549

The complexes also have emissive property in the solution state. The high intensity absorption near 290 nm has been used to monitor the emission spectral features of all the complexes. The relative intensities of all the complexes are not equal in magnitude. The 3-methyl substituted analogue has the most intense band among the others. The descending order of relative emission intensities is **11** > **15** > **13** > **17** > **19** for the chloride containing complexes (Figure 6.3). The bromide containing complexes are having slightly less intensities than the corresponding chloride containing analogous. However, the relative order is same to that of the chloride containing complexes. Again the emission is sensitive to the polarity of the solvent both in relative position and intensity. With the increase of solvent polarity

the emission band sifts towards the lower energy for both chloride containing complexes as well as the bromide containing complexes (Figure 6.3).

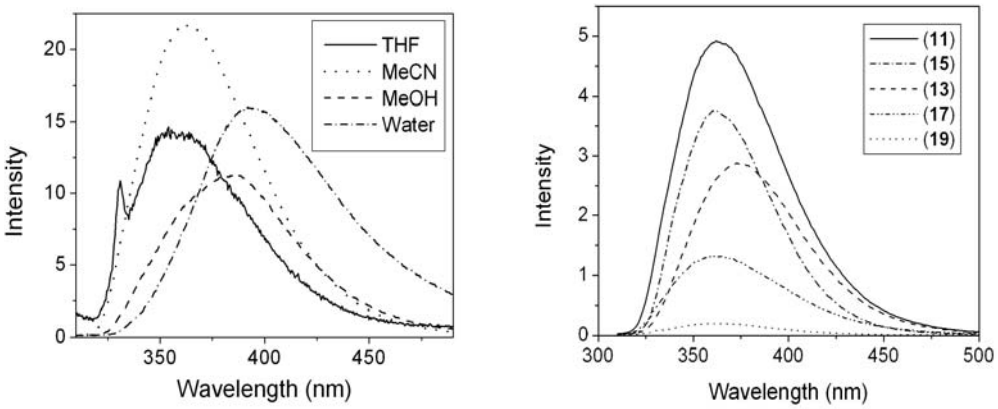

Figure 6.3. The solvent dependent emission spectra of **[Cu(3-Me-pyp)Br]** (**12**) (left) and the emission profiles of the chloride containing complexes in acetonitrile solutions (right).

Table 6.6. The wavelength (nm) of the emission band (λ_{max}) of all the ten complexes in water, methanol (MeOH), acetonitrile (MeCN) and tetrahydrofuran (THF).

Solvent	11	12	13	14	15	16	17	18	19	20
Water	392	394	394	396	384	385	396	391	388	384
MeOH	383	384	384	384	374	374	390	388	357	358
MeCN	363	363	374	372	362	361	362	362	364	362
THF	374	357	363	363	357	357	355	353	–	–

6.3.3. Description of molecular structures

The complexes crystallize in $P\bar{1}$, $P2_1/c$, and Pbca space groups. The asymmetric units of **13** and **14** contain a full complex molecule with one methanol and one water molecule, respectively. In rest of the case, a single complex molecule is present in the asymmetric unit except in **19**, where two complex molecules are observed in the asymmetric unit. In all the complexes the metal ion is coordinated to the pyridine-N, the imine-N and the phenolate-O donor tridentate ligand and the

halide. Complexes **13** and **14** are mononuclear species, while complexes **11**, **12**, **17**, **18** and **20** exist as centrosymmetric dimeric species in the solid state. On the other hand, complexes **15**, **16** and **19** are one-dimensional polymeric species. In **13** and **14** (4-Me substituted ligand), the metal ion is in N_2OX square-planar geometry. Except in **17** and **18** (6-Me substituted ligand) in all other cases, the metal ion is in square-pyramidal N_2OX_2 geometry, where the apical site is occupied by a halogen atom from a neighbouring molecule. In **17** and **18**, the coordination geometry around each metal ion can be best described as trigonal-bipyramidal. The imine-N atom and the two bridging halogen-atoms form the trigonal equatorial plane and the pyridine-N and the phenolate-O occupy the axial sites. All these structures are depicted in Figures 6.4 and 6.5. Selected bond lengths and angles are listed in Tables 6.7 and 6.8. The Cu–O (phenolate), the Cu–N (imine) and the Cu–N (pyridine) bond lengths are comparable with the bond lengths reported for copper(II) complexes having the same coordination atoms.[23] The equatorial Cu–X bond lengths are significantly shorter than the apical Cu–X' distances in the square-pyramidal copper(II) containing species (**11**, **12**, **15**, **16**, **19** and **20**). In general, the interaction at the apical site of the metal ion is weak. However, for **20** it is very weak as reflected by the significantly longer Cu–Cl' distances compared to that of the others (Tables 6.7 and 6.8). It may be noted that in **20**, the Cl-atom at 4-position of the phenolate ring is involved in the interaction with the metal ion at the apical position, while the metal coordinated halogen atom is at the apical site in rest of the square-pyramidal species. For **17** and **18**, in the trigonal equatorial plane both Cu–X and Cu–X' bond lengths are essentially identical. However, these are longer than the equatorial Cu–X bond lengths observed in the other species (Tables 6.7 and 6.8).

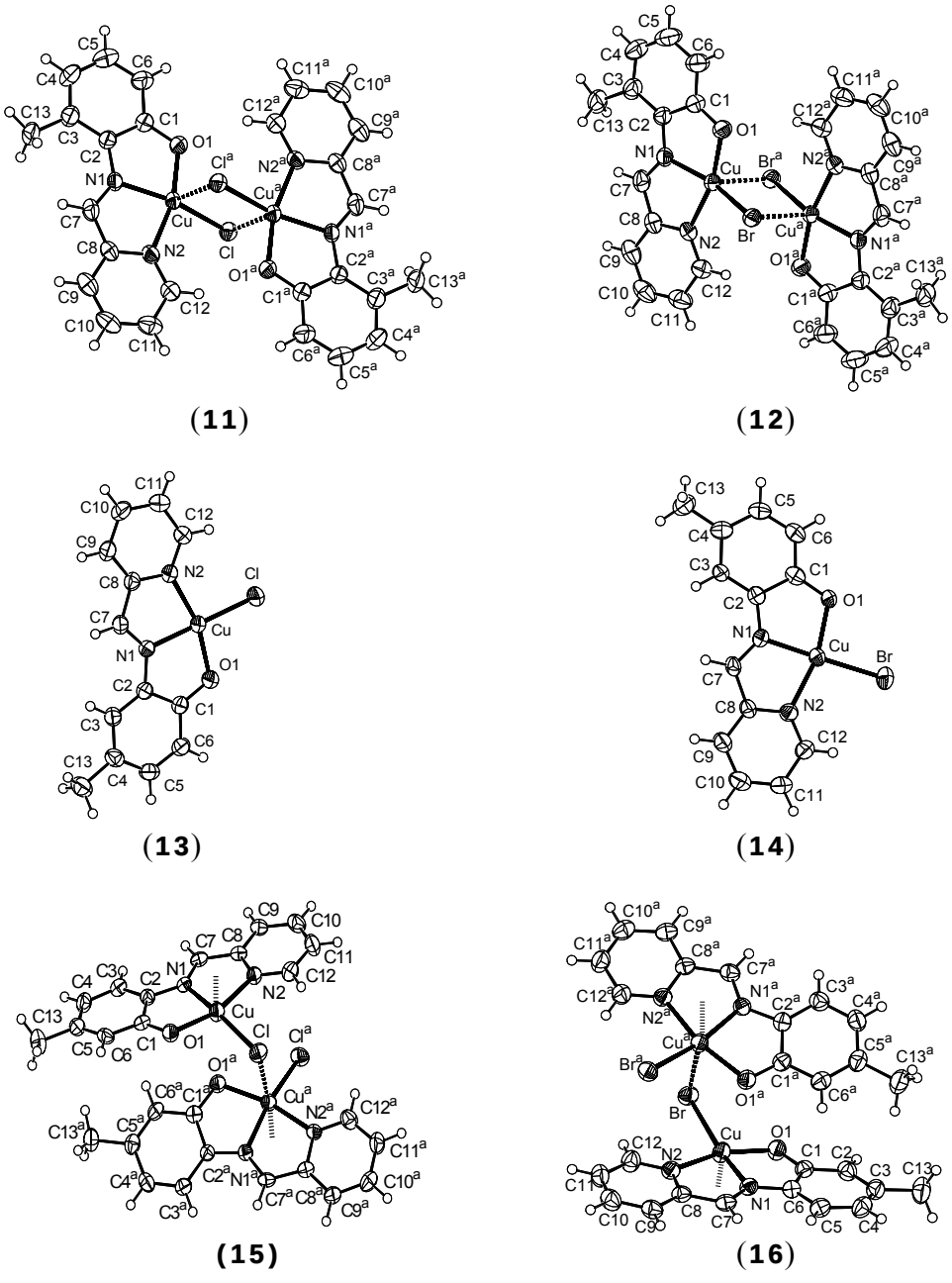

Figure 6.4. Structure of the dimeric form of **11**, **12**, **15** and **16**, and the monomeric form of **13** and **14** with the atom-labeling scheme. All non-hydrogen atoms are represented by their 50% probability thermal ellipsoids.

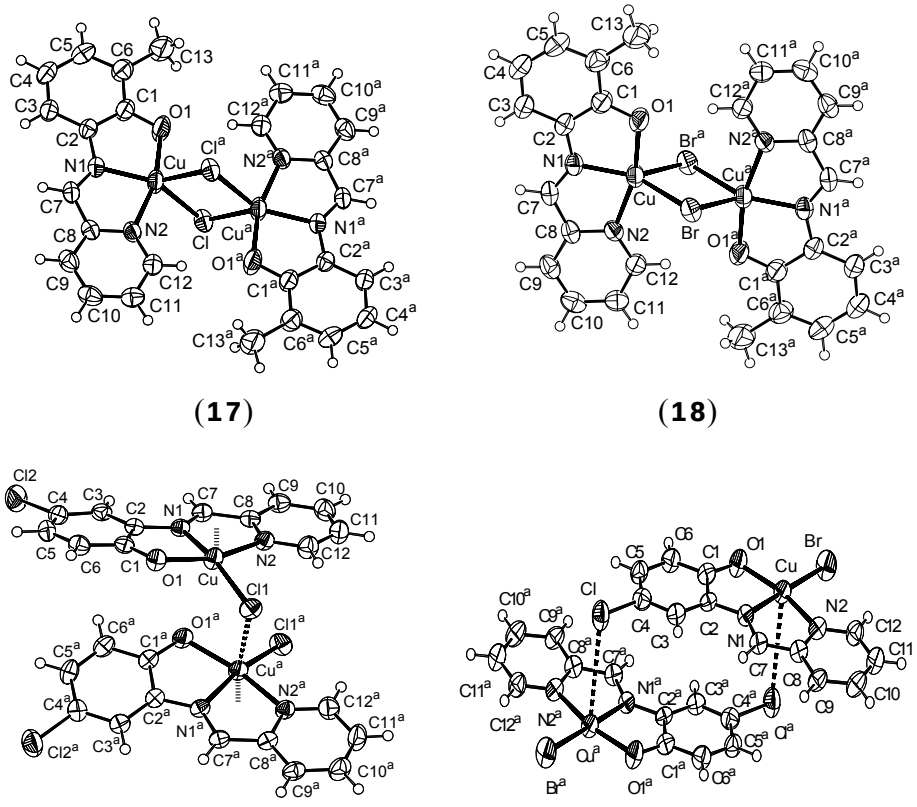

Figure 6.5. Structure of the dimeric form of **17**, **18**, **19** and **20** with the atom-labeling scheme. All non-hydrogen atoms are represented by their 50% probability thermal ellipsoids.

Table 6.7. Selected bond lengths (Å) and angles (°) for **11**, **13**·CH_3OH, **15**, **17** and **19**.

Complex	**11**	**13**·CH_3OH	**15**	**17**	**19**
Cu-O(1)	1.920(2)	1.940(2)	1.959(2)	1.935(3)	1.949(2)
Cu-N(1)	1.981(2)	1.960(2)	1.950(3)	1.955(3)	1.953(2)
Cu-N(2)	2.010(2)	2.020(2)	2.034(3)	2.022(3)	2.029(2)
Cu-Cl	2.2824(8)	2.2030(7)	2.2299(11)	2.4445(10)	2.2257(7)
O(1)-C(1)	1.309(3)	1.327(3)	1.324(4)	1.315(4)	1.319(3)
N(1)-C(7)	1.286(4)	1.271(3)	1.283(4)	1.281(4)	1.273(3)
Cu-Cl[a]	2.6790(9)	–	3.0730(12)	2.4309(10)	2.9464(8)
O(1)-Cu-N(1)	83.46(9)	83.63(7)	84.01(11)	83.31(11)	84.22(8)
N(1)-Cu-N(2)	81.38(10)	80.35(7)	80.05(13)	80.36(11)	80.02(9)
N(2)-Cu-Cl	96.10(7)	99.20(6)	95.92(9)	95.98(8)	97.16(7)
O(1)-Cu-Cl	97.10(6)	96.84(5)	101.40(8)	96.11(11)	100.06(6)
O(1)-Cu-N(2)	164.56(9)	163.71(7)	162.27(11)	163.66(11)	162.48(8)
N(1)-Cu-Cl	159.78(7)	179.33(5)	165.53(9)	136.58(8)	164.35(7)
O(1)-Cu-Cl[a]	95.27(7)	–	81.96(8)	96.87(12)	86.18(6)
N(1)-Cu-Cl[a]	106.18(7)	–	90.84(9)	132.39(8)	90.53(6)
N(2)-Cu-Cl[a]	91.79(7)	–	90.53(9)	93.89(9)	87.61(6)
Cl-Cu-Cl[a]	93.92(3)	–	103.15(4)	90.91(3)	105.66(3)
Cu-Cl-Cu[a]	86.08(3)	–	88.77(9)	89.09(3)	87.21(2)

Table 6.8. Selected bond lengths (Å) and angles (°) for **12**, **14**·H_2O, **16**, **18** and **20**.

Complex	**12**	**14**·H_2O	**16**	**18**	**20**
Cu-O(1)	1.917(2)	1.928(5)	1.952(2)	1.925(4)	1.940(3)
Cu-N(1)	1.977(2)	1.956(5)	1.954(2)	1.955(4)	1.963(4)
Cu-N(2)	2.015(2)	2.020(6)	2.043(2)	2.014(4)	2.020(4)
Cu-Br	2.4251(4)	2.3461(13)	2.3805(4)	2.5455(11)	2.3264(8)
O(1)-C(1)	1.310(3)	1.335(8)	1.314(3)	1.313(6)	1.319(6)
N(1)-C(7)	1.284(3)	1.287(8)	1.285(3)	1.283(7)	1.286(6)
Cu-Br[a]	2.7944(4)	–	3.0548(5)	2.5947(11)	3.204(2)[#]
O(1)-Cu-N(1)	83.50(7)	83.4(2)	83.85(8)	83.70(18)	83.36(16)
N(1)-Cu-N(2)	81.48(7)	80.7(2)	79.81(9)	80.44(18)	84.45(17)
N(2)-Cu-Br	96.30(5)	100.67(17)	96.48(6)	96.11(13)	99.06(13)
O(1)-Cu-Br	96.83(5)	95.22(14)	100.84(5)	95.73(15)	97.13(11)
O(1)-Cu-N(2)	164.81(7)	164.1(2)	162.67(8)	164.14(17)	163.80(16)
N(1)-Cu-Br	158.24(6)	178.27(17)	162.50(6)	138.72(13)	179.16(12)
O(1)-Cu-Br[a]	95.11(6)	–	85.18(6)	96.85(16)	94.91(13)*
N(1)-Cu-Br[a]	104.88(6)	–	95.12(6)	126.52(13)	84.52(12)*
N(2)-Cu-Br[a]	90.89(5)	–	90.52(6)	92.68(12)	83.67(12)*
Br-Cu-Br[a]	96.78(1)	–	102.05(1)	94.63(3)	94.75(4)*
Cu-Br-Cu[a]	83.22(1)	–	89.37(3)	85.37(3)	–

it is Cu–Cl distance; * angles are listed associated with chloride.

6.3.4. Supramolecular architectures

In the previous chapter, we have seen that [Cu(pyp)X] has perfect or nearly perfect square-planar geometry despite the presence of H_2O or MeOH in the crystal lattice. Depending upon the solvent of crystallization they form zipper structure or columnar structure assisted by mainly π-stacking expected for a plate-like species. In the present series of complexes, we have used the methyl or chloro substituted Hpyp as the ligand. There is a drastic change in the coordination geometry of the metal ion from square-planar to square-pyramidal to trigonal-bipyramidal due to the presence of the substituent on the tridentate ligand. Such changes are due to moderately strong to weak intermolecular interactions involving the coordinatively unsaturated metal ion.

We have systematically investigated the intermolecular non-covalent interactions and the resulting supramolecular architectures for all the complexes described in this chapter. A wide variety of non-covalent interactions such as C–H···X (with metal bound halide) and C–H···O (with incorporated solvent molecule) along with its stronger counter part O–H···O hydrogen bonding and π···π stacking are detected in this homologated family of simple complexes. As expected from the electronic back ground, the azomethine-CH and the *para*-CH of the pyridyl ring, the most electro-positive among the available hydrogens participate in the intermolecular C–H···O/X interactions. In some cases we have found that solvent molecules incorporated in the crystal lattice also support to hold the overall supramolecular structures. In the following sections we have discussed the molecular self-assembly of the present series of complexes in terms of their topological recognitions.

6.3.4.1. Staircase structure

The molecules of the 3-methyl substituted ligand containing complexes **11** and **12** are dimeric 'Z' type units due to equatorial-apical bridging by the metal bound halide in a reciprocal manner (Figure 6.4). This 'Z' units form staircase-like structure along *a*-axis through π···π interaction mainly involving the chelate rings formed by the pyridine-N and the imine-N. The staircases are interconnected through C–H···X interactions to afford a 2D network (Figure 6.6). The *para*-CH of the metal coordinated pyridine ring and the metal coordinated halide are involved in this C–H···X interactions. Finally these 2D sheets are connected via C–H···π interactions to build 3D framework. This C–H···π interaction involves the 3-methyl proton and the phenolate ring. The parameters associated with π···π, C–H···X and C–H···π interactions are listed in Table 6.9.

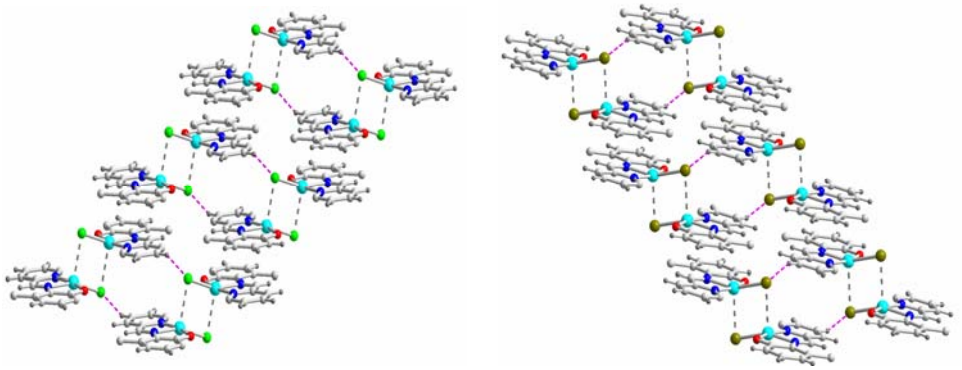

Figure 6.6. The staircase structure of **11** (left) and **12** (right) *via* apical metal-halide and stacking interactions. The parallel stairs are again connected through C–H···X interactions.

Table 6.9. The geometrical parameters associated with π···π, C–H···X and C–H···π interactions.

Complex	Interplanar Distance (Å)	Cg···Cg[#] distance (Å)	Offset angle (°)	Cu···Cu distance (Å)
11	3.386	3.407	6	5.016
12	3.413	3.462	10	5.114
Complex	Interaction	*d* (Å)	*D* (Å)	*θ* (°)
11	C–H···Cl	2.719	3.590	156
12	C–H···Br	2.816	3.685	156
	H···Cg distance (Å)	C···Cg distance (Å)	C– H···Cg angle (°)	
11	2.77	3.607	146	
12	2.78	3.638	150	

[#]The shortest Cg···Cg distances listed

6.3.4.2. Ladder structure

The solvent interspersed 4-methyl substituted ligand bearing complexes **13**·CH_3OH and **14**·H_2O reveal solvent mediated hydrogen bonded 1D ladder structure along the *b*-axis. The chloride ligated complex (**13)** shows double chain ladder structure through O–H···O (methanol-OH with phenolate-O), C–H···O (azomethine-

CH with methanol-O) and C–H···Cl (para-CH of pyridyl ring with metal bound chloride) interactions. Whereas in bromide ligated hydrated complex (**14**), the water molecule interacts with the complex molecule through two O–H···O (water-OH with phenolate-O) and one C–H···O (azomethine-CH with water O-atom) interactions to assist the formation of uniform ladder structure (Figure 6.7). In both the structures, the one-dimensional parallel ladders form 2D sheet structure through intermolecular π···π interactions between the planar complex molecules involving the chelate ring formed by pyridine-N and imine-N and pyridine ring. The ladder structure of **14**·H_2O is more uniform because both the complex and water molecules serve as three connector nodes. On the other hand, the complex molecule acts as four connector node and the methanol molecule acts as two connector node in the ladder structure formed by **13**·CH_3OH. The methanol and the complex molecule forms a finite square structures, which are again connected through C–H···Cl to form the final ladder structure. All the hydrogen bonding and the stacking parameters are given in Table 6.10.

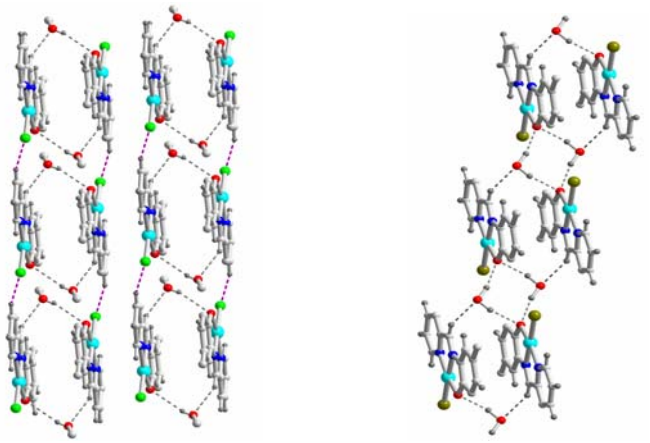

Figure 6.7. The ladder structures of **13**·CH_3OH (left) and **14**·H_2O (right) through hydrogen bonding with the incorporated solvent molecules.

Table 6.10. The geometrical parameters associated with π···π and H-bonding interactions.

	Interplanar Distance (Å)	Cg···Cg[#] distance (Å)	Offset angle (°)	Cu···Cu distance (Å)
13·CH_3OH	3.315	3.410	14	4.880
14·H_2O	3.299	3.391	13	5.055
	Interaction	*d* (Å)	*D* (Å)	*θ* (°)
13·CH_3OH	O−H···O	2.236	2.832	158
	C−H···O	2.673	3.548	157
	C−H···Cl	2.841	3.727	160
14·H_2O	O−H···O	1.921	2.863	167
	O−H···O	1.973	2.848	151
	C−H···O	2.395	3.242	151

[#]The shortest Cg···Cg distances listed

6.3.4.3. Square-grid structure

The 5-methyl substituted ligand containing species (**15** and **16**) prefer the metal-halide apical interaction in alternate mode instead of the reciprocal mode observed for the 3-methyl substituted ligand bearing complexes (**11** and **12**). Due to this alternate metal-halide apical interaction **15** and **16** form a polymeric chain structure. The metal bound halide also participates in intermolecular C−H···X interaction involving the azomethine-CH group. As a result, each complex molecule is serving as a four connector node to assist the formation of 2D square-grid structure (Figure 6.8). The parameters associated with the Cu···X' and C–H···X interactions are given in Table 6.11.

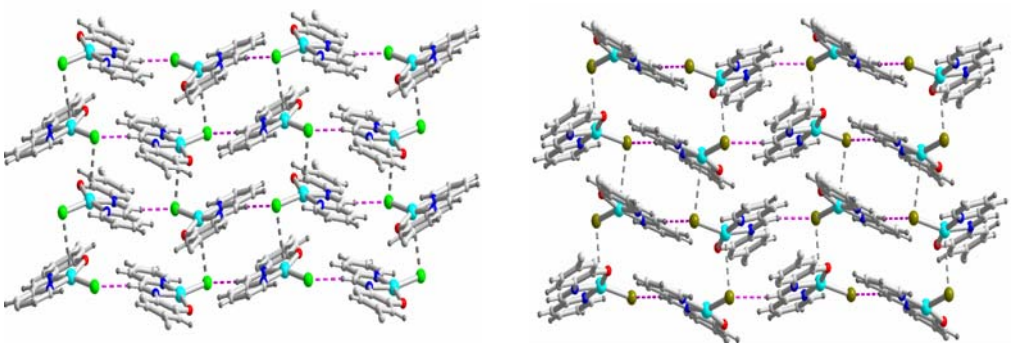

Figure 6.8. The square-grid structures of **15** (left) and **16** (right) through Cu···X and C–H···X interactions.

Table 6.11. The geometrical parameters for Cu···X and C–H···X interactions.

	Interaction	Cu···X distance (Å)	Cu–X···Cu' angle (°)	Cu···Cu' distance (Å)
15	Cu···Cl	3.073	89	3.758
16	Cu···Br	3.055	89	3.852
	Interaction	*d* (Å)	*D* (Å)	*θ* (°)
15	C–H···Cl	2.674	3.601	176
16	C–H···Br	2.796	3.720	173

6.3.4.4. Molecular brick wall

The complexes of the 6-methyl substituted ligand (**17** and **18**) have more symmetric dihalo bridged dimeric structure with respect to the Cu−Cl distances in the Cu_2Cl_2 core. In these dimeric molecules the metal ions have trigonal bipyramidal coordination geometry. Due to this type of dimerization whole molecule has two planar wings suitable to undergo stacking interactions. The stacking of the molecules is very similar to the arrangement of bricks in a wall. We have mentioned this structural motif as 'molecular brick wall' (Figure 6.9). Both the five membered chelate rings and the pyridyl rings participate in the stacking interactions. The wall structures are parallel to the crystallographic *ab*-plane. The geometrical parameters associated with the stacking interactions are given in Table 6.12.

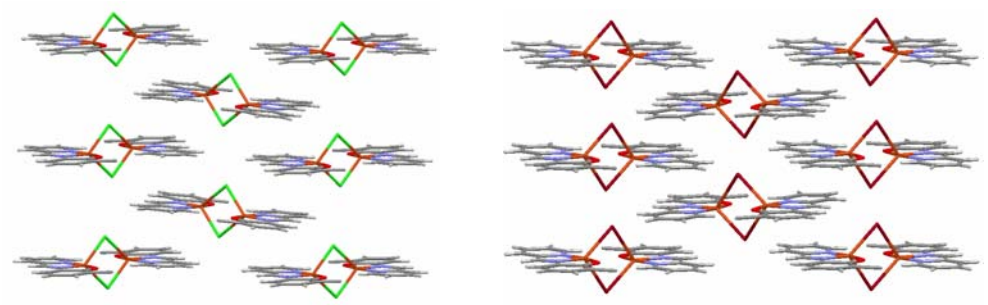

Figure 6.9. The π-stacking interactions assisted 'molecular brick wall' structures of **17** (left) and **18** (right).

Table 6.12. The geometric parameters associated with the π···π interactions.

Complex	Interplanar distance (Å)	Cg···Cg[#] distance (Å)	Offset angle (°)	Cu···Cu distance (Å)
17	3.372	3.525	17	6.353
18	3.378	3.542	17	6.485

[#]The shortest Cg···Cg distances listed

6.3.4.5. The effect of chloro substitution

We have seen that the complexes with the 4-methyl substituted ligand (**13** and **14**) provide solvent assisted ladder structures in the crystal lattice. It is well known that methyl and chloro substituted molecules which are otherwise identical give similar crystal structures due to their similar volumes.[24] Keeping this 'chloro-methyl' exchange rule in mind we have prepared complexes **19** and **20**, where the ligand contains a chloro group at the 4-position of the phenolate ring. However, **13** and **14** crystallized as **13**·CH_3OH and **14**·H_2O, while there is no solvent molecule in the crystal lattices of **19** and **20**. In all the previous cases (**11** and **12**; **13**·CH_3OH and **14**·H_2O; **15** and **16**; **17** and **18**), the molecular as well as supramolecular structural motifs for each pair of chloride and bromide ligated complexes are identical or very similar. But this is not the case for the complexes **19** and **20**. A 1D structure of the chloride ligated complex (**19**) is formed due to equatorial-apical bridging by the metal bound chloride. These parallel 1D structures are further connected by C−H···Cl−Cu interactions involving the azomethine-CH groups. As these Cu−Cl···Cu and

C−H···Cl−Cu interactions are roughly orthogonal a 2D square-grid net is formed (Figure 6.10). In contrast the bromide ligated species (**20**) form a dimeric structure *via* much weaker apical Cu···Cl interaction in a reciprocal manner involving the Cl-atom on the phenolate ring. These dimeric units form a 1D chain structure *via* π···π interactions (Figure 6.10) involving the five membered chelate rings and the pyridyl ring. The parameters associated with the non-covalent interactions observed for **19** and **20** are given in Table 6.13.

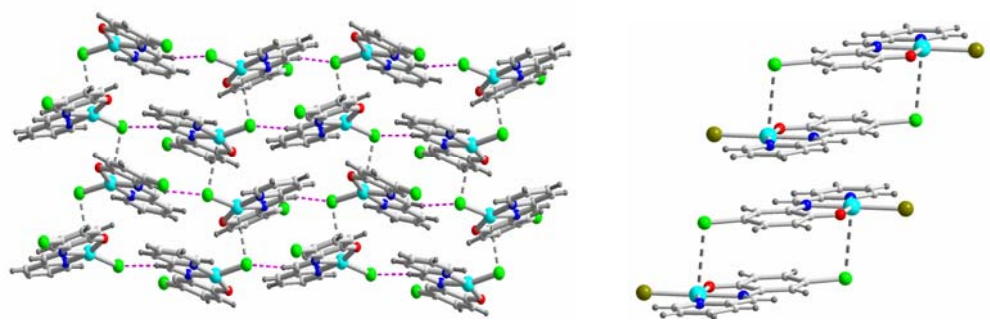

Figure 6.10. The square-grid structure of **19** (left) and the 1D chain of **20** (right).

Table 6.13. The geometrical parameters associated with non-covalent interactions in **19** and **20**.

Complex	Interaction	*d* (Å)	*D* (Å)	*θ* (°)
19	Cu···Cl'	2.946	3.605	87
	C–H···Cl	2.744	3.670	174
Complex	Interaction	Interplanar distance (Å)	Cg···Cg[#] distance (Å)	Offset angle (°)
20	π···π	3.228	3.403	17

[#]The shortest Cg···Cg distances listed

6.4. Conclusion

The molecular flexibility and the position of the peripheral functionality are expected to influence the self-assembly process and the resulting supramolecular structures. In the last chapter, we have seen how the nature of the solvent present in the crystal lattice influences the supramolecular architecture formed by very similar

host molecules having relatively rigid molecular frame. In this chapter, we have taken the same rigid molecular frame of copper(II) species and introduced and varied the position of the methyl substituent on the ligand to monitor the variation in the crystal packing patterns. In this process, we have realized staircase, ladder, brick-wall and square-grid supramolecular architectures with the variation of substitutional position on the ligand backbone. The susbstituent position not only affected the structural patterns but also caused the change in the energetic part of the complexes, which has been reflected in the electronic spectral feature.

Reference

32 Bond, A. D.; Jones, W. In *Supramolecular Organization and Materials Design*; Jones, W., Rao, C. N. R., Eds.; Cambridge University Press: Cambridge, 2002.

33 Desiraju, G. R. *Crystal Engineering. The Design of Organic Solids*; Elsevier: Amsterdam, 1989.

34 Moulton, B.; Zaworotko, M. J. *Chem. Rev.* **2001**, *101*, 1629.

35 Hoeben, F. J. M.; Jonkheijm, P.; Meijer, E. W.; Schenning, A. P. H. J. *Chem. Rev.* **2005**, *105*, 1491.

36 Kitagawa, S.; Uemura, K. *Chem. Soc. Rev*. **2005**, *34*, 109.

37 Pollino, J. M.; Weck M. *Chem. Soc. Rev*. **2005**, *34*, 193.

38 Braga, D.; Brammer, L.; Champness, N. R. *CrystEngComm* **2005**, *7*, 1.

39 Erk, P.; Hengelsberg, H.; Haddow, M. F.; Gelder, R. V. *CrystEngComm* **2004**, *6*, 474.

40 Nishio, M. *CrystEngComm* **2004**, *6*, 130.

41 Beatty, A. M. *Coord. Chem. Rev*. **2003**, *246*, 131.

42 Beatty, A. M. *CrystEngComm* **2001**, *51*, 1.

43 Alcock, N. W.; Barker, P. R.; Haider, J. M.; Hannon, M. J.; Painting, C. L.; Pikramenou, Z.; Plummer, E. A.; Rissanen, K.; Saarenketo, P. *J. Chem. Soc., Dalton Trans.* **2000**, 1447.

44 Lehn, J.-M. *Science* **2002**, *295*, 2400.

45 Sinnokrot, M. O.; Cherrill, C. D. *J. Am. Chem. Soc.* **2004**, *126*, 7690.

46 Hunter, C. A.; Sanders, J. K. M. *J. Am. Chem. Soc.* **1990**, *112*, 5525.

47 Hatfield, W. E. *Theory and Applications of Molecular Paramagnetism*; Boudreaux, E. A.; Mulay, L. N., Eds.; Wiley, New York, 1976; pp. 491.

48 *SMART*; 5.630, Eds.; *SAINTPLUS*; 6.45, Eds.; Bruker AXS, Inc.: Madison, WI, USA, 2003.

49 *SADABS*; 2.10, Eds.; Bruker AXS, Inc.: Madison, WI, USA, 2003.

50 Sheldrick, G. M. *SHELX-97* Structure Determination Software, University of Go¨ttingen, Go¨ttingen, Germany, 1997.
51 McArdle, P. *J. Appl. Crystallogr.* **1995**, *28*, 65.
52 Spek, A. L. *Platon98* Molecular Graphics Software, University of Glasgow, UK, 1998.
53 Nakamoto, K. *Infrared and Raman Spectra of Inorganic and Coordination Compounds;* Wiley, New York, 1986; pp. 241–244.
54 Pal, S. N.; Pal, S. *Inorg. Chem.* **2001**, *40*, 4807.
55 Desiraju, G. R.; Sarma, J. A. R. P. *Proc. Indian Acad. Sci. (Chem. Sci.)* **1986**, *96*, 599.

Chapter 7

Coordination polymers assembled by rigid and conformationally flexible spacers

Three three-dimensional succinate bridged coordination polymers, $\{[Cu(suc)(bpy)(H_2O)_2]\cdot(H_2O)_2\}_n$ (**21**), $\{[Ni(suc)(bpy)(H_2O)_2]\cdot(H_2O)_2\}_n$ (**22**) and $[Cu_2(suc)_2(pz)]_n$ (**23**) {where suc^{2-} = dianionic deprotonated succinic acid; bpy = 4,4'-bipyridine and pz = pyrazine} have been synthesized and characterized. In the cases of **21** and **22**, the chiral *gauche* conformation of the succinate leads to homo-chiral cylindrical helices along the crystallographic *c*-axis. The left handed or *M*-form of succinate produces left handed helix in the case of **21**, while the right handed or *P*-form of succinate produces right handed helix in the case of **22**. Both the distorted octahedral metal centers show twisting chiral $7^5.9$ net with the helix incorporated within it. On the other hand **23** depicts the 2-fold interpenetrating primitive cubic network. The thermo-gravimetric analysis (TGA) and magnetic properties of these coordination polymers are discussed in details.

7.1. Introduction

'Crystal engineering', the term coined by Schmidt about three decade ago[1] is the most suitable tool for the development of rational strategies in designing new crystalline materials, in particular those with functional properties.[2,3] The specific network topology of a coordination polymer can be controlled by a careful selection of the metal coordination geometry and the organic bridging ligand.[4,5] In the field of metal-organic frameworks (MOFs), a strong interaction such as metal-ligand coordination together with intermolecular non-covalent interactions are utilized to assemble supramolecular networks with desired topologies from their constituent building blocks. In recent times, considerable efforts have been devoted on the design, synthesis and characterization of novel multidimensional MOF architectures and topologies for their potential applications in a wide range of research areas such

as functional solid materials, ion exchange, catalysis, gas storage,[6–10] and the development of optical, electronic, and magnetic devices.[11–16] The designed synthesis of noncentrosymmetric solids is a challenging problem for the fabrication of materials with ferro-, pyro- and piezoelectric, and nonlinear optical (NLO) properties.[17,18] Due to the lack of inversion centre helical motif is one of the strategic architecture found in many acentric solids. However, an equally large group of materials that contain helical chains do have inversion centers. In general, how to design or make a noncentrosymmetric solid from inorganic helices relies on our understanding of ligand effects and crystal packing. Here we have tried to explain the role of the length and conformation of the bridging ligand and the helical symmetry on the formation of the two noncentrosymmetric compounds, $\{[Cu(suc)(bpy)(H_2O)_2]\cdot(H_2O)_2\}_n$ (**21**) and $\{[Ni(bpy)(suc)(H_2O)_2]\cdot(H_2O)_2\}_n$ (**22**) (where 'suc' and 'bpy' represents dianionic succinate and 4,4'-bipyridine, respectively) and the centrosymmetric compound $[Cu_2(suc)_2(pz)]_n$ (**23**) (where 'pz' represents pyrazine).

7.2. Experimental section

7.2.1. Materials

All the chemicals and solvents used in this work were of analytical grade available commercially and were used without further purification.

7.2.2. Physical measurements

Microanalytical (C, H, N) data were obtained with a Thermo Finnigon Flash EA1112 elemental analyzer. The infrared spectra were collected by using a KBr pellet on a Jasco-5300 FT-IR spectrophotometer. A Shimadzu 3101-PC UV/vis/NIR spectro-photometer was used to record the electronic spectra. DSC was performed on a Mettler Toledo DSC 822e module and TGA was performed on a Mettler Toledo TGA/SDTA 851e module. The typical sample size is 4-6 mg for DSC and 9-12 mg for TGA. A SQUID magnetometer was used for the magnetic susceptibilities measurements in the temperature range 20–300 K. A diamagnetic correction calculated from Pascal's constants,[19] was used to obtain the molar paramagnetic susceptibilities.

7.2.3. Synthesis

[Cu(suc)(bpy)(H_2O)$_2$]·2H_2O (21)

A DMF solution of 4,4'-bipyridine (31 mg, 0.2 mmol) was added to an aqueous solution of $Cu(NO_3)_2·3H_2O$ (48 mg, 0.2 mmol) with stirring at room temperature. After 10 min. an aqueous solution of disodium succinate (32 mg, 0.2 mmol) was added slowly with stirring. After ½ hr stirring the mixture was heated to 120°C for 3 days and cooled slowly to room temperature. The blue needle shaped crystals deposited were collected by filtration, washed thoroughly with water and dried in air (yield: 68%). Anal. calcd. for $CuC_{14}H_{20}N_2O_8$: C, 41.23; H, 4.94; N, 6.87. Found: C, 41.85; H, 4.39; N, 6.41. Selected IR bands (cm^{-1}): 3369(br), 2980(m), 2901(m), 1616(s), 1558(s), 1419(s), 1072(s), 821(s).

[Ni(suc)(bpy)(H_2O)$_2$]·2H_2O (22)

This compound was prepared using $Ni(NO_3)_2·6H_2O$ instead of $Cu(NO_3)_2·3H_2O$ by following the same procedure as described for **21**. Blocked shape bluish crystals were obtained in about 74% yield. Anal. calcd. for $NiC_{14}H_{20}N_2O_8$: C, 41.72; H, 5.00; N, 6.95. Found: C, 41.90; H, 4.71; N, 6.49. Selected IR bands (cm^{-1}): 3364(br), 2890(m), 1616(s), 1541(s), 1419(s), 1068(s), 819(s).

[Cu$_2$(suc)$_2$(pz)] (23)

A water solution of pyrazine (16 mg, 0.2 mmol) was added to an aqueous solution of $Cu(NO_3)_2·3H_2O$ (97 mg, 0.4 mmol) with stirring at room temperature. After 10 min. an aqueous solution of disodium succinate (65 mg, 0.4 mmol) was added slowly with stirring. After ½ hr stirring the mixture was heated to 120°C for 3 days and cooled slowly to room temperature. The green needle shaped crystals deposited were collected by filtration, washed thoroughly with water and dried in air (yield: 77%). Anal. calcd. for $CuC_6H_6NO_4$: C, 32.81; H, 2.75; N, 6.38. Found: C, 32.37; H, 2.39; N, 5.85. Selected IR bands (cm^{-1}): 3107(w), 3036(w), 2961(w), 2939(w), 1591(s), 1493(m), 1406(s), 1242(s), 1049(s), 814(s), 686(s), 451(s).

7.2.4. X-ray crystallography

Unit cell parameters and the intensity data for **21**, **22** and **23** are obtained on a Bruker-Nonius SMART APEX CCD single crystal diffractometer, equipped with a graphite monochromator and a Mo Kα fine-focus sealed tube (λ = 0.71073 Å) operated at 2.0 kW. The detector was placed at a distance of 6.0 cm from the crystal. Data are collected at 298 K with a scan width of 0.3º in ω and an exposure time of 10 sec/frame. In each case, the SMART software was used for data acquisition and the SAINT-Plus software was used for data extraction.[20] An absorption correction was performed with the help of SADABS program.[21] All the structures were solved by direct methods and refined on F^2 by full-matrix least-squares procedures. All non-hydrogen atoms were refined anisotropically. The protons of the solvent molecules in all the cases were located in the corresponding difference maps and refined with $U_{iso}(H) = 1.5U_{eq}(O)$, respectively. Other hydrogen atoms were included in the structure factor calculation at idealized positions by using a riding model. The SHELX-97[22] programs were used for structure solution and refinement. The Platon[23] packages were used for molecular graphics. Significant crystallographic data are summarized in Table 7.1.

Table 7.1. Crystallographic parameters for **21**, **22**, and **23**.

Complex	**21**	**22**	**23**
Chemical formula	$CuC_{14}H_{20}N_2O_8$	$NiC_{14}H_{20}N_2O_8$	$CuC_6H_6NO_4$
Formula weight	407.86	403.03	219.67
Crystal system	Hexagonal	Hexagonal	Monoclinic
Space group	$P6_522$	$P6_122$	C2/m
T(K)	298	298	298
a (Å)	11.0818(3)	11.1996(4)	9.7726(12)
b (Å)	11.0818(3)	11.1996(4)	11.6654(15)
c (Å)	24.9892(14)	24.2343(18)	7.4758(9)
α (°)	90	90	90
β (°)	90	90	119.250(2)
γ (°)	120	120	90
2θ range	4.24–52.04	4.20–52.02	5.92–56.60
V (Å^3)	2657.68(18)	2632.5(2)	743.59(16)
Z	6	6	8
μ (mm^{-1})	1.276	1.149	2.911
N-collected	27840	14646	4072
N-unique	1757	1731	891
N [$I \geq 2\sigma(I)$]	1620	1566	823
Parameters	128	128	58
Flack parameter	0.01(2)	0.01(3)	–
*R*1[a], *wR*2[b] [$I \geq 2\sigma(I)$]	0.0327, 0.0749	0.0345, 0.0763	0.0345, 0.0832
*R*1[a], *wR*2[b] [all data]	0.0372, 0.0770	0.0406, 0.0790	0.0384, 0.0861
GOF[c] (F^2)	1.121	1.055	1.087
Largest peak and hole (*e* Å^{-3})	0.329, −0.157	0.366, −0.190	0.885, −0.438

[a] $R1 = \sum||F_o| - |F_c||/\sum|F_o|$. [b] $wR2 = \{\sum[(F_o^2 - F_c^2)^2]/\sum[w(F_o^2)^2]\}^{1/2}$.

[c] $GOF = \{\sum[w(F_o^2 - F_c^2)^2]/(n - p)\}^{1/2}$ where n is the number of reflections and p is the number of parameters refined; $w = 1/[\sigma^2(F_o^2) + (aP)^2 + bP]$.

7.3. Results and discussion

7.3.1. Synthesis and some properties

All the compounds have been synthesized in moderate yield from dmf-water media by solvo-thermal process. Compounds are insoluble in water and common organic solvents.

In the infrared spectra, compounds **21** and **22** has display a medium intensity broad band at ~3370 cm^{-1} due to the water molecules present in them. The sharp band at ~1616 cm^{-1} is most likely associated with the coordinated carboxylate functionalities. The sharp band observed at 1591 cm^{-1} in the spectrum of **23** is assigned to the ν_{asy} of the bridging carboxylate moieties.[24]

7.3.2. Description of the crystal structures

[Cu(suc)(bpy)(H_2O)$_2$]·2H_2O (**21**)

The compound **21** crystallizes in $P6_522$ space group. The asymmetric unit contains half of Cu^{2+}, half of succinate, half of 4,4'-bipyridine, one coordinated and one uncoordinated water molecule. As shown in Figure 7.1, the Cu^{2+} centre is in tetragonally elongated N_2O_4 octahedral coordination sphere. The nitrogen atoms belong to two bpy ligands, the oxygen atoms to two H_2O molecules and two monodentate succinate ions. The two pyridyl nitrogen atoms as well as the two carboxylate oxygen atoms are *trans* to each other and form the equatorial plane. The Cu–N bond lengths are 1.996(3) and 2.015(3) Å and Cu–O (carboxylate-O) bond length is 1.958(2) Å. The aqua oxygen atoms occupy the elongated axial positions with the Cu–O bond length 2.529(2) Å. The larger axial Cu–O bond lengths are indicative of Jahn-Teller distortion due to the d9 configuration of the metal ion. The *cis* and *trans* bond angles about the central Cu-atom are in the ranges 86-94 and 177-180º, respectively. Among the two crystallographically distinct water molecules, one is hydrogen bonded to a coordinating aqua oxygen atom as well as to one non-coordinating carboxylate oxygen atom and the second one is hydrogen bonded to the other crystal water oxygen atom as well as to another non-coordinating carboxylate

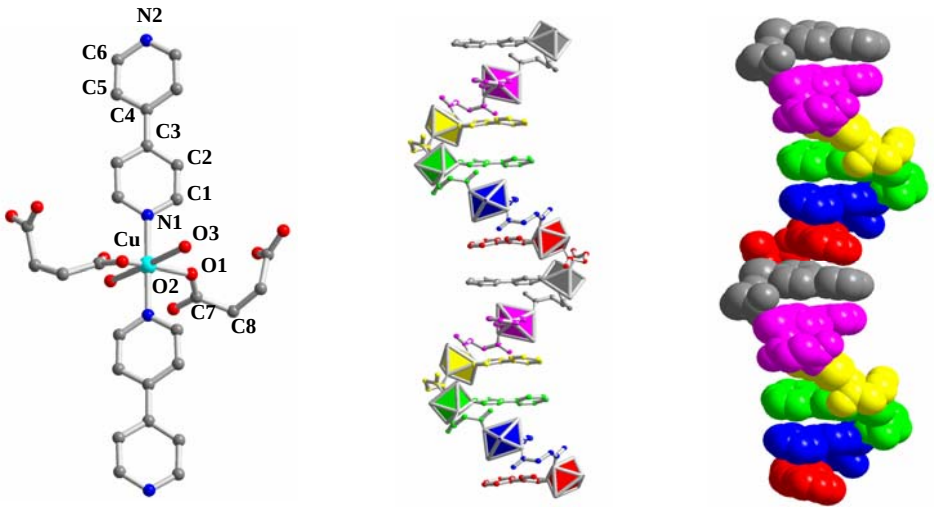

Figure 7.1. Crystal structure of **21** with the atom-labeling scheme (left), the polyhedral representation (middle) and the space-filling model (right) of the helical assembly.

oxygen atom. Three rotamer are possible for the succinate ion. These are *trans* or *anti*, *cis* or *eclipsed* and *gauche* forms (Figure 7.2). The *gauche* form is chiral. One of the enantiomers has the right handed (*P*) form and the other one has the left handed (*M*) form (Figure 7.2). The left handed *gauche* conformation of succinate ligands in **21** (torsion angle for the skeleton carbon chain of succinate anion is 69.82(6)º) leads to a striking structural feature: alternating assembly of the left handed homo-chiral cylindrical 6_1 helices along the crystallographic *c*-axis (Figure 7.1). The helices are further interconnected by 4,4'-bipyridine ligands, which are aligned parallel to the [100], [010] and [110] axis. These interconnection lead to a novel 3D framework providing channels in the same directions in which the crystal H_2O molecules are located (Figure 7.3). The intrahelical Cu···Cu separation (7.061 Å) through the succinato group is significantly smaller than the interhelical metal-metal separation (11.082 Å) through the 4,4'-bipyridine ligand. The Cu···Cu distance of the repeating period in the helical column is about 21.591 Å. Another unusual feature of the structure is that each helix is connected with six adjacent helices by 4,4'-bipyridine ligands. As shown in Figure 7.1, six 4,4'-bipyridine ligands of one hexagon have six

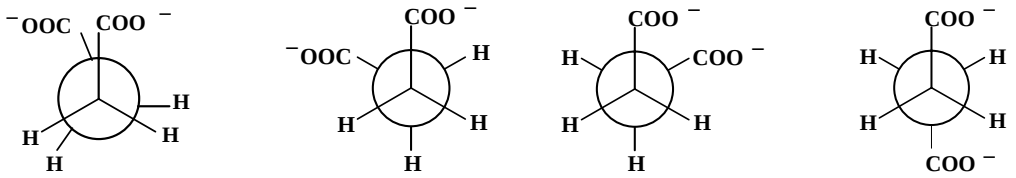

Figure 7.2. The four possible rotamers of succinate.

different orientations and each of them connects to another adjacent helix, respectively (Figure 7.3). The stacking is inherently orientated and appears to manifest itself in two salient characters. First, for each cylindrical column, only one helical orientation is involved in the crystal structure, which crystallizes in the asymmetric space group, $P6_522$. Second, adjacent helices are staggered by one-sixth of the column length. All the important bond distances and angles has depicted in the Table 7.2.

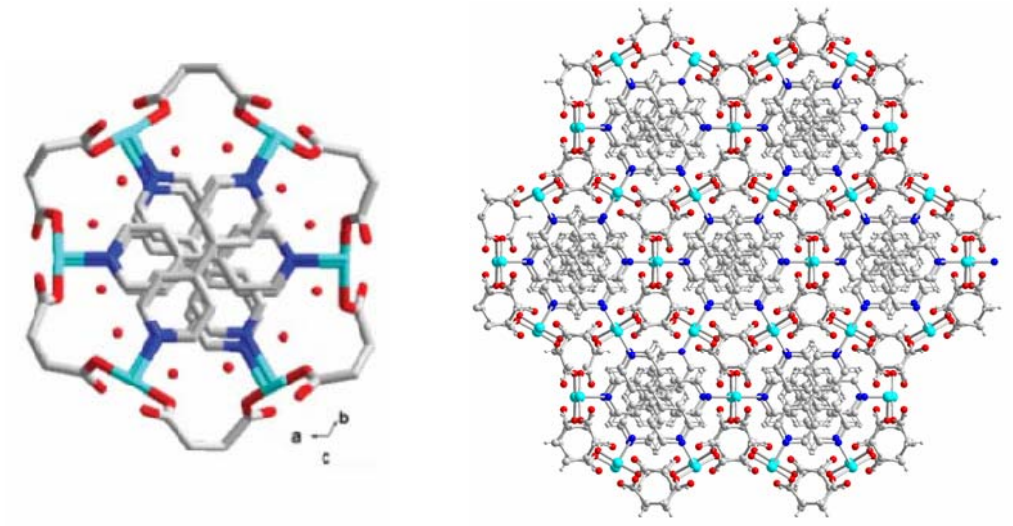

Figure 7.3. Stick representation of the channels between the helices filled by guest water molecules (left); stick representation of the connecting mode of helices (right).

The Cu atoms act as four-coordinate planar centers (the axial water ligands do not bridge). There are two different ligands, so the network can be represented

topologically simply by the Cu nodes and the two types of connectors (bridging 4,4'-bipyridine and succinate ligands) between them. There are two different node-node distances in the structure reported here, and the angles concerning the nodes are not 90º. Three adjacent nodes between two succinate ligands form an arc, which further leads to form a single helix (Figure 7.1). Figure 7.4 reveals the unusual 'dense' $7^5.9$ network displayed by this structure. The main feature of this net is that it is a strongly twisting 'dense' $7^5.9$ net and incorporates helix sub-structures with the same accessibility. The maximum symmetry of the net is hexagonal. Compared to the regular 'dense' $7^5.9$ net, there are several differences in the present one: (i) this net contains only one type of node, but there are two types of links; (ii) the angle between all the nodes are not 90º, so it cannot be classed as either a ''regular'' [all vertices, edges, and angles are equivalent (related by symmetry)] or ''quasi-regular'' [all vertices and edges (but not angles) are equivalent] net;[25] (iii) due to the helix substructure, the 3_1 helical disposition in the regular 'dense' $7^5.9$ net changes to the higher 6_1 helical structure.

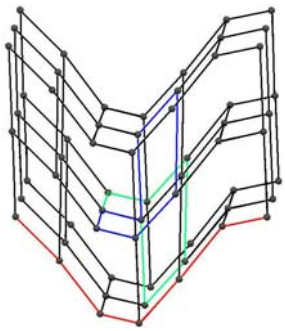

Figure 7.4. The twisting 'dense' $7^5.9$ net; single helix (red) and two seven-membered shortest circuits (green and blue) are highlighted.

It may noted that the structure of **21** has been reported earlier.[26,27] However, the space group assigned to them are different and hence ambiguous in these reports. These are $P6_1$ (No. 169)[26] and $P6_5$ (No. 170)[27]. However, during data processing and refinement of **21**, we found that this copper(II) compound possesses a 6_5 crystallographic axis passing through the centre of C(3) and C(4), and a twofold crystallographic axis passing through Cu, N(1), C(3), C(4) and N(2). The space group

was unambiguously determined to be $P6_522$ for **21**. Recently the analogous Co(II) complexes has been reported[28] in the same space group in which we have solved the structure of **21**.

[Ni(suc)(bpy)(H_2O)$_2$]·2H_2O (**22**)

The nickel(II) analogue (**22**) of the previous compound (**21**) crystallizes in $P6_122$ space group and the asymmetric unit contains half of Ni^{2+}, half of succinate anion, half of 4,4'-bipyridine, one coordinated and one uncoordinated water molecules (Figure 7.5). The overall structural motifs of both **21** and **22** are almost identical except few major differences. As expected, Ni^{2+} forms stronger axial bonds than Cu^{2+}. The axial Ni–O bond distances are 2.134(2) Å. As a result, N2O4 coordination geometry around the metal centre constituted by two succinate O-atoms, two water O-atoms and two pyridyl N-atoms is very close to octahedral symmetry. Another major difference is the handedness of the helix, which propagates along the *c*-axis. Here it is right handed (Figure 7.5) rather than left handed (**21**) (Figure 7.1). The selected bond lengths and angles are given in Table 7.2. This difference in

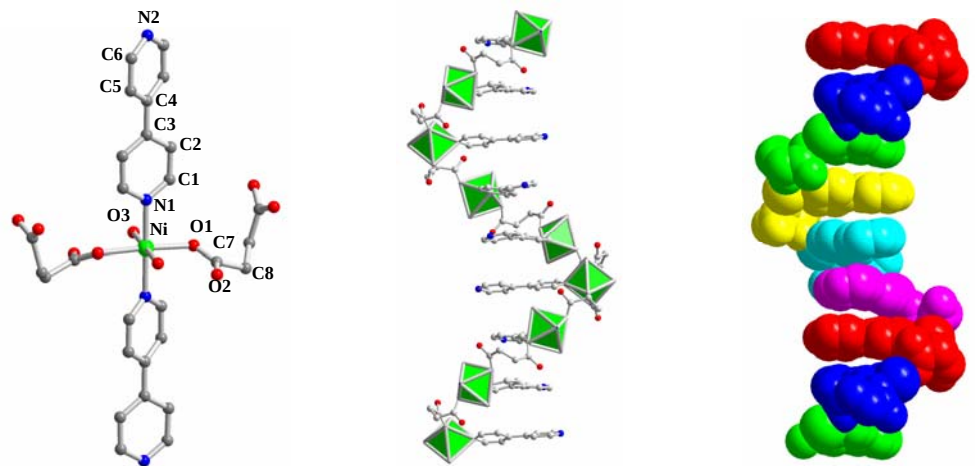

Figure 7.5 Crystal structure of **22** with the atom-labeling scheme (left), the polyhedral representation (middle) and the space-filling model (right) of the helical assembly.

handedness of the helices is due to the difference in the conformations of succinate in **21** and **22**. In **22**, bridging succinate is in right handed *gauche* form. The torsion angle for the skeleton carbon chain of succinate anion is 69.94(8)º in **22**. Thus the handedness of the bridging succinate is translated to the same handedness of the helical superstructure observed for **21** and **22**. The intrahelical Ni···Ni separation through the succinato group is 7.296 Å and that of through the 4,4'-bipyridine ligand is 11.200 Å. Whereas the Ni···Ni distance of the repeating period in the helical column is about 21.089 Å. Except the handedness of the helices all other features of crystal packing are identical for both **21** and **22** (Figures 7.3 and 7.6).

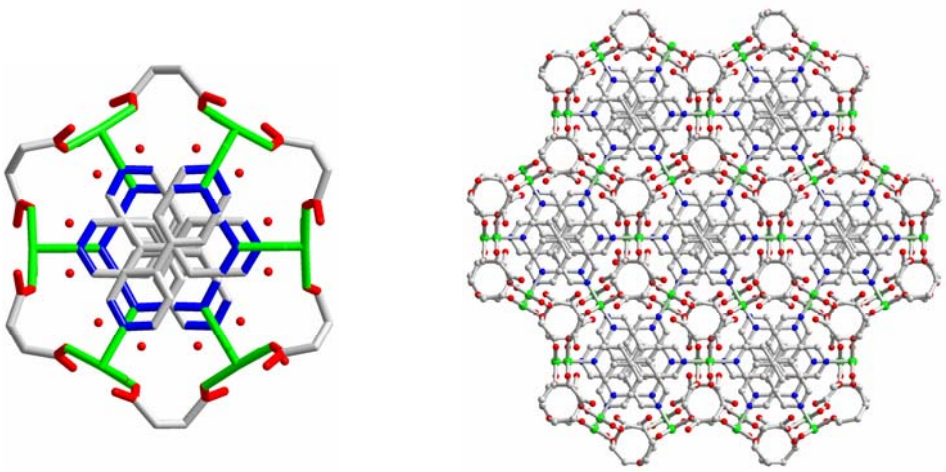

Figure 7.6. Stick representation of the channels between the helices filled by guest water molecules (left); stick representation of the connecting mode of helices (right).

[Cu_2(suc)$_2$(pz)] (23)

The compound **23** crystallizes in C2/m space group, where the asymmetric unit contains half Cu^{2+}, half succinate anion and one third pyrazine molecule. Unlike in the previous two compounds, here the succinate ion is in *anti* or *trans* conformation. Each Cu^{2+} ion is octahedrally coordinated to four oxygen atoms from four bridging succinates at the equatorial sites, while the axial sites are occupied by the nitrogen atoms of two bridging pyrazine molecules (Figure 7.7). The equatorial Cu–O bond lengths and the axial Cu–N bond lengths indicate a Jahn-Teller elongation of the

N_2O_4 coordination sphere. The selected bond lengths and angles are listed in Table 7.2. The Cu···Cu distances in this $\{Cu_2(\mu\text{-}O_2CR)_4\}$ core is 2.590(8) Å. These succinate bridged paddle-wheel binuclear Cu_2^{4+} units (Figure 7.7) form distorted two-dimensional (2D) square-grids of $\{Cu_2(suc)_4\}$ units parallel to the *bc*-plane (Figure 7.8). These 2D square-grids are further pillared by pyrazine (parallel to the *a*-axis) to

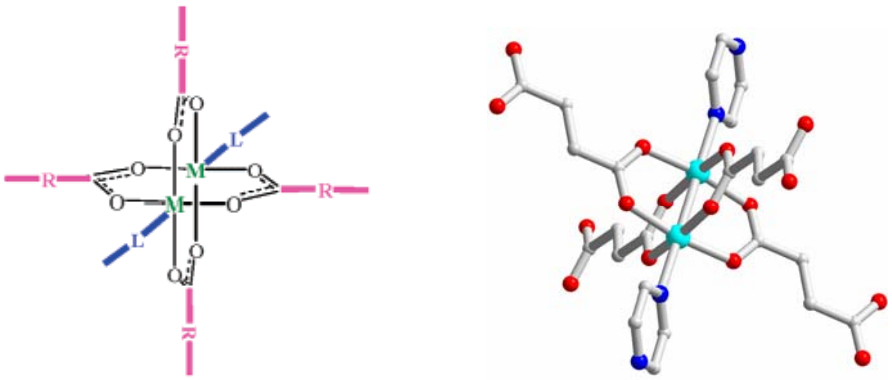

Figure 7.7. Schematic diagram (left) and the ball-stick representation (right) of the basic binuclear paddle-wheel unit in **23**.

form a three-dimensional (3D) structure (Figure 7.8). The topology of **23** can be best described as a primitive cubic (α-Po) net (Figure 7.8). The overall structure of **23** can be described as a doubly interpenetrating 3D network by the mutual interpenetration of two identical α-Po nets of $\{Cu_2(suc)_2(pz)\}$ (Figure 7.9). The pores of **23** along the 2D square-grid of $\{Cu_2(suc)_4\}$ units are filled by the pyrazine molecules from another α-Po net, while the pores viewed along the rectangular grid of $\{Cu_2(suc)_2(pz)\}$ are significantly reduced due to double interpenetration of the 3D frameworks (Figure 7.9). Overall, there exists a 1D channel along the rectangular diagonal of the paddle-wheel clusters which can be access for the guest molecules.

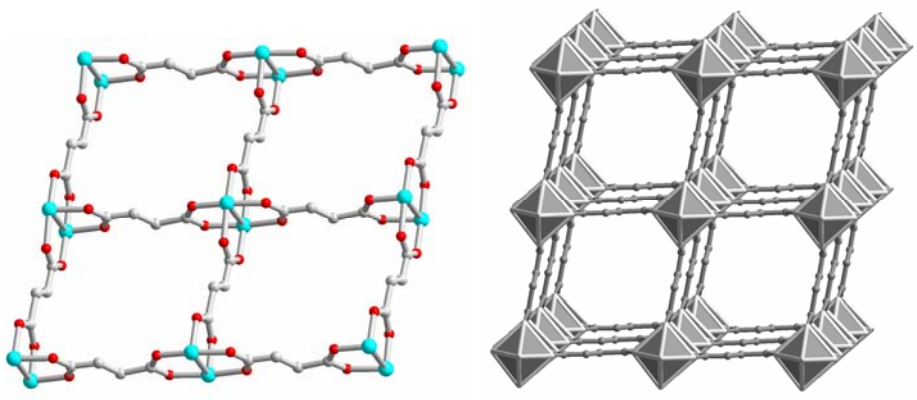

Figure 7.8. The ball-stick representation of 2D square-grid structure of $\{Cu_2(suc)_4\}$ (left) and the 3D network of **23** resembling the α–Po framework (right).

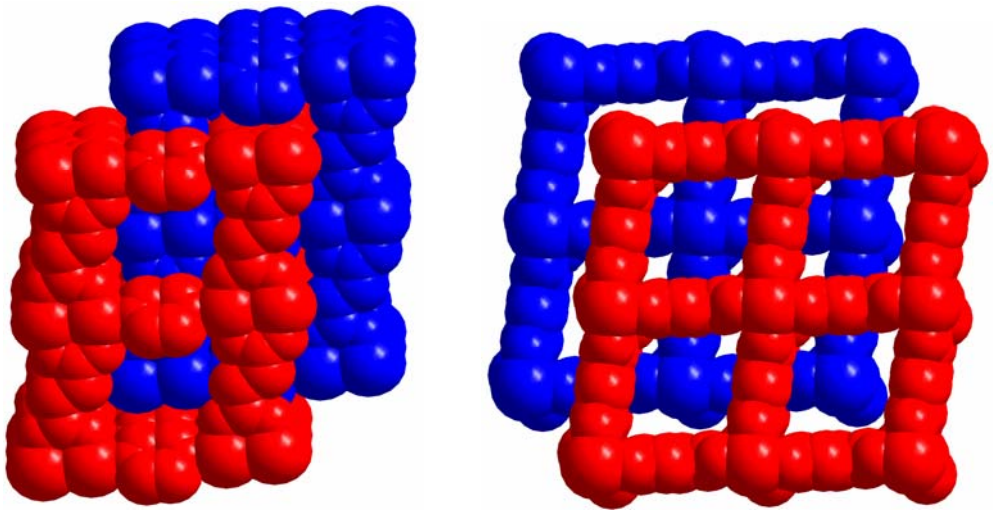

Figure 7.9. Space-filling representation of the side view of doubly interpenetrating frameworks indicating the pores in the 2D square grid of $\{Cu_2(suc)_4\}$ (blue) are filled with pyrazine molecules from another α–Po net (red) (left). The pores viewed along the rectangular grid of $\{Cu_2(suc)_2(pz)\}$ units are significantly reduced by the framework interpenetration (right).

Table 7.2. Selected bond lengths (Å) and angles (°) for **21**, **22** and **23**.

Compound **21**			
Cu-O(1)	1.9581(17)	O(1)-Cu-O(3)	93.76(8)
Cu-N(1)	2.015(3)	O(1)-Cu-O(3)^{a}	86.30(8)
Cu-N(2)^{b}	1.996(3)	O(1)^{a}-Cu-O(1)	176.98(11)
Cu-O(3)	2.529(2)	N(2)^{b}-Cu-N(1)	180.0
O(1)-C(7)	1.260(3)	N(1)-Cu-O(3)	91.06(6)
O(2)-C(7)	1.246(4)	N(2)^{b}-Cu-O(3)	88.94(6)
O(1)-Cu-N(1)	88.49(5)	O(3)^{a}-Cu-O(3)	177.88(12)
O(1)-Cu-N(2)^{b}	91.51(5)	O(2)-C(7)-O(1)	124.5(3)
Compound **22**			
Ni-O(1)	2.0489(19)	O(1)-Ni-O(3)	92.43(9)
Ni-N(2)^{d}	2.059(3)	O(1)-Ni-O(3)^{c}	87.58(9)
Ni-N(1)	2.071(3)	N(1)-Ni-O(3)	90.24(8)
Ni-O(3)	2.134(2)	N(2)^{c}-Ni-O(3)	89.76(8)
O(1)-C(7)	1.249(3)	O(1)-Ni-O(1)^{c}	176.51(12)
O(2)-C(7)	1.258(4)	N(2)^{d}-Ni-N(1)	180.0
O(1)-Ni-N(1)	88.26(6)	O(3)^{c}-Ni-O(3)	179.51(16)
O(1)-Ni-N(2)^{d}	91.74(6)	O(1)-C(7)-O(2)	124.5(3)
Compound **23**			
Cu(1)-O(1)	1.9678(19)	O(2)^{e}-Cu(1)-O(2)^{f}	89.56(14)
Cu(1)-O(2)^{e}	1.9612(19)	O(2)^{e}-Cu(1)-O(1)	169.66(8)
Cu(1)-N(1)	2.2628(19)	O(1)-Cu(1)-O(1)^{g}	88.22(14)
Cu(1)-Cu(1)^{e}	2.5901(8)	O(2)^{e}-Cu(1)-N(1)	95.01(7)
O(1)-C(1)	1.259(3)	O(2)^{e}-Cu(1)-Cu(1)^{e}	84.37(6)
O(2)-C(1)	1.259(3)	O(1)-Cu(1)-Cu(1)^{e}	85.32(6)
Cu(1)-Cu(1)^{e}	2.5901(8)	N(1)-Cu(1)-Cu(1)^{e}	179.12(5)
O(1)-Cu(1)-N(1)	95.31(7)	O(1)-C(1)-O(2)	125.3(2)
O(2)^{f}-Cu(1)-O(1)	90.18(11)		

Symmetry transformations used to generate equivalent atoms: a = x-y, -y, -z; b = x-1, y, z; c = x-y+1, -y+2, -z; d = x+1, y, z; e = -x, -y, -z; f = -x, y, -z; g = x, -y, z.

7.3.3. Magnetic properties

Temperature dependence of the magnetic susceptibilities (χ_M) of **21** and **22** were measured at a magnetic field of 10 kOe (Figure 7.10). The μ_{eff} (per Cu^{2+} ion) for **21** at room temperature (300 K) is 1.57 μ_B, which increases to 1.79 μ_B upon cooling upto 180 K. Below 180 K the increase in the moment is relatively less. At 20 K the μ_{eff} is 1.90 μ_B. Thus there are two segments in the plot of χ_M^{-1} *vs.* T for **21**. The data within temperature ranges 300-180 K and 180-20 K were fit using the Curie Weiss law. The '*C*' and 'θ' values are 0.23 and 81.1 K and 0.41 and 2.9 K for these two temperature ranges. These values indicate the presence of ferromagnetic coupling between Cu^{2+} ions in **21**. In contrast, the temperature dependence of χ_M^{-1} *vs.* T plot shows typically Curie paramagnetic behavior of **22**. The '*C*' and 'θ' values obtained for 22 are 1.02 and 1.9 K, respectively.

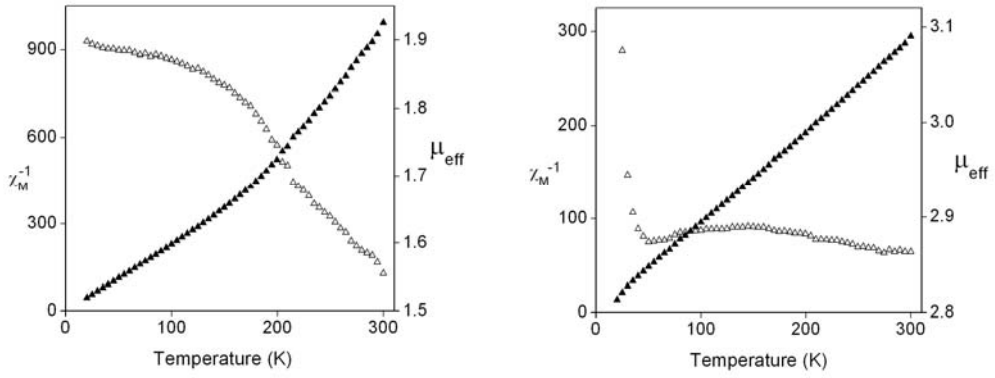

Figure 7.10. Inverse molar magnetic susceptibility (▲) and effective magnetic moment (Δ) of **21** (left) and **22** (right) as a function of temperature.

The temperature dependence of the inverse magnetic susceptibilities (χ_M^{-1}) and the effective magnetic moments (μ_{eff}) of **23** has been depicted in the Figure 7.11. The magnetic susceptibilities were measured at a fixed magnetic field of 10 kOe. The μ_{eff} (per Cu^{2+} ion) value at 300 K is 1.40 μ_B, which decreases smoothly upon cooling to ca. 80 K and reaches the value of 0.82 μ_B and then increases to value of 0.94 μ_B at 20 K. Between 80 K to 40 K the μ_{eff} remains almost constant (Figure 7.11). The decrease of the μ_{eff} can be attributed to the strong antiferromagnetic coupling between the two

copper(II) centers bridged by four carboxylates. Ferromagnetic coupling between the pyrazine bridged binuclear Cu_2 system is possibly responsible for the increase of moment below 40 K. We have tried to fit the data using the Bleany-Bowers equation.[29,30] However, the best least-squares fit could be obtained only with a very high (19%) S = ½ paramagnetic impurity. The g, J and J' values obtained are 2.06, –174(4) and +35(2) cm^{-1} respectively.

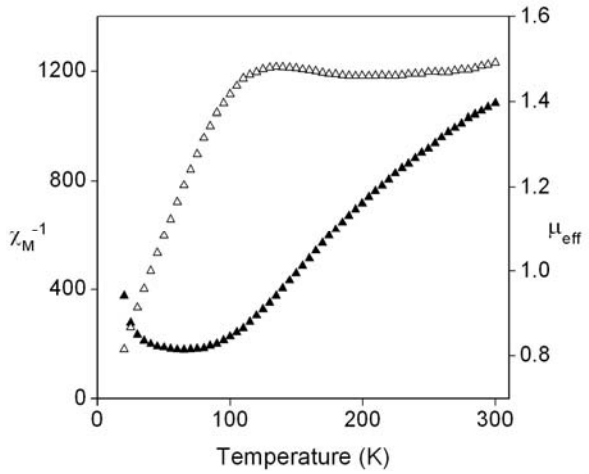

Figure 7.11. Inverse molar magnetic susceptibility (Δ) and effective magnetic moment (▲) of **23** as a function of temperature.

7.3.4. Thermal analysis

The TGA measurements of all the compounds under flowing nitrogen gas has been performed in the temperature range 30 to 400º C. Compounds **21** and **22** showed that, the endothermic desolvation starts and ends in the temperature ranges 61−118º C and 68−134º C, respectively. The observed weight losses of 17.22 % and 17.82 % correspond well to the calculated values of 17.67 % and 17.88 % for the four water molecules per formula unit for **21** and **22**, respectively. Upon further heating the insolated residue starts to decompose in two-three overlapping steps at ~172 and 197º C for **21** and **22**, respectively. The decomposition continued beyond 400º C. The differential scanning calorimetric measurements also correspond well with the TGA data (Figure 7.12).

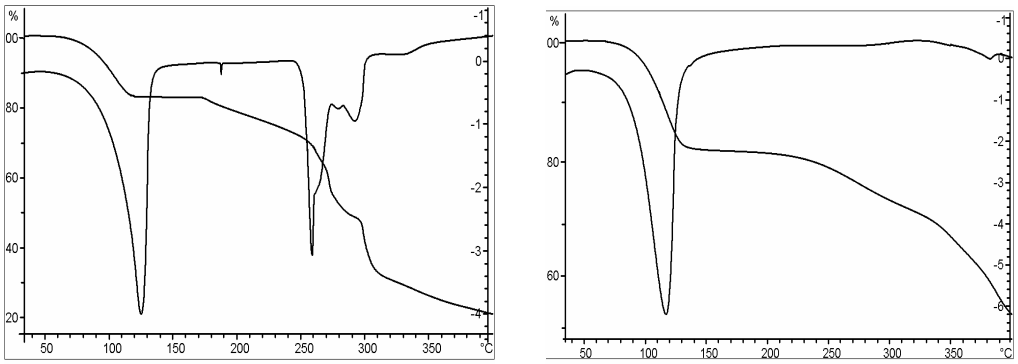

Figure 7.12. The thermo gravimetric and the differential scanning calorimetric plots for **21** (left) and **22** (right).

7.4. Conclusion

The architecture of a metal-organic framework from a coordination polymer is expected to depend strongly on the preference of the metal ion for particular coordination geometry, conformational flexibility and the length of the bridging ligands. The compounds **21**, **22** and **23** are coordination polymers containing mixed ligand bridges. The conformational flexibility of the first bridging ligand (succinate) and the length of the second (longer 4,4'-bipyridine or shorter pyrazine) are the two variable in these species. We have seen the conformationally flexible spacer succinate can acquire gauche (in **21** and **22**) as well as the *anti* or *trans* (in **23**) conformations. Due to the angular orientation of the carboxylates in the *gauche* conformation the structure took the helical shape in **21** and **22**. The partner spacer, 4,4'-bipyridine in **21** and **22** allows enough space for the formation and propagation of the homo-chiral helical structural motifs in the crystal lattice. As a result, **21** and **22** crystallize in non-centrosymmetric space groups. On the other hand, in **23** the *anti* or *trans* conformation of the succinate most likely due to shorter partner spacer, pyrazine leads to the formation of paddle-wheel type binuclear $\{Cu_2(\mu\text{-}O_2CR)_4\}$ unit as building blocks. These paddle-wheel units connected through the *anti* or *trans* succinate ligands form 2D square-grids, which are again bridged by pyrazine leading to the formation of primitive cubic network of **23**.

Reference

1 Schmidt, G. M. J. *Pure Appl. Chem.* **1971**, *27*, 647.
2 Desiraju, G. R. Crystal Engineering: The Design of Organic Solids, Elsevier, Amsterdam, 1989.
3 Lehn, J. M. *Science*, **2002**, *295*, 2400.
4 Reinhoudt, D. N.; Crego-Calama, M. *Science*, **2002**, *295*, 2403.
5 Hollingsworth, M. D. *Science*, **2002**, *295*, 2410.
6 Moulton, B.; Zaworotko, M. J. *Chem. Rev*. **2001**, *101*, 1629.
7 Hagrman, P. J.; Hagrman, D.; Zubieta, J. *Angew. Chem., Int. Ed*. **1999**, *38*, 2638.
8 Yaghi, O. M.; Li, H.; Davis, C.; Richardson, D.; Groy, T. L. *Acc. Chem. Res.* **1998**, *31*, 474.
9 Yaghi, O. M.; O'Keeffe, M.; Ockwig, N. W.; Chae, H. K.; Eddaoudi, M.; Kim, J. *Nature* **2003**, *423*, 705.
10 Eddaoudi, M.; Moler, D. B.; Li, H.; Chen, B.; Reineke, T. M.; O'Keeffe, M.; Yaghi, O. M. *Acc. Chem. Res.* **2001**, *34*, 319.
11 Ma, B. Q.; Gao, S.; Su, G.; Xu, G. X. *Angew. Chem., Int. Ed*. **2001**, *40*, 434.
12 Yeung, W. F.; Man, W. L.; Wong, W. Y.; Lau, T. C.; Gao, S. *Angew. Chem., Int. Ed*. **2001**, *40*, 3031.
13 Inoue, K.; Imai,H.; Ghalsasi, P. S.; Kikuchi, K.; Ohba, M.; Okawa, H.; Yakhmi, J. V. *Angew. Chem., Int. Ed.* **2001**, *40*, 4242.
14 Ermer, O. *Adv. Mater*. **1991**, *3*, 608.
15 Inoue, K.; Hayamizu, T.; Iwamura, H.; Hashizume, D.; Ohashi, Y. *J. Am. Chem. Soc.* **1996**, *118*, 1803.
16 Fujita, M.; Kwon, Y. J.; Washizu, S.; Ogura, K. *J. Am. Chem. Soc.* **1994**, *116*, 1151.
17 Maggard, P. A.; Stern, C. L.; Poeppelmeier, K. R. *J. Am. Chem. Soc.* **2001**, *123*, 7742.
18 Evans, O. R.; Lin, W. *Acc. Chem. Res.* **2002**, *35*, 511.
19 Hatfield, W. E. *Theory and Applications of Molecular Paramagnetism*; Boudreaux, E. A.; Mulay, L. N., Eds.; Wiley, New York, 1976; pp. 491.
20 *SMART*; 5.630, Eds.; *SAINTPLUS*; 6.45, Eds.; Bruker AXS, Inc.: Madison, WI, USA, 2003.
21 *SADABS*; 2.10, Eds.; Bruker AXS, Inc.: Madison, WI, USA, 2003.
22 Sheldrick, G. M. *SHELX-97* Structure Determination Software, University of Go¨ttingen, Go¨ttingen, Germany, 1997.

23 Spek, A. L. *Platon98* Molecular Graphics Software, University of Glasgow, UK, 1998.
24 Nakamoto, K. *Infrared and Raman Spectra of Inorganic and Coordination Compounds;* Wiley, New York, 1986; pp. 241–244.
25 O'Keeffe, M.; Hyde, B. G. *Crystal structures I: patterns and symmetry*; Mineralogical Society of America, Washington, D.C., 1996.
26 Zheng, Y.-Q.; Kong, Z.-P. *Z. Anorg. Allg. Chem.* **2003**, *629*, 1469.
27 Ying, S.-M.; Mao, J.-G.; Sun, Y.-Q.; Zeng, H.-Y.; Dong, Z.-C. *Polyhedron* **2003**, *22*, 3097.
28 Zhang, J.; Kang, Y.; Zhang, R.-B.; Li, Z.-J.; Cheng, J.-K.; Yao, Y.-G. *CrystEngComm* **2005**, *7*, 177.
29 Chandramouli, G. V. R.; Balagopalakrishna, C.; Rajasekharan, M. V.; Manoharan, P. T. *Comput. Chem.* **1996**, *20*, 353.
30 Bleany, B.; Bowers, K. D. *Proc. R. Soc. London, Ser. A* **1952**, *214*, 451.

Appendix I

Tables for atomic coordinates (× 10^4), equivalent isotropic displacement parameters (Å^2 × 10^3), U(eq) is defined as one third of the trace of the orthogonalized U_{ij} tensor.

Table AI.1. For **[Cu(bhac)(dmpz)]** (**1**)

Chapter 2				
Atom	x	y	z	U(eq)
Cu	1339(1)	377(1)	8985(1)	35(1)
O(1)	2246(3)	2130(2)	10100(2)	43(1)
O(2)	189(3)	-1333(2)	7806(2)	44(1)
N(1)	44(3)	979(2)	7709(2)	37(1)
N(2)	-963(3)	-39(2)	6651(2)	40(1)
N(3)	2728(3)	-305(2)	10266(2)	37(1)
N(4)	3621(3)	597(2)	11357(2)	39(1)
C(1)	2882(5)	4462(3)	10898(3)	57(1)
C(2)	1951(4)	3220(2)	9861(2)	40(1)
C(3)	898(4)	3285(3)	8788(2)	44(1)
C(4)	-89(4)	2201(3)	7738(2)	40(1)
C(5)	-1295(5)	2476(3)	6676(3)	59(1)
C(6)	-768(3)	-1187(3)	6807(2)	37(1)
C(7)	-1692(4)	-2413(3)	5780(2)	39(1)
C(8)	-2710(5)	-2357(3)	4679(3)	58(1)
C(9)	-3541(5)	-3502(3)	3740(3)	69(1)
C(10)	-3374(5)	-4729(3)	3875(3)	65(1)
C(11)	-2386(5)	-4799(3)	4958(3)	71(1)
C(12)	-1540(5)	-3652(3)	5906(3)	57(1)
C(13)	2635(4)	-2660(3)	9317(3)	50(1)
C(14)	3294(4)	-1416(3)	10340(2)	39(1)
C(15)	4541(4)	-1188(3)	11482(2)	44(1)
C(16)	4712(3)	97(3)	12108(2)	41(1)
C(17)	5829(4)	907(3)	13363(2)	56(1)

Table AI.2. For **[Cu(bhac)(pyz)]**·C_2H_5OH (**2**·C_2H_5OH)

Chapter 3				
Atom	x	y	z	U(eq)
Cu	3323(1)	5882(1)	4549(1)	45(1)
O(1)	4433(2)	5719(1)	6070(1)	53(1)
O(2)	2362(2)	6131(1)	3004(1)	55(1)
O(3)	-1679(5)	6099(6)	2337(4)	185(2)
N(1)	5011(2)	7545(1)	4674(1)	47(1)

Table AI.2. Continued …

Chapter 3				
Atom	x	y	z	U(eq)
N(2)	4811(2)	8019(1)	3661(1)	51(1)
N(3)	1316(2)	4286(1)	4380(1)	47(1)
N(4)	1258(2)	3646(2)	5236(2)	53(1)
C(1)	6005(4)	6409(2)	8024(2)	75(1)
C(2)	5616(3)	6684(2)	6839(2)	53(1)
C(3)	6495(3)	7871(2)	6643(2)	54(1)
C(4)	6254(3)	8280(2)	5587(2)	50(1)
C(5)	7459(3)	9592(2)	5540(2)	64(1)
C(6)	3398(2)	7220(2)	2873(2)	49(1)
C(7)	2950(3)	7591(2)	1744(2)	57(1)
C(8)	3492(4)	8892(2)	1625(2)	71(1)
C(9)	3060(6)	9210(3)	569(3)	97(1)
C(10)	2034(6)	8259(4)	-377(3)	106(1)
C(11)	1503(7)	6985(4)	-271(2)	110(1)
C(12)	1925(4)	6645(3)	788(2)	78(1)
C(13)	-190(3)	3643(2)	3541(2)	62(1)
C(14)	-1204(3)	2570(2)	3878(3)	75(1)
C(15)	-247(3)	2616(2)	4950(2)	68(1)
C(16)	-2494(7)	6630(6)	1476(4)	127(2)
C(17)	-1960(8)	8058(6)	1590(5)	142(2)

Table AI.3. For **[Cu(bhac)(imd)]** (**3**)

Chapter 3				
Atom	x	y	z	U(eq)
Cu	2991(1)	1917(1)	1631(1)	48(1)
O(1)	3901(1)	202(3)	1153(1)	62(1)
O(2)	2065(1)	3506(2)	2154(1)	51(1)
N(1)	3068(1)	38(3)	2501(1)	45(1)
N(2)	2451(1)	717(3)	3031(1)	43(1)
N(3)	2725(1)	3798(3)	747(1)	52(1)
N(4)	2621(1)	4854(3)	-401(1)	59(1)
C(1)	4896(2)	-2916(5)	884(2)	79(1)
C(2)	4282(1)	-1693(4)	1406(1)	58(1)
C(3)	4167(2)	-2667(4)	2086(1)	57(1)
C(4)	3566(1)	-1855(3)	2617(1)	48(1)
C(5)	3511(2)	-3269(4)	3305(1)	58(1)
C(6)	1956(1)	2496(3)	2775(1)	43(1)
C(7)	1197(1)	3413(3)	3207(1)	43(1)
C(8)	811(1)	5598(4)	3043(1)	52(1)
C(9)	69(2)	6395(4)	3411(1)	61(1)
C(10)	-289(2)	5057(5)	3952(1)	66(1)
C(11)	90(2)	2914(5)	4123(1)	67(1)

Table AI.3. Continued …

Chapter 3				
Atom	x	y	z	U(eq)
C(12)	820(2)	2061(4)	3750(1)	54(1)
C(13)	2261(2)	5891(4)	691(1)	60(1)
C(14)	2195(2)	6558(4)	-18(1)	65(1)
C(15)	2927(2)	3232(4)	73(1)	55(1)

Table AI.4. For **[Cu(bhac)(py)]** (**4**)

Chapter 3				
Atom	x	y	z	U(eq)
Cu(1)	6021(1)	3716(1)	432(1)	35(1)
O(2)	6318(1)	2594(2)	-549(1)	44(1)
O(1)	5812(1)	4923(2)	1384(1)	45(1)
N(2)	7976(2)	3770(2)	50(2)	38(1)
N(3)	4721(2)	2643(2)	370(2)	36(1)
N(1)	7462(2)	4398(2)	639(2)	36(1)
C(1)	6233(2)	6521(3)	2748(2)	55(1)
C(2)	6564(2)	5768(2)	1976(2)	39(1)
C(3)	7574(2)	6000(2)	1933(2)	42(1)
C(4)	8020(2)	5354(2)	1280(2)	39(1)
C(5)	9147(2)	5771(3)	1333(3)	63(1)
C(6)	7312(2)	2843(2)	-515(2)	37(1)
C(7)	7716(2)	1978(2)	-1138(2)	38(1)
C(8)	8881(2)	1795(3)	-794(2)	52(1)
C(9)	9240(3)	917(3)	-1337(3)	62(1)
C(10)	8453(3)	220(3)	-2226(3)	59(1)
C(11)	7291(3)	405(3)	-2591(3)	58(1)
C(12)	6926(2)	1284(2)	-2051(2)	51(1)
C(13)	4401(2)	1608(2)	-261(2)	51(1)
C(14)	3516(3)	859(3)	-330(3)	61(1)
C(15)	2925(2)	1178(3)	279(3)	56(1)
C(16)	3239(2)	2239(3)	918(3)	56(1)
C(17)	4130(2)	2952(2)	949(2)	45(1)

Table AI.5. For **[Cu(bhs)(dmpz)]** (**5**)

Chapter 4				
Atom	x	y	z	U(eq)
Cu	4058(1)	1747(1)	9812(1)	33(1)
O(1)	4653(2)	1178(3)	10632(1)	41(1)
O(2)	3377(2)	1953(2)	8974(1)	38(1)
N(1)	2500(2)	492(3)	9856(1)	35(1)

Table AI.5. Continued …

Chapter 4				
Atom	x	y	z	U(eq)
N(2)	1795(2)	212(3)	9291(1)	39(1)
N(3)	5582(2)	3221(3)	9764(1)	33(1)
N(4)	6406(2)	3292(3)	10279(1)	37(1)
C(1)	3982(3)	511(4)	11058(1)	37(1)
C(2)	4550(3)	402(4)	11658(1)	44(1)
C(3)	3929(3)	-340(4)	12115(1)	52(1)
C(4)	2716(3)	-984(5)	11996(1)	56(1)
C(5)	2130(3)	-876(4)	11413(1)	48(1)
C(6)	2733(3)	-136(4)	10933(1)	38(1)
C(7)	2065(3)	-165(4)	10335(1)	40(1)
C(8)	2378(2)	1014(3)	8867(1)	34(1)
C(9)	1866(2)	776(3)	8218(1)	34(1)
C(10)	2447(2)	1638(4)	7764(1)	38(1)
C(11)	2024(3)	1422(4)	7158(1)	43(1)
C(12)	1024(3)	331(4)	6994(1)	47(1)
C(13)	436(3)	-524(4)	7441(1)	52(1)
C(14)	853(3)	-308(4)	8048(1)	43(1)
C(15)	6086(3)	4253(3)	9362(1)	36(1)
C(16)	7216(3)	4957(4)	9628(1)	44(1)
C(17)	7396(3)	4300(4)	10211(1)	44(1)
C(18)	5467(3)	4545(4)	8734(1)	46(1)
C(19)	8440(3)	4532(5)	10712(2)	65(1)

Table AI.6. For **[Cu(bhs)(pyz)]**·0.5H_2O (**6**·0.5H_2O)

Chapter 4				
Atom	x	y	z	U(eq)
Cu(1)	5267(1)	7870(1)	95(1)	40(1)
O(1)	5637(2)	6747(3)	-422(1)	43(1)
O(2)	4827(2)	9046(4)	591(1)	46(1)
N(1)	4246(2)	7068(4)	-301(2)	37(1)
N(2)	3750(2)	7541(4)	-28(2)	42(1)
N(3)	6315(2)	8399(4)	639(2)	36(1)
N(4)	6915(2)	7606(5)	589(2)	41(1)
C(1)	5218(3)	5979(5)	-931(2)	42(1)
C(2)	5572(3)	5499(6)	-1324(2)	51(1)
C(3)	5187(3)	4640(6)	-1847(2)	60(1)
C(4)	4417(3)	4191(6)	-2010(2)	57(1)
C(5)	4059(3)	4662(5)	-1653(2)	49(1)
C(6)	4426(2)	5571(5)	-1114(2)	40(1)
C(7)	3990(2)	6118(5)	-777(2)	42(1)
C(8)	4116(2)	8591(5)	431(2)	39(1)
C(9)	3698(2)	9353(5)	772(2)	37(1)

Table AI.6. Continued …

Chapter 4				
Atom	x	y	z	U(eq)
C(10)	2926(2)	9766(5)	507(2)	43(1)
C(11)	2560(3)	10544(6)	837(2)	52(1)
C(12)	2942(3)	10854(6)	1435(2)	55(1)
C(13)	3703(3)	10421(6)	1701(2)	59(1)
C(14)	4074(3)	9702(6)	1369(2)	52(1)
C(15)	6591(3)	9228(5)	1156(2)	44(1)
C(16)	7374(3)	8949(6)	1435(2)	51(1)
C(17)	7554(2)	7892(6)	1060(2)	46(1)
Cu(2)	10555(1)	3641(1)	839(1)	43(1)
O(3)	10883(2)	2946(4)	238(1)	46(1)
O(4)	10170(2)	4190(4)	1445(1)	47(1)
N(5)	9526(2)	3027(4)	406(2)	37(1)
N(6)	9037(2)	3325(4)	701(2)	42(1)
N(7)	11576(2)	4564(5)	1314(2)	46(1)
N(8)	12087(2)	5021(5)	1086(2)	46(1)
C(18)	10460(2)	2202(5)	-277(2)	40(1)
C(19)	10818(3)	1652(6)	-650(2)	50(1)
C(20)	10426(3)	881(6)	-1191(2)	57(1)
C(21)	9649(3)	598(6)	-1387(2)	56(1)
C(22)	9286(3)	1099(5)	-1028(2)	52(1)
C(23)	9668(2)	1899(5)	-470(2)	40(1)
C(24)	9246(2)	2324(5)	-111(2)	39(1)
C(25)	9440(3)	3921(5)	1238(2)	39(1)
C(26)	9032(2)	4317(5)	1629(2)	37(1)
C(27)	8355(2)	3446(5)	1558(2)	46(1)
C(28)	7985(3)	3862(6)	1932(2)	52(1)
C(29)	8274(3)	5114(7)	2361(2)	61(1)
C(30)	8950(3)	5978(6)	2441(2)	57(1)
C(31)	9324(2)	5547(6)	2080(2)	46(1)
C(32)	11851(3)	5221(6)	1860(2)	57(1)
C(33)	12538(3)	6091(7)	1976(3)	71(2)
C(34)	12664(3)	5928(6)	1469(3)	58(1)
O(5W)	7519(2)	4800(5)	-7(2)	55(1)

Table AI.7. For **[Cu(bhs)(imd)]**·CH_3OH (**7**·CH_3OH)

Chapter 4				
Atom	x	y	z	U(eq)
Cu	4670(1)	97(1)	6172(1)	34(1)
O(1)	6144(2)	15(2)	5614(2)	43(1)
O(2)	3200(2)	14(2)	6802(2)	44(1)
O(3)	2702(2)	5776(2)	6139(2)	60(1)
N(1)	4645(2)	-1604(2)	6458(2)	34(1)

Table AI.7. Continued …

Chapter 4				
Atom	x	y	z	U(eq)
N(2)	3611(2)	-2033(2)	6802(2)	36(1)
N(3)	4645(2)	1865(2)	6125(2)	36(1)
N(4)	4028(3)	3736(2)	6150(2)	49(1)
C(1)	6882(2)	-887(3)	5739(2)	38(1)
C(2)	8013(3)	-695(3)	5447(2)	49(1)
C(3)	8828(3)	-1597(4)	5536(3)	56(1)
C(4)	8559(3)	-2726(4)	5909(3)	59(1)
C(5)	7469(3)	-2942(3)	6187(2)	49(1)
C(6)	6604(2)	-2040(3)	6114(2)	37(1)
C(7)	5485(2)	-2357(2)	6419(2)	37(1)
C(8)	2942(2)	-1102(2)	6972(2)	35(1)
C(9)	1825(2)	-1349(3)	7419(2)	39(1)
C(10)	991(3)	-447(3)	7408(2)	48(1)
C(11)	-40(3)	-636(4)	7849(3)	60(1)
C(12)	-244(3)	-1717(4)	8310(3)	61(1)
C(13)	579(3)	-2625(3)	8325(3)	55(1)
C(14)	1604(3)	-2452(3)	7882(2)	46(1)
C(15)	3754(3)	2577(3)	6280(2)	41(1)
C(16)	5140(3)	3778(3)	5899(3)	52(1)
C(17)	5522(3)	2630(3)	5878(2)	44(1)
C(18)	1902(3)	6081(4)	5402(3)	69(1)

Table AI.8. For **[Cu(bhs)(py)]** (**8**)

Chapter 4				
Atom	x	y	z	U(eq)
Cu	4356(1)	162(1)	6302(1)	38(1)
O(1)	2857(2)	-596(1)	4497(1)	42(1)
O(2)	5978(2)	1174(1)	8070(1)	44(1)
N(1)	3764(2)	1750(2)	6329(2)	37(1)
N(3)	4564(2)	-1602(2)	6573(2)	39(1)
N(2)	4781(3)	2765(2)	7476(2)	42(1)
C(1)	1554(3)	-211(2)	3798(2)	38(1)
C(2)	380(3)	-1013(2)	2550(2)	47(1)
C(3)	-1000(3)	-681(3)	1767(2)	54(1)
C(4)	-1293(3)	468(3)	2185(2)	55(1)
C(5)	-149(3)	1280(2)	3400(2)	48(1)
C(6)	1283(3)	979(2)	4227(2)	38(1)
C(7)	2424(3)	1908(2)	5471(2)	40(1)
C(8)	5886(3)	2344(2)	8300(2)	37(1)
C(9)	7109(3)	3285(2)	9589(2)	39(1)
C(10)	8534(4)	3019(2)	10422(2)	55(1)
C(11)	9668(4)	3899(3)	11618(2)	66(1)

Table AI.8. Continued …

Chapter 4				
Atom	x	y	z	U(eq)
C(12)	9376(4)	5044(3)	12002(2)	65(1)
C(13)	7953(4)	5325(2)	11185(2)	62(1)
C(14)	6845(4)	4460(2)	9983(2)	51(1)
C(15)	5654(4)	-1676(2)	7706(2)	51(1)
C(16)	5863(4)	-2846(2)	7912(2)	62(1)
C(17)	4933(4)	-4000(2)	6921(3)	59(1)
C(18)	3831(4)	-3930(2)	5751(2)	58(1)
C(19)	3674(3)	-2724(2)	5613(2)	48(1)

Table AI.9. For **[Cu(pyp)Cl]**·$2H_2O$ (**9a**)

Chapter 5				
Atom	x	y	z	U(eq)
Cu	4730(1)	2500	2398(1)	15(1)
Cl	3440(1)	2500	3931(1)	29(1)
O(1)	3110(2)	2500	1000(2)	16(1)
N(1)	5824(3)	2500	1005(2)	12(1)
N(2)	6715(3)	2500	3442(2)	17(1)
C(1)	3515(3)	2500	-149(3)	15(1)
C(2)	2537(3)	2500	-1301(3)	17(1)
C(3)	3021(3)	2500	-2459(3)	18(1)
C(4)	4473(3)	2500	-2518(3)	17(1)
C(5)	5464(3)	2500	-1392(3)	16(1)
C(6)	4980(3)	2500	-215(3)	13(1)
C(7)	7188(3)	2500	1310(3)	16(1)
C(8)	7738(3)	2500	2699(3)	16(1)
C(9)	9170(3)	2500	3202(3)	20(1)
C(10)	9572(4)	2500	4525(3)	26(1)
C(11)	8541(4)	2500	5290(3)	31(1)
C(12)	7111(4)	2500	4710(3)	25(1)
O(2)	900(2)	9637(4)	1134(3)	53(1)

Table AI.10. For **[Cu(pyp)Cl]**·CH_3OH (**9b**)

Chapter 5				
Atom	x	y	z	U(eq)
Cu	2038(1)	5573(1)	1892(1)	33(1)
Cl	1895(1)	6974(1)	3799(1)	57(1)
O(1)	2539(2)	7162(2)	952(1)	39(1)
O(2)	5766(3)	9159(2)	2089(2)	54(1)
N(1)	2258(2)	4307(2)	223(2)	31(1)

Table AI.10. Continued …

Chapter 5				
Atom	x	y	z	U(eq)
N(2)	1531(2)	3568(2)	2356(2)	33(1)
C(1)	2844(3)	6640(2)	-258(2)	34(1)
C(2)	3331(3)	7549(2)	-1117(2)	40(1)
C(3)	3633(3)	6939(3)	-2365(2)	43(1)
C(4)	3497(3)	5412(3)	-2809(2)	45(1)
C(5)	3021(3)	4490(2)	-1987(2)	40(1)
C(6)	2692(3)	5092(2)	-733(2)	32(1)
C(7)	2104(3)	2910(2)	167(2)	34(1)
C(8)	1693(3)	2442(2)	1366(2)	33(1)
C(9)	1529(3)	984(2)	1500(2)	41(1)
C(10)	1153(3)	664(3)	2686(2)	48(1)
C(11)	942(3)	1804(3)	3677(2)	49(1)
C(12)	1144(3)	3246(2)	3487(2)	41(1)
C(13)	6110(4)	9439(3)	3457(3)	61(1)

Table AI.11. For **[Cu(pyp)Br]**·$2H_2O$ (**10a**)

Chapter 5				
Atom	x	y	z	U(eq)
Cu	4740(1)	2500	7331(1)	15(1)
Br	3352(1)	2500	8903(1)	26(1)
O(1)	3125(2)	2500	5940(2)	17(1)
N(1)	5839(3)	2500	5966(2)	13(1)
N(2)	6711(3)	2500	8384(3)	16(1)
C(1)	3532(3)	2500	4819(3)	15(1)
C(2)	2553(3)	2500	3669(3)	17(1)
C(3)	3041(3)	2500	2536(3)	18(1)
C(4)	4491(4)	2500	2498(3)	18(1)
C(5)	5474(3)	2500	3618(3)	16(1)
C(6)	4994(3)	2500	4768(3)	14(1)
C(7)	7192(3)	2500	6301(3)	15(1)
C(8)	7736(3)	2500	7661(3)	16(1)
C(9)	9162(3)	2500	8183(3)	20(1)
C(10)	9549(4)	2500	9491(3)	25(1)
C(11)	8518(4)	2500	10226(3)	28(1)
C(12)	7102(4)	2500	9632(3)	23(1)
O(2)	894(3)	9645(5)	6125(3)	68(1)

Table AI.12. For **[Cu(pyp)Br]**·CH_3OH (**10b**)

Chapter 5				
Atom	x	y	z	U(eq)
Cu	2092(1)	550(1)	1879(1)	31(1)
Br	1981(1)	2003(1)	3886(1)	53(1)
O(1)	2561(3)	2137(2)	975(2)	37(1)
O(2)	5803(4)	4129(3)	2059(3)	55(1)
N(1)	2272(3)	-663(2)	220(2)	30(1)
N(2)	1598(3)	-1440(2)	2319(2)	31(1)
C(1)	2837(4)	1637(3)	-232(3)	32(1)
C(2)	3297(4)	2568(3)	-1063(3)	37(1)
C(3)	3572(4)	1977(4)	-2301(3)	42(1)
C(4)	3432(5)	484(4)	-2757(3)	43(1)
C(5)	2980(4)	-448(3)	-1959(3)	38(1)
C(6)	2680(4)	130(3)	-714(3)	31(1)
C(7)	2123(4)	-2050(3)	144(3)	34(1)
C(8)	1749(4)	-2537(3)	1321(3)	33(1)
C(9)	1593(4)	-3979(3)	1429(3)	41(1)
C(10)	1268(5)	-4330(4)	2579(4)	47(1)
C(11)	1083(5)	-3233(4)	3583(3)	48(1)
C(12)	1251(4)	-1790(3)	3426(2)	40(1)
C(13)	6279(4)	4412(3)	3403(2)	61(1)

Table AI.13. For **[Cu(3-Me-pyp)Cl]** (**11**)

Chapter 6				
Atom	x	y	z	U(eq)
Cu	2644(1)	10399(1)	5574(1)	34(1)
Cl	4166(1)	11186(1)	3478(1)	37(1)
O(1)	1768(3)	12406(2)	6564(2)	42(1)
N(1)	580(3)	10069(3)	7051(2)	32(1)
N(2)	2910(3)	8285(3)	4876(3)	35(1)
C(1)	383(4)	12549(4)	7688(3)	38(1)
C(2)	-438(5)	13916(4)	8576(4)	51(1)
C(3)	-1916(6)	14052(5)	9718(4)	64(1)
C(4)	-2635(5)	12849(5)	10051(4)	61(1)
C(5)	-1900(4)	11486(4)	9228(3)	45(1)
C(6)	-376(4)	11333(4)	8039(3)	36(1)
C(7)	330(4)	8786(4)	6895(3)	41(1)
C(8)	1594(4)	7751(4)	5694(3)	36(1)
C(9)	1516(5)	6326(4)	5397(4)	49(1)
C(10)	2806(5)	5415(4)	4242(4)	52(1)
C(11)	4132(5)	5941(4)	3434(4)	51(1)
C(12)	4158(4)	7383(4)	3768(3)	42(1)
C(13)	-2729(5)	10223(6)	9618(4)	62(1)

Table AI.14. For **[Cu(3-Me-pyp)Br]** (**12**)

Chapter 6				
Atom	x	y	z	U(eq)
Cu	1961(1)	10446(1)	4381(1)	39(1)
Br	-411(1)	11330(1)	6598(1)	40(1)
O(1)	833(2)	12413(2)	3407(2)	46(1)
N(1)	4305(2)	10140(2)	2910(2)	38(1)
N(2)	3787(2)	8357(2)	5054(2)	39(1)
C(1)	2054(3)	12564(3)	2292(2)	43(1)
C(2)	1507(4)	13908(3)	1417(3)	59(1)
C(3)	2831(5)	14057(4)	283(3)	71(1)
C(4)	4713(5)	12905(4)	-43(3)	67(1)
C(5)	5351(4)	11550(4)	767(3)	51(1)
C(6)	3996(3)	11383(3)	1939(2)	40(1)
C(7)	5810(3)	8872(3)	3040(3)	45(1)
C(8)	5588(3)	7851(3)	4229(2)	42(1)
C(9)	7082(4)	6461(3)	4513(3)	54(1)
C(10)	6730(4)	5568(3)	5667(3)	59(1)
C(11)	4906(4)	6066(3)	6481(3)	57(1)
C(12)	3450(4)	7473(3)	6154(3)	48(1)
C(13)	7411(4)	10340(5)	391(3)	69(1)

Table AI.15. For **[Cu(4-Me-pyp)Cl]**·CH_3OH (**13**·CH_3OH)

Chapter 6				
Atom	x	y	z	U(eq)
Cu	1774(1)	533(1)	6922(1)	34(1)
Cl	1281(1)	1853(1)	8656(1)	48(1)
O(1)	2466(3)	2210(2)	6126(2)	42(1)
O(2)	4198(4)	5970(3)	2825(3)	74(1)
N(1)	2183(3)	-656(2)	5381(2)	31(1)
N(2)	1322(3)	-1541(2)	7327(2)	35(1)
C(7)	2023(3)	-2070(3)	5307(2)	36(1)
C(3)	3719(3)	2225(3)	3076(2)	42(1)
C(6)	2695(3)	225(3)	4528(2)	33(1)
C(1)	2843(3)	1761(3)	5005(2)	36(1)
C(8)	1518(3)	-2630(2)	6398(2)	34(1)
C(12)	897(4)	-1936(3)	8362(2)	41(1)
C(9)	1314(4)	-4121(3)	6496(2)	43(1)
C(13)	3834(4)	192(4)	1319(2)	53(1)
C(5)	3027(3)	-294(3)	3352(2)	38(1)
C(11)	682(4)	-3412(3)	8521(2)	50(1)
C(2)	3412(3)	2754(3)	4235(2)	41(1)
C(4)	3533(3)	697(3)	2597(2)	41(1)
C(10)	906(4)	-4524(3)	7579(3)	50(1)
C(14)	4088(6)	5747(4)	1581(4)	78(1)

Table AI.16. For **[Cu(4-Me-pyp)Br]**·H_2O (**14**·H_2O)

Chapter 6				
Atom	x	y	z	U(eq)
Cu	1647(1)	10499(1)	3327(1)	37(1)
Br	1634(2)	12173(1)	2073(1)	58(1)
O(1)	3192(8)	12330(5)	4669(4)	40(1)
N(1)	1745(9)	9151(7)	4398(5)	31(1)
N(2)	93(9)	8209(7)	2233(5)	37(1)
C(1)	3600(11)	11826(9)	5600(6)	36(2)
C(2)	4752(12)	12893(9)	6663(7)	41(2)
C(3)	5077(11)	12295(9)	7590(6)	41(2)
C(4)	4263(12)	10580(10)	7517(7)	42(2)
C(5)	3165(11)	9489(8)	6459(6)	35(2)
C(6)	2816(11)	10076(8)	5512(6)	33(2)
C(7)	881(11)	7562(8)	3979(6)	34(2)
C(8)	-121(11)	6986(8)	2762(6)	34(2)
C(9)	-1140(13)	5326(9)	2182(7)	47(2)
C(12)	-778(12)	7794(10)	1128(6)	44(2)
C(13)	4574(14)	9986(11)	8558(7)	56(2)
C(10)	-2025(15)	4920(11)	1027(7)	60(2)
C(11)	-1876(15)	6150(10)	493(7)	56(2)
O(2)	7315(9)	4595(7)	4609(6)	57(2)

Table AI.17. For **[Cu(5-Me-pyp)Cl]** (**15**)

Chapter 6				
Atom	x	y	z	U(eq)
Cu	4420(1)	7065(1)	1886(1)	35(1)
Cl	3411(1)	8248(1)	2742(2)	41(1)
O(1)	5729(2)	7609(2)	616(4)	34(1)
N(1)	5403(3)	6005(2)	1829(4)	26(1)
N(2)	3257(3)	6164(2)	2819(4)	30(1)
C(6)	6526(3)	6171(2)	1199(5)	27(1)
C(7)	4949(4)	5285(2)	2396(5)	29(1)
C(9)	3109(4)	4636(3)	3609(5)	33(1)
C(2)	7730(3)	7276(3)	-173(5)	32(1)
C(5)	7486(3)	5579(3)	1228(5)	33(1)
C(1)	6631(4)	7048(3)	534(5)	30(1)
C(12)	2141(4)	6277(3)	3279(6)	40(1)
C(8)	3736(3)	5347(2)	2975(5)	28(1)
C(3)	8669(4)	6698(3)	-146(6)	35(1)
C(10)	1947(4)	4772(3)	4075(6)	40(1)
C(13)	9841(4)	6966(3)	-919(6)	51(1)
C(4)	8542(4)	5845(3)	577(6)	37(1)
C(11)	1448(4)	5592(3)	3889(6)	43(1)

Table AI.18. For **[Cu(5-Me-pyp)Br]** (**16**)

Chapter 6				
Atom	x	y	z	U(eq)
Cu	10649(1)	7024(1)	3229(1)	40(1)
Br	11738(1)	8249(1)	2258(1)	41(1)
O(1)	9328(2)	7586(1)	4404(3)	41(1)
N(1)	9603(2)	6008(1)	3207(3)	33(1)
N(2)	11777(2)	6110(1)	2270(3)	36(1)
C(8)	11252(2)	5323(2)	2064(3)	34(1)
C(7)	10016(2)	5293(2)	2601(3)	36(1)
C(4)	6436(2)	5914(2)	4450(4)	45(1)
C(1)	8409(2)	7057(2)	4480(3)	35(1)
C(6)	8477(2)	6194(2)	3827(3)	35(1)
C(9)	11850(3)	4612(2)	1421(4)	41(1)
C(3)	6347(2)	6746(2)	5190(4)	43(1)
C(2)	7316(2)	7305(2)	5210(4)	40(1)
C(12)	12909(2)	6197(2)	1836(4)	44(1)
C(5)	7499(2)	5631(2)	3798(4)	40(1)
C(11)	13567(3)	5514(2)	1206(4)	48(1)
C(10)	13029(3)	4719(2)	994(4)	47(1)
C(13)	5185(3)	7036(2)	5957(5)	59(1)

Table AI.19. For **[Cu(6-Me-pyp)Cl]** (**17**)

Chapter 6				
Atom	x	y	z	U(eq)
Cu	9045(1)	810(1)	5342(1)	66(1)
Cl	10113(1)	1493(1)	4406(1)	45(1)
O(1)	9590(2)	2047(4)	6073(2)	89(1)
N(1)	7918(2)	1629(3)	5725(1)	36(1)
N(2)	8149(2)	-244(3)	4700(2)	41(1)
C(1)	8984(2)	2782(4)	6450(2)	50(1)
C(2)	9235(3)	3722(5)	7026(2)	54(1)
C(3)	8560(3)	4480(4)	7378(2)	53(1)
C(4)	7644(3)	4327(4)	7208(2)	51(1)
C(5)	7390(2)	3396(4)	6668(2)	43(1)
C(6)	8058(2)	2620(4)	6291(2)	38(1)
C(7)	7179(2)	1156(4)	5449(2)	40(1)
C(8)	7280(2)	96(4)	4858(2)	36(1)
C(9)	6571(2)	-514(4)	4483(2)	48(1)
C(10)	6753(3)	-1486(4)	3927(2)	51(1)
C(11)	7635(2)	-1829(4)	3767(2)	47(1)
C(12)	8315(2)	-1190(4)	4169(2)	47(1)
C(13)	10214(3)	3864(7)	7225(3)	86(2)

Table AI.20. For **[Cu(6-Me-pyp)Br]** (**18**)

Chapter 6				
Atom	x	y	z	U(eq)
Cu	4062(1)	890(1)	4675(1)	65(1)
Br	5124(1)	1600(1)	5661(1)	51(1)
O(1)	4592(3)	2166(6)	3964(3)	81(2)
N(1)	2966(3)	1634(5)	4266(2)	41(1)
N(2)	3203(3)	-220(5)	5298(2)	44(1)
C(8)	2355(3)	87(6)	5130(3)	42(1)
C(10)	1853(4)	-1490(6)	6066(3)	53(2)
C(7)	2253(3)	1124(6)	4537(3)	44(1)
C(11)	2704(4)	-1816(6)	6228(3)	48(1)
C(6)	3105(3)	2625(6)	3705(3)	43(1)
C(4)	2709(4)	4329(7)	2776(3)	58(2)
C(5)	2458(4)	3371(6)	3306(3)	50(1)
C(12)	3361(4)	-1172(6)	5834(3)	48(1)
C(1)	4006(4)	2857(7)	3569(3)	53(2)
C(3)	3595(4)	4539(7)	2638(3)	61(2)
C(9)	1673(4)	-536(6)	5504(3)	51(2)
C(13)	5212(4)	4059(10)	2847(4)	92(3)
C(2)	4251(4)	3833(7)	3010(3)	60(2)

Table AI.21. For **[Cu(4-Cl-pyp)Cl]** (**19**)

Chapter 6				
Atom	x	y	z	U(eq)
Cu(1)	4417(1)	6142(1)	2190(1)	36(1)
Cu(2)	9368(1)	6932(1)	2209(1)	36(1)
Cl(3)	10248(1)	5720(1)	1764(1)	42(1)
Cl(1)	5374(1)	7330(1)	1736(1)	41(1)
Cl(2)	3202(1)	4220(1)	4724(1)	61(1)
Cl(4)	8812(1)	8891(1)	4767(1)	62(1)
O(2)	8138(3)	6414(1)	2855(1)	38(1)
O(1)	3214(3)	6694(1)	2822(1)	37(1)
N(1)	4331(3)	5081(1)	2654(1)	31(1)
N(3)	9398(3)	8004(1)	2668(1)	31(1)
N(2)	5267(3)	5238(1)	1624(1)	34(1)
C(13)	8149(4)	6981(2)	3279(1)	33(1)
N(4)	10335(3)	7796(1)	1641(1)	34(1)
C(7)	4853(3)	4359(2)	2431(1)	33(1)
C(18)	8829(3)	7855(2)	3214(1)	31(1)
C(1)	3130(4)	6140(2)	3249(1)	32(1)
C(6)	3713(3)	5254(2)	3192(1)	31(1)
C(5)	3734(4)	4651(2)	3642(1)	34(1)
C(19)	10020(3)	8706(2)	2437(1)	32(1)
C(16)	8489(4)	8182(2)	4182(1)	40(1)

Table AI.21. Continued …

Chapter 6				
Atom	x	y	z	U(eq)
C(4)	3141(4)	4939(2)	4149(1)	39(1)
C(8)	5379(3)	4417(2)	1848(1)	32(1)
C(17)	9011(4)	8453(2)	3662(1)	34(1)
C(20)	10544(3)	8618(2)	1856(1)	32(1)
C(9)	5917(4)	3697(2)	1534(1)	37(1)
C(2)	2471(4)	6384(2)	3777(1)	39(1)
C(14)	7544(4)	6759(2)	3817(1)	41(1)
C(10)	6324(4)	3831(2)	975(1)	44(1)
C(21)	11180(4)	9313(2)	1539(1)	40(1)
C(3)	2485(4)	5799(2)	4218(1)	41(1)
C(22)	11627(4)	9147(2)	983(1)	49(1)
C(23)	11423(5)	8307(2)	769(1)	54(1)
C(11)	6211(4)	4664(2)	747(1)	46(1)
C(12)	5693(4)	5354(2)	1089(1)	44(1)
C(24)	10766(4)	7646(2)	1112(1)	46(1)
C(15)	7734(4)	7346(2)	4262(1)	42(1)

Table AI.22. For **[Cu(4-Cl-pyp)Br]** (**20**)

Chapter 6				
Atom	x	y	z	U(eq)
Cu	850(1)	10572(1)	4037(1)	36(1)
Br	-264(1)	11608(1)	3349(1)	55(1)
Cl	5326(2)	9642(1)	6607(1)	53(1)
O(1)	1686(5)	11442(2)	4622(2)	44(1)
N(2)	259(6)	9418(3)	3598(2)	35(1)
N(1)	1811(5)	9690(3)	4608(2)	31(1)
C(3)	4127(7)	11103(4)	6001(2)	39(1)
C(1)	2492(7)	11051(3)	5078(2)	35(1)
C(11)	-836(8)	8476(4)	2822(3)	49(2)
C(6)	2599(7)	10092(3)	5110(2)	31(1)
C(9)	684(7)	7816(3)	3648(2)	39(1)
C(7)	1741(7)	8856(3)	4449(2)	34(1)
C(5)	3431(7)	9650(3)	5581(2)	35(1)
C(2)	3313(8)	11535(3)	5539(2)	41(1)
C(8)	882(7)	8675(3)	3887(2)	34(1)
C(4)	4190(7)	10161(4)	6018(2)	38(1)
C(12)	-580(7)	9311(4)	3079(2)	41(1)
C(10)	-213(8)	7718(4)	3112(3)	49(2)

Table AI.23. For **[Cu(suc)(bpy)(H_2O)$_2$]**·2H_2O (**21**)

Chapter 7				
Atom	x	y	z	U(eq)
Cu	5146(1)	0	0	28(1)
O(1)	4333(2)	-1718(2)	422(1)	34(1)
O(2)	5417(2)	-931(2)	1198(1)	51(1)
O(3)	5883(3)	1560(3)	815(1)	49(1)
O(4)	4522(4)	3078(5)	1051(2)	85(1)
N(1)	6964(2)	0	0	27(1)
N(2)	13345(2)	0	0	30(1)
C(1)	8175(3)	1163(3)	100(1)	33(1)
C(2)	9434(3)	1203(3)	110(1)	34(1)
C(3)	9490(3)	0	0	29(1)
C(4)	10818(3)	0	0	31(1)
C(5)	10879(3)	-1201(3)	83(1)	44(1)
C(6)	12131(3)	-1172(3)	78(1)	42(1)
C(7)	4753(3)	-1884(3)	870(1)	32(1)
C(8)	4478(3)	-3338(3)	997(1)	36(1)

Table AI.24. For **[Ni(suc)(bpy)(H_2O)$_2$]**·2H_2O (**22**)

Chapter 7				
Atom	x	y	z	U(eq)
Ni	4575(1)	10000	0	27(1)
N(2)	-3587(3)	10000	0	34(1)
O(1)	3602(2)	8165(2)	418(1)	36(1)
N(1)	2726(3)	10000	0	29(1)
O(3)	5167(3)	11168(2)	746(1)	42(1)
O(2)	3388(3)	8861(2)	1250(1)	55(1)
C(3)	225(3)	10000	0	31(1)
C(4)	-1094(3)	10000	0	34(1)
C(2)	1467(3)	11197(3)	79(1)	39(1)
C(7)	3064(3)	7950(3)	885(1)	36(1)
C(8)	1896(3)	6507(3)	1010(1)	45(1)
C(1)	2680(3)	11156(3)	71(1)	36(1)
C(5)	-2331(3)	8815(3)	109(1)	43(1)
O(4)	2793(5)	8043(5)	2339(2)	107(2)
C(6)	-3544(3)	8851(3)	103(1)	44(1)

Table AI.25. For **[Cu$_2$(suc)$_2$(pz)]** (**23**)

Chapter 7				
Atom	x	y	z	U(eq)
Cu(1)	1332(1)	0	18(1)	12(1)
N(1)	3639(2)	0	-5(3)	20(1)
O(1)	1958(2)	1174(2)	2167(3)	31(1)
O(2)	-356(2)	1184(2)	2099(3)	32(1)
C(1)	1051(3)	1491(2)	2821(4)	21(1)
C(3)	4291(3)	977(2)	-10(5)	30(1)
C(2)	1669(3)	2307(3)	4616(4)	28(1)

List of Publications

Thesis Work

1. A one-dimensional assembly of a square-planar copper(II) complexes with alternate short and long Cu···Cu distances: Metal ion spin-exchange *via* π-π interactions.
   S. Das, G. P. Muthukumaragopal, S. Pal and S. Pal
   New J. Chem. **2003**, *27*, 1102-1107.

2. Self-assembly of copper(II) complexes with dibasic tridentate ligand and monodentate N-heterocycles: Structural, magnetic and EPR studies.
   S. Das and S. Pal
   J. Mol. Struc. **2005**, *741*, 183-192.

3. Copper(II) complexes with tridentate N-(benzoyl)-N'-(salicylidene)-hydrazine and monodentate N-heterocycles: Investigation of inter-molecular interactions in the solid state.
   S. Das and S.Pal
   J. Mol. Struc. **2005**, *753*, 68-79.

4. Non-oligomeric zipper from planar copper(II) complexes.
   S. Das and S. Pal
   (Manuscript under preparation).

5. Supramolecular architecture of a family of homologated copper(II) complexes: Effect of ligand substituent position.
   S. Das and S. Pal
   (Manuscript under preparation).

6. Coordination polymer based on cobridging of rigid and flexible spacer: The role of length and conformational flexibility of the spacers.
   S. Das and S. Pal
   (Manuscript under preparation).

Other Publications

7. Cyclopalladated complexes with N-(benzoyl)-N'-(2,4-dimethoxy-benzylidene)hydrazine: Synthesis, characterization and structural studies.
   S. Das and S. Pal
   J. Organomet. Chem. **2004**, *689*, 352-360.

8. Unique asymmetric (Cu^{II}_4) double-stranded helicate from a hexadentate piperazine-based ligand: Ligand conformation isomerism upon coordination.
   A. R. Paital, P. K. Nanda, **S. Das**, G. Aromi and D. Ray
   Inorg. Chem. **2006**, *45*, 505-507.

9. Synthesis, characterization and structural studies of palladium(II) complexes with N-(aroyl)-N'-(2,4-dimethoxy-benzylidene)hydrazines.
   S. Das and S. Pal
   J. Organomet. Chem. In press.